AMEGHINIANA
A GONDWANAN PALEONTOLOGICAL JOURNAL

THE SKULL BENEATH THE SKIN: CRANIAL OSTEOLOGY OF *SKORPIOVENATOR BUSTINGORRYI* (DINOSAURIA, THEROPODA, ABELISAURIDAE) FROM THE LATE CRETACEOUS OF PATAGONIA, ARGENTINA

JUAN I. CANALE[1,2]
MAURICIO A. CERRONI[1,3]
MATTIA A. BAIANO[1,2,4]
JORGE G. MESO[1,4]
DAMIANO PALOMBI[1,2]
ARIANA PAULINA CARABAJAL[1,5]

[1]Consejo Nacional de Investigaciones Científicas y Técnicas (CONICET).
[2]Área Laboratorio e Investigación, Museo Municipal "Ernesto Bachmann" (MEB), Dr. Natali S/N 8311, Villa El Chocón, Neuquén, Argentina. Universidad Nacional de Río Negro (UNRN), Sede Alto Valle y Valle Medio, Gral. Roca, Río Negro, Argentina.
[3]Laboratorio de Anatomía Comparada y Evolución de los Vertebrados, Museo Argentino de Ciencias Naturales "Bernardino Rivadavia", CONICET, Av. Patricias Argentinas 480, (C1405) Buenos Aires, Argentina.
[4]Instituto de Investigaciones en Paleobiología y Geología. (IIPG). Av. Roca 1242, (R8332EXZ) General Roca, Río Negro, Argentina.
[5]Instituto de Investigaciones en Biodiversidad y Medio Ambiente (INIBIOMA). Pje Gutiérrez 1415 (8400), San Carlos de Bariloche, Río Negro, Argentina.

Submitted: 27 August 2025 - **Accepted:** 20 August 2026 - **Published:** 21 August 2026

To cite this article: Juan I. Canale, Mauricio A. Cerroni, Mattia A. Baiano, Jorge G. Meso, Damiano Palombi, & Ariana Paulina Carabajal (2027). The skull beneath the skin: cranial osteology of *Skorpiovenator bustingorryi* (Dinosauria, Cheropoda, Abelisauridae) from the Late Cretaceous of Patagonia, Argentina. *Ameghiniana*, *64*(1), xx–xx.

To link to this article: http://dx.doi.org/10.5710/AMGH.20.08.2026.3665

PLEASE SCROLL DOWN FOR ARTICLE

XXXXXXXXXXXXXXX
XXXXXXXXXXXX

XXXXXXXXXXXXXXXXXXXXXXX
XXXXXXXXXXXXXXXXXXXXXXX
XXXXXXXXXXXXXXXXXXXXXXX
XXXXXXXXXXX

XXXXXXXXXXXXXXX
XXXXXXXXXXXX

XXXXXXXXXXXXXXXXXXXXXXX
XXXXXXXXXXXXXXXXXXXXXXX
XXXXXXXXXXXXXXXXXXXXXXX
XXXXXXXXXXX

XXXXXXXXXXXXXXX
XXXXXXXXXXXX

XXXXXXXXXXXXXXXXXXXXXXX
XXXXXXXXXXXXXXXXXXXXXXX
XXXXXXXXXXXXXXXXXXXXXXX
XXXXXXXXXXX

ISSN 0002-7014
AMEGHINIANA - 2027 - Volume 64(1): xx–xx
GONDWANAN PERSPECTIVES

THE SKULL BENEATH THE SKIN: CRANIAL OSTEOLOGY OF *SKORPIOVENATOR BUSTINGORRYI* (DINOSAURIA, THEROPODA, ABELISAURIDAE) FROM THE LATE CRETACEOUS OF PATAGONIA, ARGENTINA

JUAN I. CANALE[1,2], MAURICIO A. CERRONI[1,3], MATTIA A. BAIANO[1,2,4], JORGE G. MESO[1,4], DAMIANO PALOMBI[1,2], AND ARIANA PAULINA CARABAJAL[1,5]

[1]Consejo Nacional de Investigaciones Científicas y Técnicas (CONICET).

[2]Área Laboratorio e Investigación, Museo Municipal "Ernesto Bachmann" (MEB), Dr. Natali S/N 8311, Villa El Chocón, Neuquén, Argentina. Universidad Nacional de Río Negro (UNRN), Sede Alto Valle y Valle Medio, Gral. Roca, Río Negro, Argentina. *jicanale@unrn.edu.ar*; *damianopalombi@icloud.com*; *mbaiano@unrn.edu.ar*

[3]Laboratorio de Anatomía Comparada y Evolución de los Vertebrados, Museo Argentino de Ciencias Naturales "Bernardino Rivadavia", CONICET, Av. Patricias Argentinas 480, (C1405) Buenos Aires, Argentina. *mauricio.cerroni@gmail.com*

[4]Instituto de Investigaciones en Paleobiología y Geología. (IIPG). Av. Roca 1242, (R8332EXZ) General Roca, Río Negro, Argentina. jgmeso@unrn.edu.ar

[5]Instituto de Investigaciones en Biodiversidad y Medio Ambiente (INIBIOMA). Pje Gutiérrez 1415 (8400), San Carlos de Bariloche, Río Negro, Argentina. *a.paulinacarabajal@conicet.gov.ar*

Abstract. We present a detailed comparative cranial anatomical description of the abelisaurid theropod *Skorpiovenator bustingorryi*, recovered from the Cenomanian—Turonian Huincul Formation near Villa El Chocón, Neuquén Province, Argentina. The specimen was thoroughly prepared and supplemented with CT scan-based reconstructions. *Skorpiovenator* represents one of the most complete abelisaurid skulls, and indeed one of the most complete of any South American theropod dinosaur documented to date. Its skull is moderately short and tall, featuring strongly ornamented facial bones, a characteristic common among abelisaurids. We re-evaluated previously proposed autapomorphies and suggest new ones to refine the diagnosis of the species, and discuss several cranial features within a phylogenetic framework to clarify its relationships among late-branching ceratosaurians. The analysis recovers *Skorpiovenator* as a brachyrostran abelisaurid, nested within a subclade alongside other early Late Cretaceous Patagonian taxa, sister group to Furileusauria. Key cranial features include two pairs of prominences on the frontals, low paired crests on the anterior portion of the nasals, an enlarged external mandibular fenestra, and a distinctive dentition. Notably, *Skorpiovenator* exhibits the highest maxillary and dentary tooth count recorded for an abelisaurid. A significant discovery is the identification of an additional small bone dorsal to the articular of the mandible, interpreted as the antarticular, likely sesamoid in origin. It represents the first record of such an ossification outside the Tetanurae lineage. The data presented in this work significantly enhance our anatomical understanding of abelisaurid crania thereby contributing to a clearer understanding of phylogenetic relationships within ceratosaurian theropod dinosaurs.

Key words. *Skorpiovenator*. Cranium. Anatomy. Ceratosauria. Braincase. Phylogeny. South America.

Resumen. OSTEOLOGÍA CRANEANA DE *SKORPIOVENATOR BUSTINGORRYI* (DINOSAURIA, THEROPODA, ABELISAURIDAE) DEL CRETÁCICO SUPERIOR DE PATAGONIA, ARGENTINA. Presentamos una descripción anatómica craneana comparativa detallada del terópodo abelisáurido *Skorpiovenator bustingorryi*, recuperado de la Formación Huincul (Cenomaniano–Turoniano), en Villa El Chocón, Provincia del Neuquén, Argentina. El espécimen fue preparado y complementado con reconstrucciones basadas en tomografías computarizadas. *Skorpiovenator* posee uno de los cráneos de abelisáuridos más completos y, efectivamente, de los más completos de cualquier dinosaurio terópodo sudamericano documentado. Su cráneo es moderadamente corto y alto, con huesos faciales fuertemente ornamentados, una característica común entre los abelisáuridos. Re-evaluamos rasgos autapomórficos del cráneo previamente propuestos, sugerimos otros para mejorar la diagnosis de la especie y discutimos varias características craneanas en un marco filogenético para dilucidar las relaciones filogenéticas entre ceratosaurios derivados. El análisis recuperó *Skorpiovenator* como un abelisáurido braquirostro, anidado en un subclado junto con otros taxones patagónicos del Cretácico Tardío temprano, grupo hermano de los Furileusauria. Algunos caracteres craneanos destacables incluyen dos pares de prominencias frontales, crestas bajas bilaterales sobre el sector anterior de los nasales, gran tamaño de la fenestra mandibular y dentición distintiva. Notablemente *Skorpiovenator* presenta el mayor número de dientes maxilares y dentarios registrados en un abelisáurido. Un descubrimiento intrigante es un pequeño hueso adicional dorsal al articular de la mandíbula, interpretado como el antarticular, probablemente de origen sesamoideo. Este representa el primer registro de un elemento de este tipo por fuera del linaje Tetanurae. Los datos obtenidos en este trabajo aumentan significativamente nuestra comprensión anatómica del cráneo de los abelisáuridos, contribuyendo así a aclarar las relaciones filogenéticas dentro de los dinosaurios terópodos ceratosaurios.

Palabras clave. *Skorpiovenator*. Cráneo. Anatomía. Ceratosauria. Caja craneana. Filogenia. América del Sur.

INTRODUCTION

The abelisaurid theropods were extremely abundant and diverse in Cretaceous faunas of the Southern Hemisphere. They were characterized by some bizarre traits, most of them concentrated in their short, tall and robust skulls, which show facial bones usually ornamented with crests, furrows and protuberances, a centrally constricted orbital fenestra; horns and protuberances on their frontal bones; and extremely kinetic articulation between dentary and postdentary bones. Undoubtedly, the best record of this group comes from South America outcrops, including several erected species, some of them represented by fairly complete specimens with partially to almost completely preserved skulls such as *Carnotaurus sastrei* (Bonaparte, 1985), *Aucasaurus garridoi* (Coria *et al*., 2002), *Eoabelisaurus mefi* (Pol & Rauhut, 2012), *Llukalkan aliocranianus* (Gianechini *et al*., 2021), *Spectrovenator ragei* (Zaher *et al*., 2020), and *Koleken inakayali* (Pol *et al*., 2024). This is complemented by abelisaurid specimens collected from Cretaceous rocks in various parts of the world, including significant cranial remains, such as *Rugops primus* from Niger (Sereno *et al*., 2004), *Majungasaurus crenatissimus* from Madagascar (Sampson *et al*., 1998), and *Arcovenator escotae* from France (Tortosa *et al*., 2014). Despite this important record compared to other theropod groups, the cranial anatomy of abelisaurids remains poorly understood. Only a few works provide detailed descriptions of the skull (Sampson & Witmer, 2007; Cerroni *et al*., 2020a) or specific regions, such as the braincase (Paulina Carabajal, 2011a, b; Paulina Carabajal & Filippi, 2018).

In the summer of 2005, a field prospecting trip carried out by Juan Ignacio Canale and Agustín Scanferla— PhD students at that time—in the Candeleros and Huincul formations (surroundings of Villa El Chocón) led to the discovery of theropod remains by Scanferla. These remains were excavated some months later. The excavation yielded one of the most complete abelisaurid theropods ever recorded: *Skorpiovenator bustingorryi* Canale *et al*., 2009, a specimen found articulated and missing only the distal two-thirds of the tail and both pectoral girdles and arms (Fig. 1A–1G). The first publication was based on the right side of the specimen, which was the first to be prepared. Subsequently, the skeleton underwent a comprehensive preparation, which included the disarticulation of the skull from the cervical vertebrae. This process, in conjunction with CT scans, enabled the complete examination of the skull, revealing one of the most remarkable features of this taxon: a double row of large, rounded foramina extending anteroposteriorly along the dorsal surface of the skull, likely related to some biological function such as thermoregulation, visual display, or the presence of sensory structures (Cerroni *et al*., 2020b).

In this contribution, we provide a detailed osteological description of the holotype skull of *Skorpiovenator bustingorryi*, including its internal spaces and the bones of the palate and medial surfaces that are otherwise hidden from view, based on direct observation and CT scan analysis. Finally, we discuss some anatomical characters and their phylogenetic implications.

Institutional abbreviations. MACN, Museo Argentino de Ciencias Naturales "Bernardino Rivadavia", Buenos Aires, Argentina; **MAU,** Museo Municipal "Argentino Urquiza", Rincón de los Sauces, Neuquén, Argentina; **MCF-PVPH,** Museo "Carmen Funes", Plaza Huincul, Neuquén, Argentina; **MMCh-PV,** Museo Muncipal "Ernesto Bachmann", Villa El Chocón, Neuquén, Argentina; **MPCA,** Museo Provincial "Carlos Ameghino", Cipolletti, Río Negro, Argentina; **MPEF-PV,** Museo Paleontológico "Egidio Feruglio", Trelew, Chubut, Argentina; **MUCPv,** Museo de la Universidad del Comahue, Lago Barreales, Neuquén, Argentina; **USNM**, National Museum of Natural History, Smithsonian Institution, Washington D.C., USA.

MATERIAL AND METHODS

Material

The holotype specimen of *Skorpiovenator bustingorryi* is housed at the Vertebrate Paleontology collection of the Museo Paleontológico "Ernesto Bachmann" of Villa El Chocón, Neuquén Province, Argentina, under the number MMCh-PV 48.

The skeleton of *Skorpiovenator* was extracted from the rock in a single plaster jacket, as it was preserved completely articulated and splitting it in the field would have entailed a high risk of fossil destruction (Fig. 1B–1G). Once in the laboratory, the skull, which was firmly attached to the atlas-axis complex, was disarticulated, requiring delicate technical work. This allowed detailed mechanical preparation and X-ray computed tomography to study internal structures.

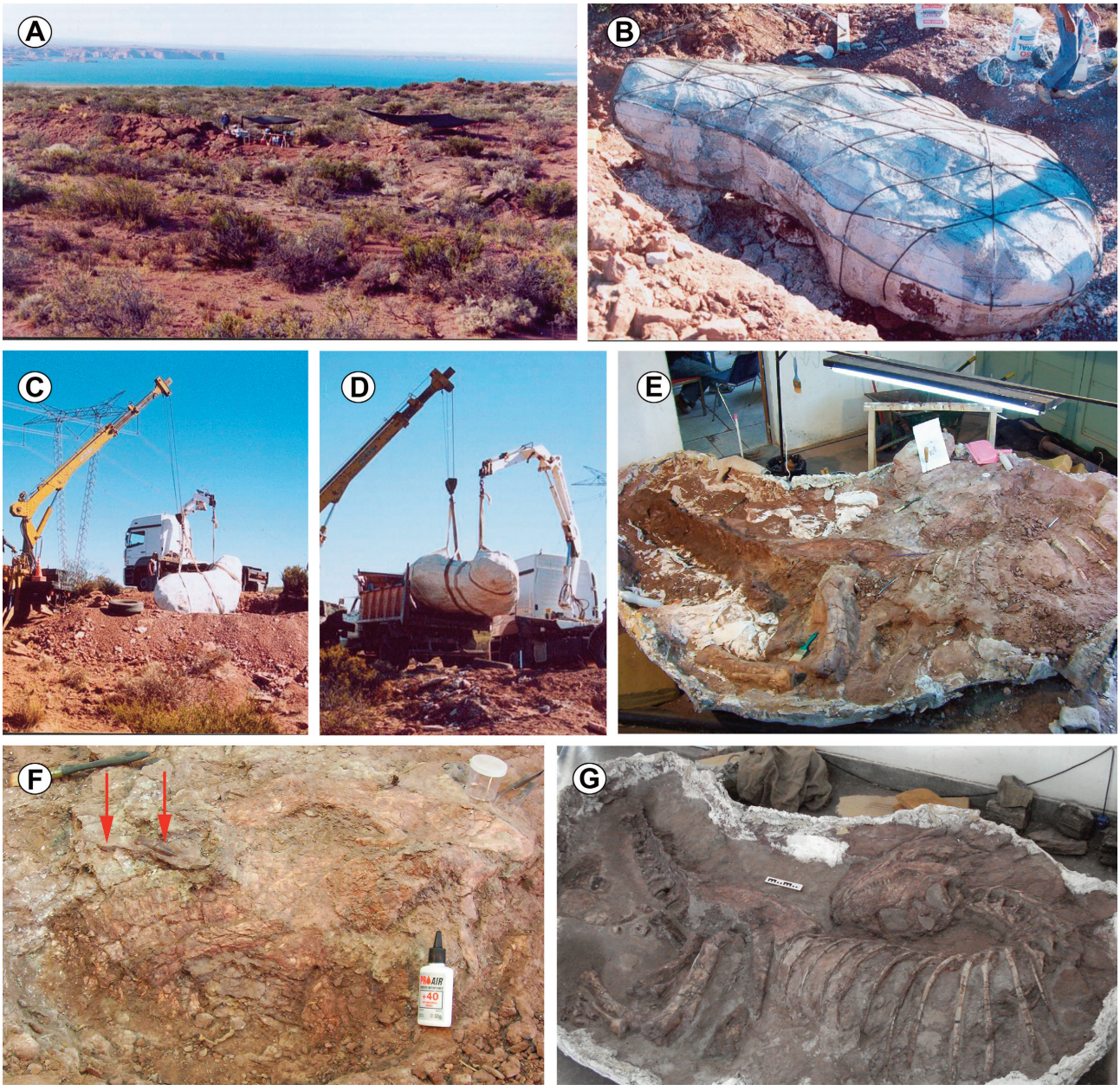


Figure 1. A–G. Extraction and preparation works on the holotype of ***Skorpiovenator bustingorryi*** **(MMCh-PV 48)**. **A,** detail of the fossil site, levels of Huincul Formation on the Bustingorry field, with the Exequiel Ramos Mexía lake in the background; **B,** construction of the iron bar net, covering the plaster jacket with the specimen; **C,** cranes lifting the plaster jacket; **D,** cranes placing the plaster jacket in the truck; **E,** preparation of the specimen in the laboratory; **F,** right lateral surface of the skull partially exposed from the rock, arrows pointing to *Skorpiovenator* loose teeth found during preparation; **G,** prepared right side of the holotype specimen, still in the plaster jacket.

Notable preservational differences exist between the sides of the skull of *Skorpiovenator* due to taphonomic processes, with the right side exhibiting better bone surface condition than the left side (Fig. 2A–2B). This is probably because the left side was close to the ground surface while still buried in rock and was, therefore, more exposed to erosive agents such as water infiltrating the sediments. Also, roots from the extant Patagonian vegetation affected portions of the medial surfaces, as seen in the palatal bones and lateral walls of the braincase.

The skull of *Skorpiovenator* shows signs of plastic shear deformation, which occurred during postburial diagenesis. This caused the right side of the skull to be displaced dorsally relative to the left (Fig. 2A–2F). Both lower jaws are articulated with the skull and remain closed; despite the general skull deformation, they are neither mediolaterally

crushed nor extremely displaced horizontally, although in the right lateral view, the right lower jaw is slightly elevated relative to the left one (Fig. 2A).

The diagenetic deformation produced disarticulation between some bones and also deformed others. The postorbital-squamosal complex rotated anteroventrally on the right side, which is evidenced by the disarticulation observed in the squamosal with respect to the quadratojugal/

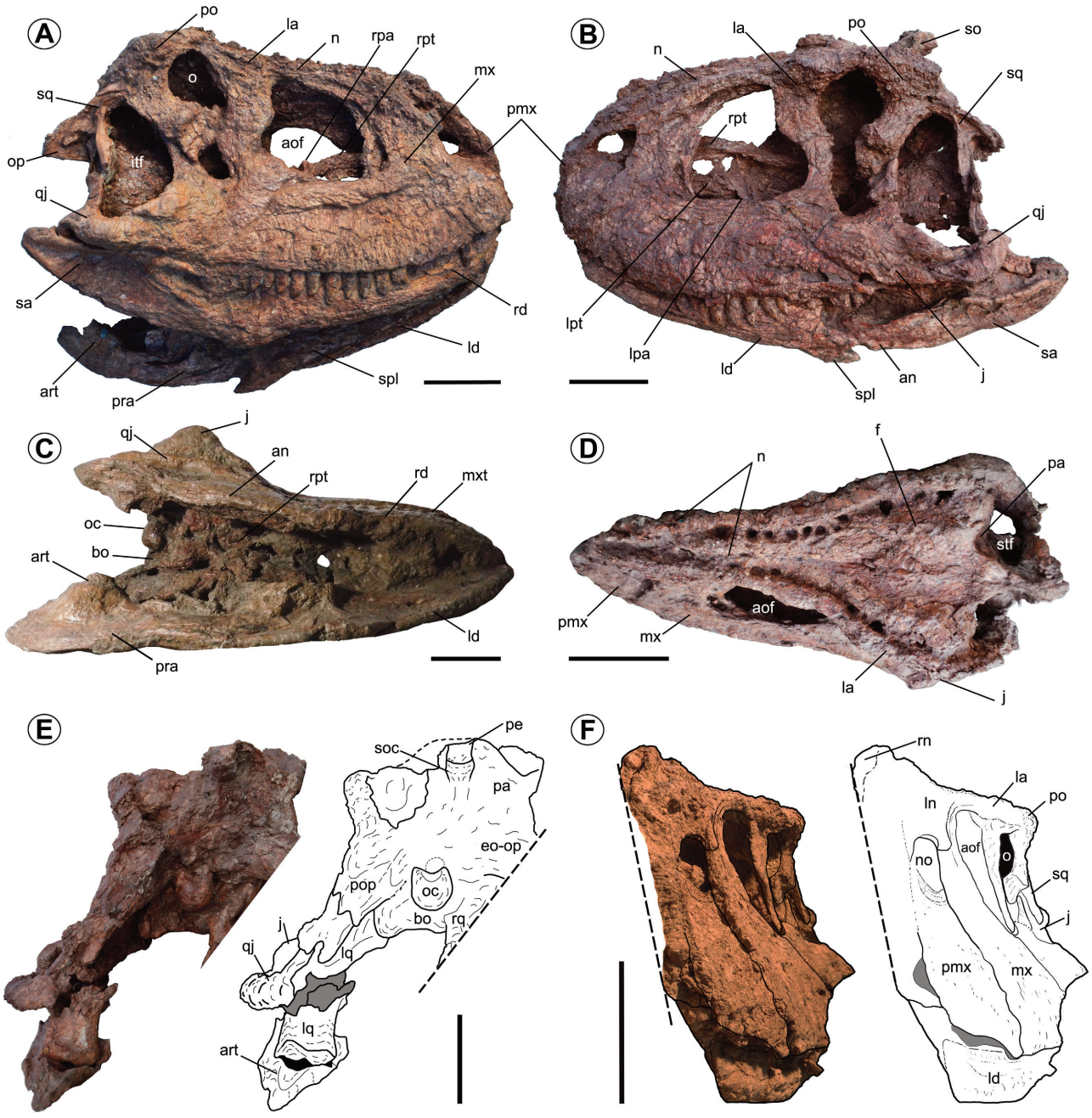


Figure 2. A–F. Skull of ***Skorpiovenator bustingorryi*** (**MMCh-PV 48**) in **A,** right lateral, **B,** left lateral, **C,** ventral, **D,** dorsal, **E,** posterior, and **F,** anterior views. Grey areas indicate broken bone surfaces; straight dashed lines in E and F represent the limit of the plaster jacket. Abbreviations: **an,** angular; **aof,** antorbital fenestra; **art,** articular; **bo,** basioccipital; **eo-op,** exoccipital-opisthotic; **itf,** infratemporal fenestra; **f,** frontal; **j,** jugal; **la,** lacrimal; **lf,** left dentary; **ln,** left nasal; **lpa,** left palatine; **lpt,** left pterygoid; **lq,** left quadrate; **mx,** maxilla; **mxt,** maxillary teeth; **n,** nasal; **no,** narial opening; **o,** orbit; **oc,** occipital condyle; **op,** opisthotic; **pa,** parietal; **pe,** parietal eminence; **pmx,** premaxilla; **pra,** prearticular; **po,** postorbital; **pop,** paroccipital process; **qj,** quadratojugal; **rd,** right dentary; **rn,** right nasal; **rpa,** right palatine; **rpt,** right pterygoid; **rq,** right quadrate; **sa,** surangular; **so,** supraoccipital; **soc**, supraoccipital crest; **spl,** splenial; **sq,** squamosal; **stf,** supratemporal fenestra. Scale bars equal 10 cm.

quadrate (Fig. 2A). Additionally, the distal end of the right postorbital is in contact with the posterior margins of the lacrimal, closing the right orbital fenestra at mid height, thus constricting the suborbital space ventrally. The right side was the first to be mechanically prepared and figured in the original publication, being reproduced in subsequent works and reconstructions since then (*e.g.*, Canale *et al.*, 2009; Novas *et al.*, 2013; Cerroni *et al.*, 2020b). However, on the left side of the skull, the orbit and suborbital space are not separated by the postorbital and lacrimal bones, which may indicate the original morphology of the circumorbital area (Fig. 2B). The distal end of the jugal ramus of the right lacrimal is displaced and laterally covered by the jugal (Fig. 2A), whereas the left lacrimal is well visible in lateral view unobscured by the jugal (Fig. 2B). This enabled a reinterpretation of the morphology of the distal end of the jugal ramus, revealing that it is not as wide as previously suggested. The aforementioned distorted bones provide evidence that deformational forces also acted in the anteroposterior (*e.g.*, postorbital-squamosal) and mediolateral (*e.g.*, distal end of the lacrimal) directions.

The deformation is also evident in the loss of bilateral symmetry of the braincase in posterior view (Fig. 2E), where the right side is displaced dorsally with respect to the left, as observed in the position of the paroccipital processes and the right parietal ala. In anterior view, the mediolateral deformation affected the lacrimal and the bilateral crest of the nasals, as they are asymmetrically arranged (Fig. 2F). The palate was also affected by deformation, as evidenced by the vomeropalatine ramus of the right pterygoid, which is dorsally located over its left counterpart and the left palatine. CT scans revealed that the U-shaped space of the right ectopterygoid is occupied by the dorsal aspect of the right surangular, and that the vomer is broken off from the anterior portion of the pterygoid and is displaced ventrally.

Finally, erosive factors such as water, wind, and plant roots mostly weathered the anterior surface of the skull, including the premaxillary processes of the nasals and palatal bones such as the palatines and pterygoids. The left side of the skull exhibits the most pronounced taphonomic alteration, resulting in the complete loss of some elements (*e.g.*, the ectopterygoid) and partial erosion of structures including the ectopterygoid and quadratic rami of the pterygoid, the jugal ramus of the palatine, and multiple maxillary teeth.

Theropod species used for comparisons. We examined firsthand the following theropod specimens, mostly abelisaurids and other ceratosaurs, for comparative purposes: *Abelisaurus comahuensis* (MPCA 11098; Bonaparte and Novas, 1985), *Arcovenator escotae* (MHNA-PV-2011.12.1, MHNA-PV-2011.12.2; Tortosa *et al.*, 2014), Abelisauridae indet. (UNPSJB-PV 247; Lamanna *et al.*, 2002), *Aucasaurus garridoi* (MCF-PVPH-236; Coria *et al*, 2002), *Carnotaurus sastrei* (MACN-CH 894; Bonaparte, 1985), *Ceratosaurus nasicornis* (USNM 4735; Gilmore, 1920), *Ekrixinatosaurus novasi* (MUCPv 294; Calvo *et al.*, 2004), *Eoabelisaurus mefi* (MPEF PV 3990; Pol and Rauhut, 2012), *Genyodectes serus* (MLP 26-39; Woodward, 1901), *Guemesia ochoai* (IBIGEO-P 103; Agnolín *et al.*, 2022), *Ilokelesia aguadagrandensis* (MCF-PVPH 35; Coria and Salgado, 1998), *Llukalkan aliocranianus* (MAU-Pv-LI-581; Gianechini *et al.*, 2021), *Niebla antiqua* (MPCN-PV 796; Aranciaga Rolando *et al.*, 2021), *Noasaurus leali* (PVL4061; Bonaparte and Powell, 1980), *Koleken inakayali* (MPEF-PV 10826; Pol *et al.*, 2024), *Tralkasaurus cuyi* (MPCA-PV 815; Cerroni *et al.*, 2020c), *Viavenator exxoni* (MAU-Pv-LI 530; Filippi *et al.*, 2016).

The following species were compared through their publications, photographs, and/or casts: *Berthasaura leopoldinae* (de Souza *et al.*, 2021), *Ceratosaurus* sp. (Madsen & Welles, 2000), *Kryptops palaios* (Sereno & Brusatte, 2008), *Majungasaurus crenatissimus* (Sampson & Witmer, 2007, MACN-PV-19776, cast), *Masiakasaurus knopfleri* (Carrano *et al.*, 2002, 2011), *Rugops primus* (Sereno *et al.*, 2004), *Spectrovenator ragei* (Zaher *et al.*, 2020).

Methods

The specimen was studied macroscopically, and details were observed with a hand magnifying glass Zeiss Gold 15 X. The CT scans were performed at the medical diagnostic institution Clinica Moguillansky (Neuquén, Argentina), using a medical tomograph GE BrightSpeed Elite, and applying an energy of 140 kv and 153 mAs, resulting in 2236 slices of 0.62 mm thickness. The segmentation of bones and their internal structures was obtained and visualized using the software 3D Slicer version 5.6.2 (Fedorov *et al.*, 2012) and Materialise Mimics 16.0 (braincase). Final illustrations were made using Adobe Photoshop (CS6). Bone measurements were taken with a digital calliper and tape measure (SOI 1, Table S1).

The 3D models of the complete skull were created using photogrammetry. A Sony DSC-H300 camera with a 20.1-megapixel Cyber-shot sensor was used. To capture a comprehensive view and ensure adequate overlaps between photos, 205 photos of the left side of the skull and 307 of the right were taken, including overlapping points from dorsal and ventral views. These images were processed with Agisoft Metashape Standard, version 1.8.4 (64-bit), a photogrammetry software for generating 3D data. After importing the images, the software's algorithm calculated the associated camera parameters. Then image matching procedures extracted and matched positions and orientations in space. The extracted features were linked to 3D points, resulting in a sparse point cloud. A dense point cloud was then created using "Dense Stereo Matching" (DSM) algorithms that employed all the pixels from the images. Finally, the points were triangulated to form a mesh model with texture containing colour information from the images. The resulting 3D model has been exported to .ply format.

The resultant 3D models derived from segmentation and phogrammetry are hosted at the repository of the Internet Archive: https://archive.org/details/20260929_20260929_1834

Dental description. The dentition of *Skorpiovenator bustingorryi* (MMCh-PV 48) was examined firsthand using an Amscope SM-8 Stereo Microscope 7X - 45X magnification. Furthermore, in order to describe the dentary teeth—hidden beneath the premaxillae and maxillae—digital reconstructions obtained through segmentation of the dentary were employed. Twelve crown-based measurements were taken: crown basal length (**CBL**); crown basal width (**CBW**); crown height (**CH)**; mesial serrated carina length (**MSL**); mesio-basal denticle density (**MB**); mesio-central denticle density (**MC**); mesioapical denticle density (**MA**); distobasal denticle density (**DB**); distocentral denticle density (**DC**); distoapical denticle density (**DA**); mid-crown length (**MCL**); and mid-crown width (**MCW**). Also, four ratios were calculated: crown base ratio (**CBR**); crown height ratio (**CHR**); mid-crown ratio (**MCR**); and denticle size density index (**DSDI**). These measurements were taken using a 150 mm caliper with an accuracy of 0.01 mm, and measurements and ratios were recorded for *in situ* and shed teeth (thirteen associated elements; see SOI 2). In order to ensure an exhaustive characterization of the teeth (*e.g.*, anatomical orientation, morphometric and anatomical terms), we followed the dental nomenclature and descriptive protocols proposed by Smith and Dodson (2003), Smith *et al.* (2005), and Hendrickx *et al.* (2015).

Phylogenetic Analysis. The new anatomical data provided by the complete preparation of the skull and CT scans help to improve the phylogenetic information available for *Skorpiovenator*. Therefore, to test the relationships between *Skorpiovenator* and other South American abelisaurids, we used a modified data matrix published by Pol *et al.* (2024), which is an updated version of the phylogenetic matrices of Carrano and Sampson (2008); Canale *et al.* (2009); Pol and Rauhut (2012); Rauhut and Carrano (2016); Langer *et al.* (2019); Baiano *et al.* (2020, 2021, 2022, 2023); Ibiricu *et al.* (2021); Cerroni *et al.* (2022). The database presented here consists of 47 taxa and 253 characters (the 245 characters from Pol *et al.* 2024, plus 8 characters added here: see SOI 1, Text S1) (SOI 3_Data_Matrix.nex). Furthermore, the unknown skull character states were almost all scored for *Skorpiovenator*, and many states in other abelisaurids were re-scored (see Discussion and SOI 1, Text S2 and Text S3 for details in this respect).

We carried out a parsimony analysis using the software TNT v.1.6 (Goloboff *et al.*, 2008; Goloboff & Morales, 2023). The heuristic search was performed under equal and implied weighted parsimonies, using traditional searches of up to 1000 independent hits, followed by TBR branch swapping until the tree buffer was filled (at 99999 trees). The implied weighting method (Goloboff, 1997) was implemented here in order to penalize homoplasy and assess the sensitivity of the results to character weighting. Previous studies have shown that implied weighting parsimony may provide better results than equal weighting parsimony (*e.g.*, Goloboff *et al.*, 2018; Ezcurra, 2024). In addition, different concavity constants were tested to explore potential topological variation, specifically k = 12, k = 9, k = 6, and k = 3 (Goloboff *et al.*, 2018).

Support values were evaluated in TNT using Bremer support, jackknife, and bootstrap (BS).

To temporally calibrate all phylogenetic hypotheses obtained from different implied weighting analyses (concavity constants with k equal to 3, 6, 9, and 12), the minimum branch length (MBL) and Cal3 methods were used (Bapst, 2012). Since Cal3 requires a fully resolved tree,

polytomies were randomly resolved prior to calibration using the 'multi2di' function in the 'ape' package for R. The parameters used and the script are provided in the SOI 4.

SYSTEMATIC PALEONTOLOGY

DINOSAURIA *sensu* Owen, 1842
SAURISCHIA *sensu* Seeley, 1887
THEROPODA *sensu* Marsh, 1881
CERATOSAURIA *sensu* Marsh, 1884
ABELISAUROIDEA *sensu* Bonaparte 1991
ABELISAURIDAE *sensu* Bonaparte and Novas, 1985
BRACHYROSTRA *sensu* Canale, Scanferla, Agnolin, Novas, 2009

Skorpiovenator bustingorryi Canale, Scanferla, Agnolin, Novas, 2009

Holoype. MMCh-PV 48: an almost complete and articulated skeleton, lacking both pectoral girdles, the forelimbs, and the distal two-thirds of the tail. The skull, which constitutes the focus of this contribution, is almost completely preserved with the jaws articulated in occlusion. The entire skull was affected by strong shear deformation during diagenesis. Some areas are slightly damaged, such as the surface of some bones on the left side, and some teeth were lost, most probably during the biostratinomic stage.

Referred material. MMCh-PV 255, the proximal end of the right tibia.

Original diagnosis. (1) ascending process of maxilla homogeneously wide rostro-caudally, (2) maxillary horizontal ramus dorsoventrally deep with subparallel dorsal and ventral margins, (3) maxilla/jugal contact subvertical, (4) 19 maxillary teeth, (5) lacrimal rostrally projected and with well-developed suborbital process, (6) quadratojugal with pronounced caudal notch, (7) dentary with caudoventral process bifurcated to receive rostral end of angular, and (8) angular with rostral end dorsoventrally deep to fit between splenial and prearticular (Canale *et al.*, 2009).

Emended diagnosis. We conducted an analysis of the cranial autapomorphies provided in the original publication of *Skorpiovenator* (Canale *et al.*, 2009), retaining some and discarding others, as well as identifying new autapomorphies. The new autapomorphy list is provided below, including the appendicular characters proposed by Cerroni *et al.* (2022). The detailed analysis of the cranial autapomorphies can be found in the "Discussion" section.

(1) *Ascending process of maxilla homogeneously wide rostro-caudally* (Canale *et al.*, 2009).

(2) *Maxillary horizontal ramus dorsoventrally deep with subparallel dorsal and ventral margins* (Canale *et al.*, 2009).

(3) *19 maxillary teeth* (Canale *et al.*, 2009).

(4) *Angular with rostral end dorsoventrally deep to fit between splenial and prearticular* (Canale *et al.*, 2009).

(5) *Antorbital fossa restricted to the maxilla. Nasal and lacrimal without development of antorbital fossa* (this work).

(6) *Double dorsal protuberances over each frontal bone* (this work).

(7) *Quadratojugal with thick jugal process, rounded in section, laterally procumbent and with strong rugosities covering the external surface* (this work).

(8) *21 dentary teeth* (this work).

(9) *Retroarticular fossa of the articular anteroposteriorly longer than lateromedially wide, and divided by a strongly oblique crest* (this work).

(10) *Dorsal margin of the central iliac blade convex in lateral view* (Cerroni *et al.*, 2022).

(11) *Preacetabular blade sub-rectangular in contour when viewed from the side* (Cerroni *et al.*, 2022).

(12) *Sub-vertically oriented swelling of iliac blade at the level of the acetabulum* (Cerroni *et al.*, 2022).

(13) *Tibial lateral condyle one-third wider than the medial condyle and with a flattened caudal margin in proximal view* (Cerroni *et al.*, 2022).

(14) *Rounded and deep pit over the proximolateral surfaces of digit IV phalanges IV1/2/3* (Cerroni *et al.*, 2022).

Differential diagnosis. Given that other abelisaurids have been described from the Huincul Formation, *Ilokelesia aguadagrandensis* (Coria & Salgado, 1998) and *Tralkasaurus cuyi* (Cerroni *et al.*, 2020c), we include a differential diagnosis specifying cranial differences between *Skorpiovenator* and these species:

Skorpiovenator differs from *Ilokelesia* in having a bulbous shape of the orbital boss of the postorbital, a more distally expanded ventral process of the postorbital, a more strongly ornamented lateral surface of the postorbital, a sigmoid distal border of the ventral process of the postorbital, and a quadrate without the lateral process over the ventral

sector of the lateral surface for the articulation with the quadratojugal.

Compared to *Tralkasaurus*, *Skorpiovenator* lacks curved crests over the maxillary body, but has a more reduced ventral portion of the antorbital fossa (although this could be related to a younger ontogenetic stage in *Tralkasaurus*: see Ratsimbaholison *et al.*, 2016), a dorsoventrally taller maxillary body, a more strongly inclined maxilla-jugal articulation, almost vertically oriented inner and outer margins of the anterior sector of the antorbital fossa, an anteroposteriorly wider ascending process, and teeth with distal denticles larger than the mesial ones.

Geographic occurrence. The specimen was found at "Estancia Bustingorry", 800 meters north of Route 237 at the entrance of Villa El Chocón, Neuquén Province, Argentina (SOI 1, Fig. S1).

Stratigraphic occurrence. Lower section of the Huincul Formation, Cenomanian–Turonian (Garrido, 2010). The specimen was recovered from a small outcrop of brownish and red pelitic levels, intermixed with fine-grained sandstone levels. Fossil vertebrates recovered from nearly equivalent levels in the area (within a radius of 5 km) primarily include sauropod dinosaurs. The titanosaur *Choconsaurus baileywillisi* (Simón *et al.*, 2017) and the rebbachisaurid *Cienciargentina sanchezi* (Simón & Salgado, 2025) were found in slightly lower strata of the same formation, 2.5 km to the southeast at the "La Antena" fossil site. The gigantic titanosaur *Bustingorrytitan shiva* (Simón & Salgado, 2023) was recovered from slightly higher levels, 4 km to the north.

DESCRIPTION

The skull of *Skorpiovenator* is relatively short, tall, and mediolaterally wide (Fig. 3A–3F), as in other abelisaurids (Bonaparte, 1991; Tykoski & Rowe, 2004; Novas, 2009), showing proportions more similar to those of *Majungasaurus* and *Spectrovenator*.

The overall skull length measured from the tip of the snout to the posterior end of the ventral condyle of the quadrate is 585 mm on the right side and 612 mm on the left side; skull height, measured from the top of the

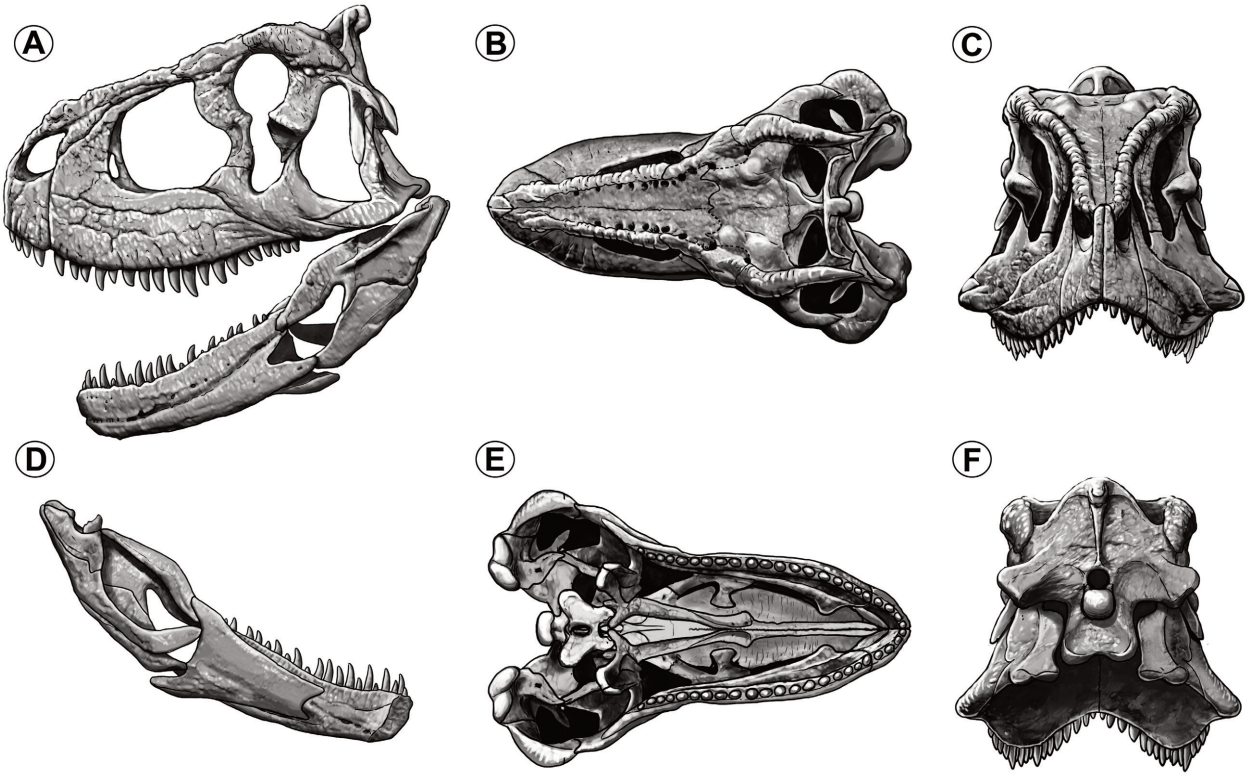


Figure 3. A–F. Drawings showing the retrodeformed skull and mandible of ***Skorpiovenator bustingorryi*** (**MMCh-PV 48**) in **A,** skull and jaw left lateral; **B,** skull, dorsal; **C,** skull anterior; **D,** left mandible, internal view; **E,** skull ventral; and **F,** skull posterior views.

postorbital to the base of the jugal, is 300 mm on the right side and 307 mm on the left side. Thus, the length/height ratio of *Skorpiovenator* is between 1.95 and 2, meaning a proportionally shorter skull than *Ceratosaurus* (R = 2.1) and *Majungasaurus* (R = 2.1), and longer than *Carnotaurus* (R = 1.6).

The surface of the facial bones is strongly ornamented with ridges and furrows (mainly in the maxilla, lacrimal and dentary), and small protuberances surrounded by an anastomosed net of grooves. Similar ornamentation is usual in other abelisaurids and is also present in other theropod groups such as carcharodontosaurids. This ornamentation is related to the mineralization of the underlying periosteum and dermis (Hieronymous & Witmer, 2003, 2004). The dorsal aspect of the skull is transversely concave on most of its surface, a condition exacerbated by the well-developed bilateral crests formed mostly by the nasals, lacrimals and postorbitals.

The cranial openings are relatively small in relation to other theropod groups. The narial opening is slightly ovoidal in lateral view, with its longest axis anteroventrally-posterodorsally oriented. The maxilla does not participate in the narial opening as was previously reported (Cerroni *et al.*, 2020a), although this condition is observable only on the left side, given that the right nasal is severely damaged at its anterolateral end.

The antorbital fenestra has a subquadrangular outline, with its opposite margins nearly parallel. Regarding the antorbital fossa, it extends only over the maxilla, being an autapomorphic trait of *Skorpiovenator*. The orbital fenestra is dorsoventrally tall with a central constriction produced by the suborbital flange of the postorbital and the suborbital process of the lacrimal. The suborbital space is also small. However, on the right side this is accentuated due to the taphonomic artifact that compresses the postorbital and the lacrimal. The supratemporal fenestra is slightly wider mediolaterally than anteroposteriorly long. It shows a parallelogram-shaped contour, with the anterior and posterior margins transversal to the main axis of the skull, and the lateral and medial margins posterolaterally directed. The infratemporal fenestra has a roughly triangular outline, with the longest side on the posterior margin and a rounded anterior rim. Due to the poor preservation of the palate, it is difficult to determine the shape of the pterygopalatine fenestra. The ventral aspect of the skull is relatively U-shaped, as is typical for abelisaurids, and through retrodeformation it shows an outline similar to that of *Majungasaurus* (Sampson & Witmer, 2007).

The mandibular fenestra exhibits an ovoidal contour, which is relatively long anteroposteriorly and wide, consistent with other abelisaurids. This opening is notably larger than those of other non-avian theropods (*e.g.*, tyrannosaurids, spinosaurids).

One of the most notable features of *Skorpiovenator* is the double line of foramina that runs anteroposteriorly over the dorsum of the skull and passes through several cranial bones. These foramina were described in detail in a previous study (Cerroni *et al.*, 2020b), which also provided hypotheses regarding their possible vascular function and palaeobiological significance.

In summary, most foramina are located on the nasal bones, with approximately seven on each side. The series continues posteriorly with foramina being bounded by different skull roof bones. The posteriormost of these corresponds in position to the small dorsal fenestra found in other abelisaurids, which in turn was termed the frontal fenestra (Tortosa *et al.*, 2014), prefrontal fenestra (Zaher *et al.*, 2020), or triosseal foramen (Cerroni *et al.*, 2020b), which is the term we use in this work. This feature has been used as a phylogenetic character in previous analyses (Canale *et al.*, 2009; Rauhut & Carrano, 2016; Pol *et al.*, 2024). In *Skorpiovenator*, this opening is similar in size to the other foramina in the series, whereas in *Spectrovenator* it is considerably larger. In *Rugops* the triosseal foramen shows irregular borders, while the nasal foramina are perfectly rounded. This latter taxon lacks the openings and fossae between the nasal foramina and the triosseal foramen, different from the condition present in *Skorpiovenator*. In *Ekrixinatosaurus* and *Arcovenator*, the nasals and lacrimals are not preserved, which prevents comparison with the rest of the foramina series. However, in the former, the size of the preserved opening is similar to that of *Skorpiovenator*, while in *Arcovenator* the fenestra is larger. Anterior to this opening, there is another broad foramen, referred to as the "middle foramen" in Cerroni *et al.* (2020b), which was determined by CT scans to be located entirely within the lacrimal bone.

It is interesting to note that, anterior to the triosseal

foramen, on both sides there is a distinct depression (Fig. 6A). CT scans do not confirm whether this depression fully perforates the skull roof. It is situated directly in line with the lateral suture between the postorbital and lacrimal, on the highest part of the orbital margin. Further blind fossae are also present in the left nasal, corresponding to positions 5 and 6 of the foramina line when counting from the anteriormost. The equivalent positions on the right nasal correspond to fully formed foramina, thus indicating bilateral asymmetry in the development of these structures. Given that the *Rugops* specimen is considered a juvenile/subadult (Carrano & Sampson, 2008) and lacks openings and fossae in the region between the line of nasal foramina and the triosseal fenestra/foramen, we can hypothesize that these blind depressions in *Skorpiovenator* are foramina still in the process of formation.

Dermatocranium

Premaxilla. Both premaxillae are present and articulated. The right premaxilla is the most complete (Fig. 4A–4I), showing some damaged bony surfaces over the anterior margin, while the left one has most of its surface eroded. The premaxilla contacts its opposite on the midline, the maxilla posteriorly, and the nasal dorsally, and presumably the vomer posteromedially, since CT scans revealed that the vomer is slightly offset from the contact with the left premaxilla.

The premaxillary body is subrectangular in lateral view, taller than long, and consistent with the morphology observed in other ceratosaur taxa such as *Carnotaurus*, *Aucasaurus*, and *Majungasaurus*. The anterior and posterior margins of the premaxillary body diverge dorsally, making its dorsal portion slightly wider (Fig. 4A), as it occurs in *Carnotaurus*. The contact with the maxilla is long, straight, and slightly posterodorsally inclined (Fig. 4B–4E). The lateral surface of the premaxillary body displays a pronounced ornamentation, characterized by a series of small irregular prominences separated by an anastomosed net of grooves. There are some small, rounded foramina scattered throughout the ventral half of the premaxillary body.

On the dorsal area of the premaxillary body, there is an abrupt change between the ornamented lateral surface and the narial fossa, which shows a completely smooth bony surface (Fig. 4A). This area corresponds to the sector of the mucous membrane of the nasal vestibule (Sampson & Witmer, 2007). The narial fossa surface of the right side forms an angle of nearly 90 degrees with the lateral surface, being almost hidden in lateral view, while on the left side it is almost continuous with the lateral surface of the premaxilla. Thus, correcting these differences produced by diagenetic deformation probably results in a narial fossa inclined with respect to the lateral surface of the premaxilla, as seen in other abelisaurids.

The nasal process is anteroposteriorly wider than in *Carnotaurus* and *Majungasaurus*, with a smooth lateral surface, forming part of the anterior border of the narial opening. This process is dorsoposteriorly oriented and gently curved, defining an angle of approximately 60 degrees with the anteroposterior axis of the skull. The precise morphology of the contact between the nasal process and the nasal is unknown because their surfaces are strongly eroded.

Both premaxillae bear four alveoli as shown by CT scans, but no erupted tooth crowns are preserved. However, some replacement teeth are recognized. The maxillary process of the premaxilla, barely visible in lateral view, can be seen in the CT scans (Fig. 4.B–4.H). It is anteroposteriorly short and posteriorly projected into a pointed end on its contact with the maxilla, resembling the condition in other abelisaurids (*e.g.*, *Majungasaurus*, *Carnotaurus*). The vomer is also visible through CT scans; however, it appears to be offset from the contact with the premaxilla.

Maxilla. The maxilla (Fig. 5A–5H) is the largest bone of the skull (SOI 1, Table S1), contacting the premaxilla anteriorly, the nasal dorsally, the jugal posteriorly and the palatine medially. Due to the articulated condition of the skull bones and the deformation that has compressed both maxillae towards the midline, information regarding the medial aspect of those bones and their articular surfaces with surrounding bones cannot be ascertained in most cases. The lateral surface of the bone is profusely ornamented, showing vertical ridges and furrows on the ventral half, over the dentigerous margin, and more rounded protuberances separated by anastomosed furrows on the dorsal region, including the ascending process (Fig. 5A–5C).

The distal tip of the ascending process of the maxilla is complete and reaches the anterior process of the lacrimal in the form of a thin lamina. This condition is better

preserved on the left side (Fig. 2B), although the lamina that contacts the lacrimal is slightly pushed medially as a consequence of taphonomic deformation. Laterally, the maxilla forms the entire anterior margin and the anterior half of the ventral margin of the antorbital fenestra. The main body of the maxilla is dorsoventrally deep, with subparallel dorsal and ventral margins, a condition considered diagnostic of the species in the original description (Canale *et al.*, 2009).

The anterior margin of the maxilla is continuous between the ventral sector and the ascending process in lateral view, as in *Ekrixinatosaurus*, without any concavity ventral to the external nares or anterior projection (Fig. 5A–5C), in contrast to the maxilla of *Majungasaurus* where a short anterior ramus of the maxilla is present. The anterior margin is straight for most of its length and is inclined posteriorly, forming an angle of about 65° with the anteroposterior axis of the skull. The ascending process rises almost

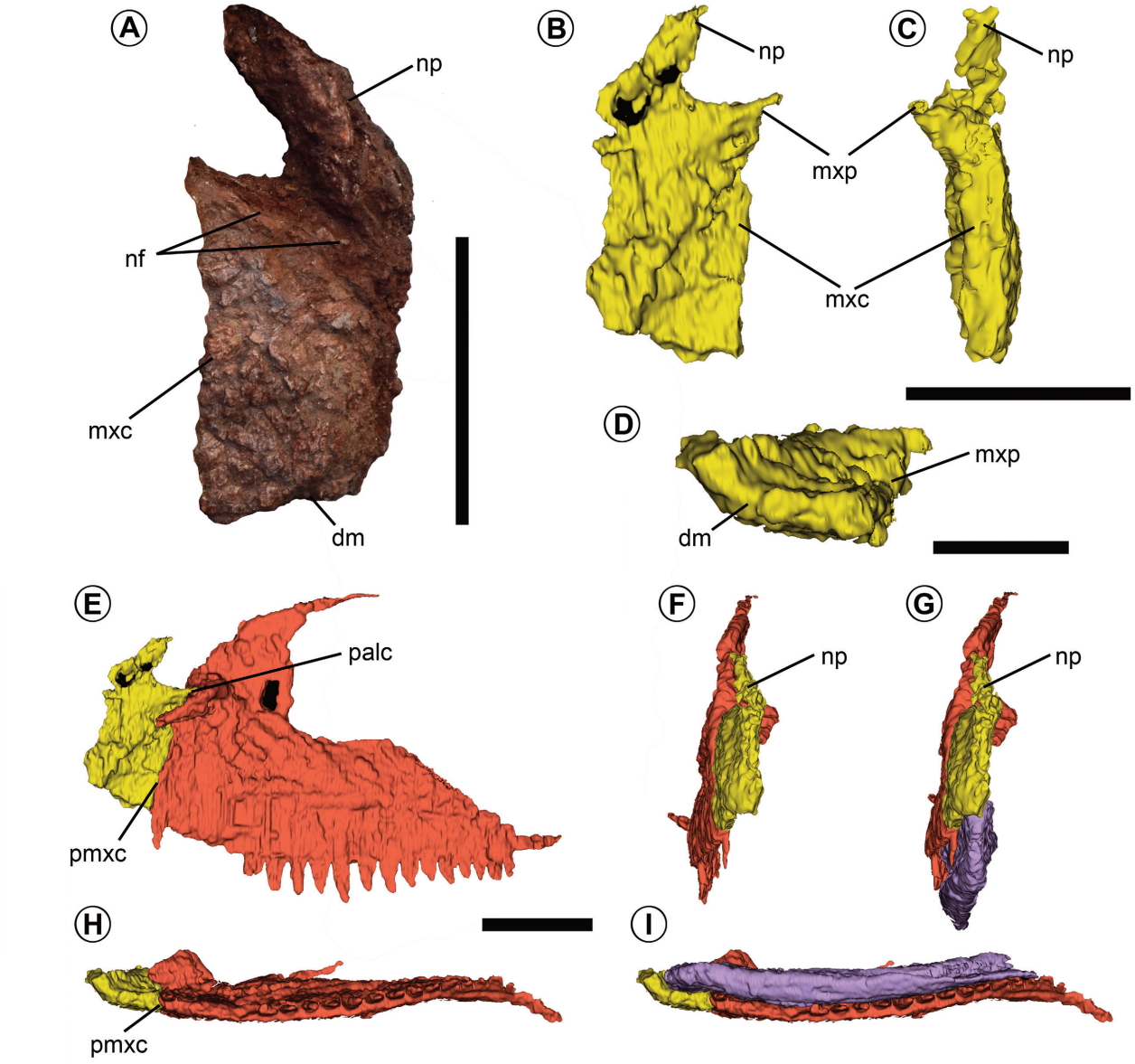


Figure 4. A–I. Right premaxilla of ***Skorpiovenator bustingorryi*** (**MMCh-PV 48**) in **A,** lateral view. Rendered right premaxilla in **B,** medial; **C,** posterior; and **D,** ventral views. Rendered right premaxilla and maxilla in articulation in **E,** medial; **F,** ventral; and **G,** anterior views; images derived from CT scan data. Rendered premaxilla in articulation with maxilla and dentary in **H,** anterior; and **I,** ventral views. Abbreviations: **dm,** dentigerous margin; **mxc,** maxillary contact; **mxp,** maxillary process; **np,** nasal process; **nf,** narial fossa; **palc,** palatal contact; **pmxc,** premaxilla-maxilla contact. Scale bars equal 10 cm (A–C, E–I) and 5 cm (D).

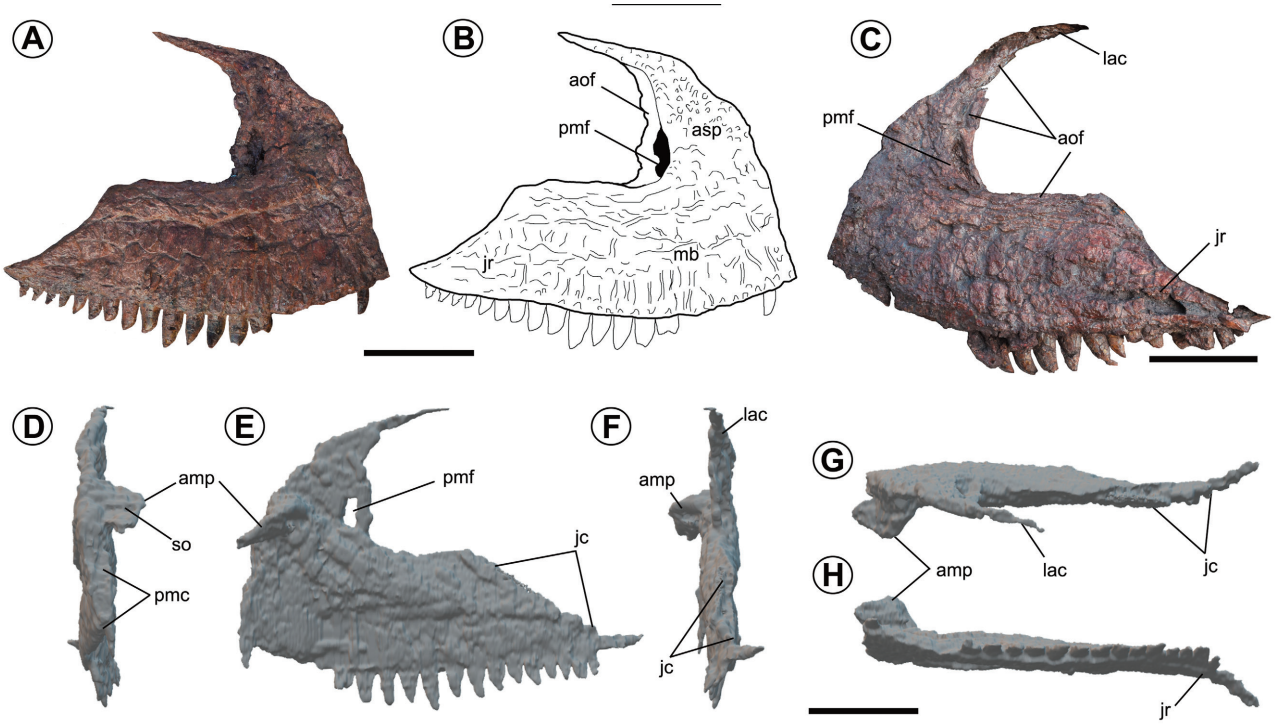


Figure 5. A–H. Maxillae of ***Skorpiovenator bustingorryi*** **(MMCh-PV 48)**. **A,** right maxilla in lateral view, and **B,** interpretative drawing. **C,** left maxilla in lateral view. Rendered right maxilla in **D,** anterior; **E,** medial; **F,** posterior; **G,** dorsal; and **H,** ventral views; images derived from CT scan data. Abbreviations: **asp,** ascending process; **amp,** anteromedial process; **aof,** antorbital fossa; **lac,** lacrimal contact; **jc,** jugal contact; **jr,** jugal ramus; **mb,** maxillary body; **pmc,** premaxillary contact; **pmf,** promaxillary fenestra; **so,** socket for articulation with premaxilla. Scale bars equal 10 cm.

vertically from the main body of the maxilla, as is typical for abelisauroids (Bonaparte & Novas, 1985; Rauhut & Carrano, 2016). At the level of the upper margin of the antorbital fenestra, the distal tip of the ascending process of the maxilla curves posteriorly, articulating under the lateral border of the nasal. The ascending process is homogeneously wide anteroposteriorly along most of its length, a feature that was proposed as an autapomorphy of the species (Canale *et al.*, 2009). On the anterior half of the lateral surface of both ascending processes, there are shallow ovoid depressions, which are anteriorly bounded by a long crest running along the nasal articulation. These depressions are probably the result of the internal collapse of the promaxillary recess during the diagenetic deformation.

As is typical in abelisaurids, the maxillary contact with the jugal is long and oblique, forming an angle of approximately 45° with the ventral margin of the bone (Fig. 5A–5C). The main contour of the contact is sigmoidal, with the posteroventral two-thirds dorsally concave and the anterodorsal third convex; into which the ventral margin of the anterior tip of the jugal fits.

Each maxilla possesses 19 alveolar positions. The right maxilla preserves 15 teeth within their alveoli, whereas the 2nd to 5th alveoli are unoccupied. In the left maxilla, only seven erupted teeth are preserved. Several isolated teeth were recovered in close proximity to the skull during the preparation of the specimen; these were probably lost during biostratinomy.

The antorbital fossa occupies the posterolateral sector of the ascending process of the maxilla, from which it is separated by a step in the form of a low crest. The anterior sector of the antorbital fossa is separated from the anterior margin of the ascending process even in its dorsal part, as in *Carnotaurus*, and unlike the condition seen in *Ekrixinatosaurus*, where the antorbital fossa covers all the dorsolateral surface of the ascending process. Notably, the antorbital fossa is poorly expanded but present in the ventral margin of the antorbital fenestra, over the dorsal surface of the maxillary body. It is separated from the lateral surface of the bone by a faint lateral crest that vanishes

posteriorly at the contact with the jugal. This ventral portion of the antorbital fossa is also present in *Spectrovenator*, *Tralkasaurus*, *Ekrixinatosaurus* and the Bajo Barreal maxilla (UNPSJB-PV 247; Lamanna *et al.*, 2002). However, this character should be taken with caution, given that it shows high variability, even in similarly sized specimens, as it was reported in *Majungasaurus* (Ratsimbaholison *et al.*, 2016).

The promaxillary fenestra is ovoidal, with its major axis slightly anterodorsally oriented (Fig. 5C) (the right promaxillary fenestra seems completely vertical due to preservational artifacts). The anterodorsal-posteroventral orientation of the promaxillary foramen is also present in most abelisaurids, such as *Carnotaurus*, *Majungasaurus* and *Tralkasaurus*. As shown by CT scans, the promaxillary fenestra in *Skorpiovenator* leads internally to the small promaxillary recess, which is globose, closed by the medial wall, and thus does not communicate with any other cavities as in other abelisauroids (*e.g.*, *Carnotaurus*, *Noasaurus*).

The CT scans show that the anteromedial process is stout and anteroposteriorly long, and is placed on the anteroventral corner of the maxillary medial wall with its main axis running anteroventrally to posterodorsally (Fig. 5D–5H). This resembles the condition in *Majungasaurus*, but differs from other abelisauroids in which the anteromedial process is horizontally displaced, as observed in *Ekrixinatosaurus*, *Noasaurus*, and Bajo Barreal maxilla (UNPSJB-PV 247). The margins of the anteromedial process get thicker posterodorsally along its contact with the ascending process; whereas the anterior surface of the process is featured by a shallow socket where it receives the maxillary process of the premaxilla.

Nasal. Although the nasals of *Skorpiovenator* were briefly described in a previous contribution focused on the nasal anatomy of abelisaurids (see Cerroni *et al.*, 2020b), we provide an expanded description in the present study. Each nasal articulates with the premaxilla anteroventrally, the maxilla ventrally, the lacrimal posteroventrally, and the frontal posteriorly (Fig. 6A). The internasal suture, despite being strongly eroded, is well defined, indicating the unfused nature of these bones.

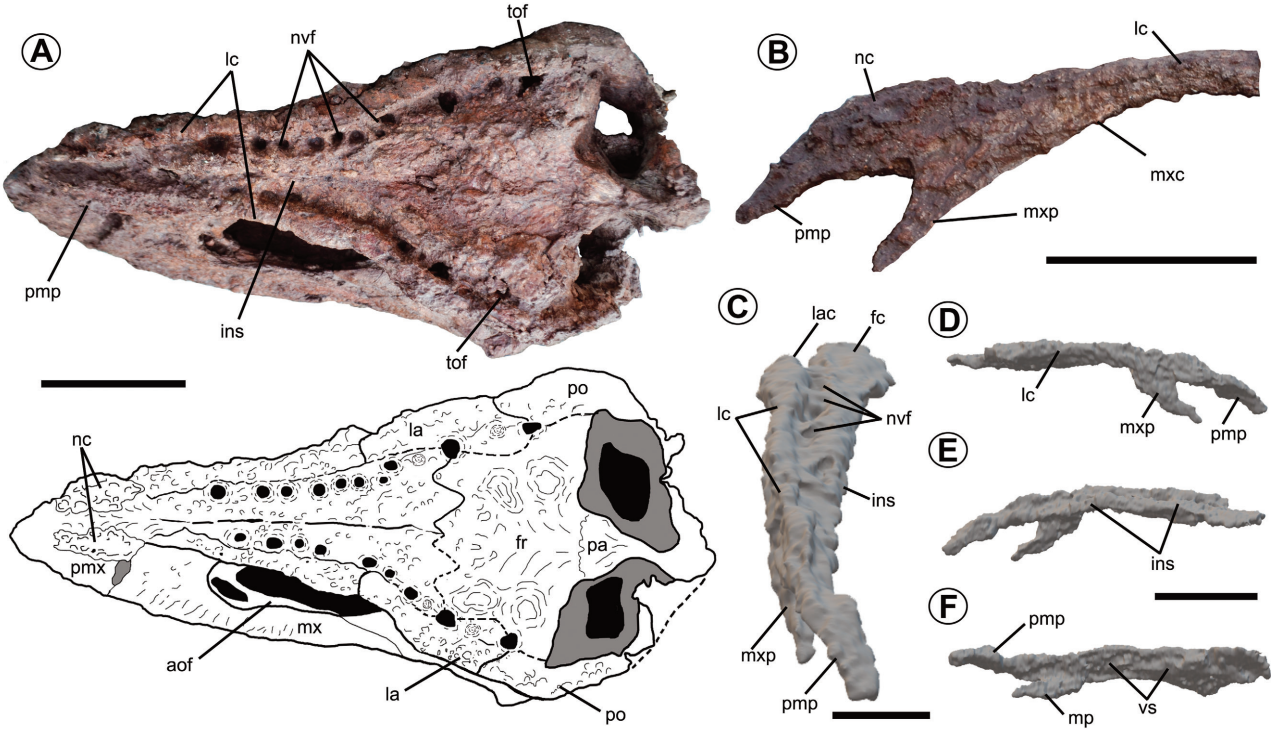


Figure 6. A–F. Nasals of ***Skorpiovenator bustingorryi*** **(MMCh-PV 48)**. **A,** skull in dorsal view (above) and interpretive drawing (below) showing nasal bones. **B,** detail of left nasal in lateral view. Rendered right nasal in **C,** anterior; **D,** lateral; **E,** medial; and **F,** ventral views; images derived from CT scan data. Abbreviations: **aof,** antorbital fossa; **fc,** frontal contact; **fr,** frontal; **ins,** internasal suture; **la,** lacrimal; **lac,** lacrimal contact; **lc,** lateral crest; **nc,** nasal crest; **nvf,** neurovascular foramina; **mx,** maxilla; **mxc,** maxillary contact; **mxp,** maxillary process; **pa,** parietal; **pmp,** premaxillary process; **pmx,** premaxilla; **po,** postorbital; **tof,** triosseal foramen; **vs,** ventral surface. Scale bars equal 10 cm (A) and 5 cm (B–F).

Each nasal forks anteriorly into two processes (= premaxillary and maxillary processes) that bound the posterodorsal corner of the narial opening (Fig. 6B–6F). In lateral view, both processes are slender and share a similar thickness, whereas the premaxillary process is slightly longer than the maxillary one. Both processes converge at a low angle, giving a U-shaped contour to the narial opening (Fig. 6B), similar to the condition in *Rugops* and *Spectrovenator*. Conversely, in other brachyrostran abelisaurids (*e.g.*, *Carnotaurus*, *Koleken*) the angle is nearly right, and the processes are short and wide. The contact with the premaxilla appears to be through a small socket, whereas it is unclear if there is a notch receiving the maxillary process, as in *Carnotaurus* (Cerroni *et al.*, 2020a: Fig. 5). The dorsal aspect of the processes is severely eroded. Dorsal to the narial openings, both nasals show anteroposteriorly elongated and mediolaterally thick ovoid protuberances covered by a papillate texture (Fig. 6B). They are separated medially by a deep depression whose surface is less ornamented than the rest of the bone. This feature is also present, but less developed, in the African abelisaurid *Rugops*.

The middle portion of the nasal body projects laterally in the form of a thick and rounded crest that overhangs the antorbital fenestra (Fig. 6A). Nevertheless, the nasals do not participate in the dorsal limits of this opening, which is bounded only by the maxilla and the lacrimal.

The most conspicuous feature of the nasals is their dorsal surface. Each nasal is relatively flat, bounded laterally by a tall and thick crest that runs anteroposteriorly, beginning at the level of the maxillary ascending process and connecting with the lacrimal crest. Each nasal has a lateral row of large foramina, presumably vascular (Cerroni *et al.*, 2020b), placed close to the lateral crest; these foramina are separated by thick bony septa (Fig. 6A). The diameter of the foramina ranges from 8 to 12 mm. The row of foramina is continuous posteriorly with two additional foramina and a small fenestra located on the skull roof.

The contact between the nasals and the bilateral crests gives the skull a transversely concave profile, a condition that, together with the presence of large foramina, is shared with only a few abelisaurids including *Rugops*, *Spectrovenator* and an undescribed abelisaurid from the Bajo Barreal Formation (Lamanna *et al.*, 2011). The nasal ornamentation is not profuse and is characterized by hummocky rugosities, with some foramina exhibiting associated vascular grooves. Furthermore, the mediolateral width of each nasal gradually increases posteriorly, notably expanding at its articulation with the lacrimal and frontal. However, the nasal-frontal suture is difficult to trace due to the state of preservation.

The thin lamina connecting the ascending process of the maxilla and the anterior process of the lacrimal articulates with the ventral surface of the nasal. However, given that both maxillae are complete and fully articulated, it is not possible to assert whether there is an articular groove. A small portion of the ventral surface of both nasals is visible in their central sector through the antorbital fenestra and lacks any foramina, unlike those reported in *Rugops* (Porter, 2015).

Each nasal of *Skorpiovenator* has a long internal canal connected with the dorsal foramina; such internal channels appear to be vascular rather than pneumatic in origin, as previously hypothesized by Cerroni *et al.* (2020b).

Lacrimal. As in some abelisaurids (*e.g.*, *Spectrovenator*, *Rugops*), the dermal lateral surface of the lacrimal is T-shaped (Fig. 7A–7H). It articulates with the nasal anteriorly, the maxilla anteroventrally, the frontal medially, the postorbital posteriorly, and the jugal ventrally. As noted in the description of the maxilla, the articulation between the lacrimal and the maxilla is usually difficult to observe in other abelisaurids because both the ascending process of the maxilla and the anterior process of the lacrimal are fragile elements reduced to thin laminae (Carrano & Sampson, 2008), and are usually incompletely preserved (*e.g.*, *Carnotaurus*, *Majungasaurus*, *Spectrovenator*). In *Skorpiovenator*, on both sides, the distal end of the ascending process of the maxilla contacts the anteroventral tip of the nasal process of the lacrimal.

In contrast to the condition in other abelisaurids, the lacrimal of *Skorpiovenator* lacks the antorbital fossa, which is restricted to the maxilla. In *Carnotaurus*, this fossa is small and restricted to the anterodorsal corner of the bone, while in *Majungasaurus*, *Llukalkan,* and *Rugops*, the fossa is more developed and clearly visible in lateral view. This fossa is widely exposed laterally in the ventral sector of the jugal process in *Eoabelisaurus*.

The lacrimal shows an expanded dorsal brow at the dorsal border of the orbital rim, as is present in *Abelisaurus*,

Spectrovenator, and *Rugops*. This brow is present in the postorbital process and is more evident on the left side (Fig. 7B), as the right lacrimal-postorbital complex strongly medially flattened by taphonomic deformation (Fig. 7A). As in other facial bones of *Skorpiovenator*, the lateral surface of the lacrimal is completely covered with dermal ornamentations, in the form of rounded protuberances surrounded by anastomosed grooves; some of these grooves are obliquely oriented relative to the lacrimal main axis (Fig. 7A–7C). The protuberances are larger on the dorsal half of the lateral surface of the lacrimal, gradually decreasing in size towards the ventral end of the bone. The ventral half of the jugal ramus, below the suborbital process, is laterally ornamented by low vertical crests and furrows (Fig. 7B). The postorbital process is short and robust due to the development of the dermal outgrowths, as in *Carnotaurus* and *Majungasaurus*. This differs from the condition in *Llukalkan*, where the process is longer and more slender (Gianechini *et al.*, 2021). However, these differences may be related to ontogenetic factors associated with outgrowth development and an increase in the size of the lacrimal body (see Ratsimbaholison *et al.*, 2016).

Unlike deeply nested abelisaurids such as *Carnotaurus* and *Abelisaurus*, *Skorpiovenator* bears a conspicuous, laterally exposed, anterior process which contacts the nasal anteriorly and medially, while its anteroventral end

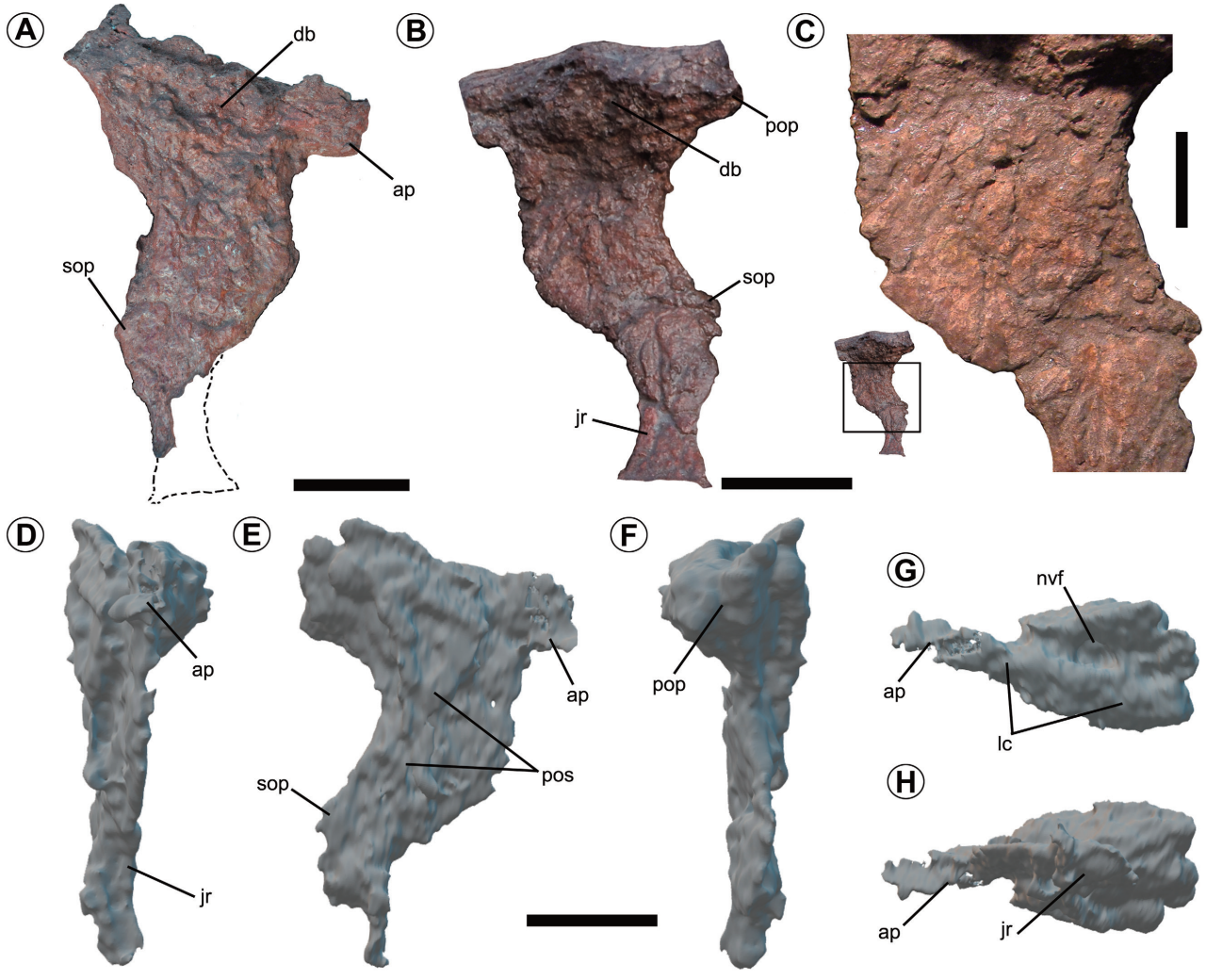


Figure 7. A–H. Lacrimals of ***Skorpiovenator bustingorryi*** **(MMCh-PV 48)**. **A,** right lacrimal in lateral view; dashed line represents hidden jugal ramus by the jugal, **B,** left lacrimal in lateral view, and **C,** close up of the external ornamentation. Rendered left lacrimal in **D,** anterior; **E,** medial; **F,** posterior; **G,** dorsal; and **H,** ventral views; images derived from CT scan data. Abbreviations: **ap,** anterior process; **db,** dorsal brow; **jr,** jugal ramus; **lc,** lateral crest; **nvf,** neurovascular foramen; **pop,** postorbital process; **pos,** preorbital strut; **sop,** suborbital process. Scale bars equal 5 cm (A–B, D–H) and 2 cm (C).

articulates with the posterodorsal end of the ascending process of the maxilla (Fig. 7A–7B). A similar process is present in *Eoabelisaurus*, *Spectrovenator* and *Llukalkan*. The lacrimals are articulated with the jugals on both sides, though their articular surfaces cannot be observed. The distal end of the jugal ramus is only observable on the left side, which shows a distally expanded and anteroventrally directed end as in *Majungasaurus* and *Carnotaurus*.

The jugal ramus is sigmoid in lateral view, being anteroposteriorly expanded dorsally and becoming progressively narrower towards its contact with the jugal (Fig. 7B), as in *Spectrovenator*, *Carnotaurus* and some specimens of *Majungasaurus*. This is observable in the left lacrimal, because in the right one the distal half of the jugal ramus is hidden by the jugal. Conversely, *Eoabelisaurus* shows only the anterior rim with a sigmoid condition, whereas *Abelisaurus* has a straight anterior rim and a sigmoid posterior border. In *Llukalkan*, the jugal ramus is rod-like and anteroposteriorly thinner along its entire length, a morphology that may be related to a possible juvenile stage of the specimen, as observed in *Majungasaurus* (Ratsimbaholison *et al.*, 2016).

In dorsal view, the lateral borders of the lacrimals correspond to the posterior continuation of the laterodorsal crests formed by the nasals (Fig. 7G–7H). These crests are medially delimited by a row of foramina, part of the neurovascular system described for some abelisaurids (Cerroni *et al.*, 2020b). CT scans revealed that one of these foramina, referred to as the "middle foramen" in Cerroni *et al.* (2020b), is located entirely within the lacrimal bone. Because the medial sutures between the lacrimal and adjacent skull roof bones are difficult to trace, they were interpreted through the CT data.

The medial surface of the lacrimal exposes the ventral portion of the preorbital strut, forming a vertically oriented crest with a rounded medial margin. This strut separates the orbital and antorbital cavities, and the adjacent bone surface is smooth. Furthermore, CT scans revealed a lacrimal recess within the lacrimal body. This recess communicates externally via a foramen on the anterior portion; however, this area is poorly preserved.

Postorbital. The postorbital (Fig. 8A–8B) contacts the lacrimal anteriorly, the squamosal posteriorly, the jugal ventrally, and the frontal/laterosphenoid medially. The contact with the lacrimal forms a thick brow that constitutes the dorsal margin of the orbit, excluding the frontal from it as in other abelisaurids and carcharodontosaurids (Bonaparte, 1991; Coria & Salgado, 1995; Sereno *et al.*, 1996; Novas *et al.*, 2013). Additionally, the postorbital forms the anterolateral border of the supratemporal fenestra and the anterodorsal border of the infratemporal fenestra. The postorbital is slightly longer anteroposteriorly than its total height, as in other abelisaurids (Carrano & Sampson, 2008; Filippi *et al.*, 2018). Tall postorbitals in abelisaurids appear to be indicative of a more advanced ontogenetic stage, as evidenced by Ratsimbaholison *et al.* (2016) for *Majungasaurus*. The lateral surface of the postorbital is strongly ornamented, as is the rest of the facial bones, with the exception of a small smooth surface over the squamosal articulation, which is better observed in the right one (Fig. 8B). The ornamentation is composed of small protuberances delimited by anastomosed grooves. However, on the dorsal surface of the postorbital, these protuberances are larger and more prominent than on the surface of the jugal process. The jugal ramus is anteroventrally oriented, with its anterior edge strongly concave, forming the posteroventral limit of the orbit, as in other abelisaurids, carcharodontosaurids, and the tyrannosaurid *Tyrannosaurus*. The posterior border of the jugal ramus is straight, as is usual in abelisaurids. The distal end of the jugal ramus is remarkably expanded as in *Carnotaurus* and *Ekrixinatosaurus*, and differs from the less expanded end present in *Spectrovenator*. This distal expansion forms a conspicuous suborbital flange in *Skorpiovenator*. The distal portion of the jugal ramus is laterally "stepped", marked by an anterodorsally-posteroventrally oriented robust ridge. In *Carnotaurus*, *Majungasaurus*, *Arcovenator*, *Llukalkan*, and *Ilokelesia* this ridge is low and sharp, while in *Abelisaurus* it is absent. This ridge delimits dorsally an anterolaterally facing fossa, which shows faint ornamentation. The distal margin of the suborbital flange is sigmoid, with a distinct concavity over the ventral third, as in *Carnotaurus* and *Majungasaurus*.

The dorsal margin of the postorbital is strongly inflated and bulked, as in *Ekrixinatosaurus* and *Arcovenator*. Below this bulge, at the junction of the postorbital rami, there is an anteroposteriorly large depression, as in *Eoabelisaurus*, *Arcovenator* and *Ilokelesia*. The squamosal ramus has the shape of an isosceles triangle, with its posterior end sharply tapered toward its contact with the squamosal.

The squamosal ramus of the postorbital rests in a fan-shaped shelf on the squamosal, a morphology also present in *Carnotaurus*, *Majungasaurus*, and *Llukalkan*. The ventral margin of the squamosal ramus is concave at its articulation with the squamosal. Proportionally, this ramus is slightly shorter than the lacrimal ramus.

Jugal. The jugal is a wide bone in lateral view, bearing four processes (Fig. 8C–8D): the anterior process forms the posteroventral corner of the antorbital fenestra, the anterodorsal process contacts the lacrimal, the posterodorsal process contacts the postorbital, and the bifurcated posterior process articulates with the quadratojugal. Additionally,

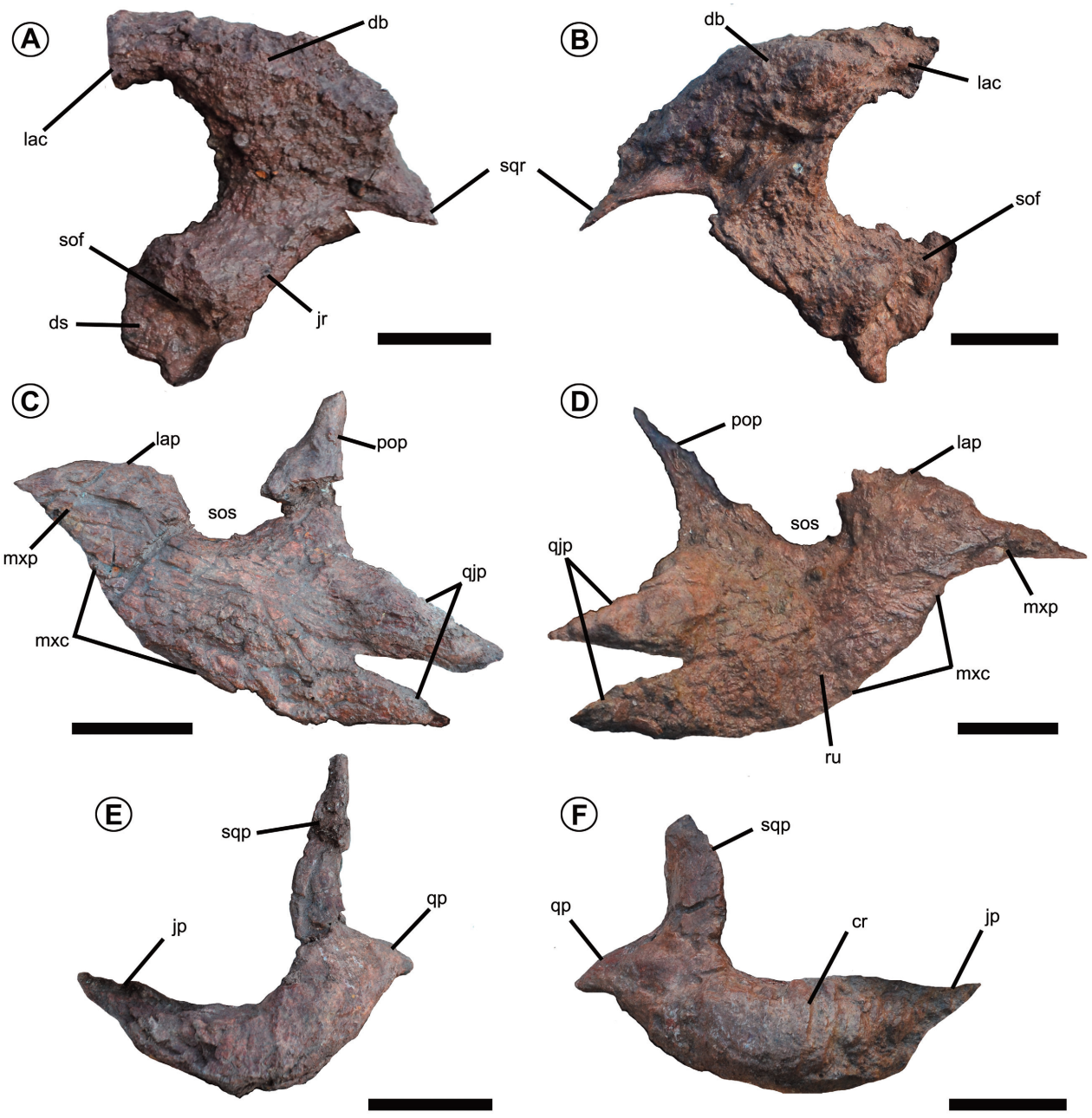


Figure 8. A–F. **A,** Left and **B,** right postorbital of ***Skorpiovenator bustingorryi*** **(MMCh-PV 48)** in lateral view. **C,** Left and **D,** right jugal in lateral view. **E,** Left and **F,** right quadratojugal in lateral view. Abbreviations: **cr,** crests; **db,** dorsal brow; **ds,** distal step; **jp,** jugal process of quadratojugal; **jr,** jugal ramus of postorbital; **lac,** lacrimal contact; **lap,** lacrimal process of jugal; **mxc,** maxillary contact; **mxp,** maxillary process of jugal; **pop,** postorbital process of jugal; **qjp,** quadratojugal processes of jugal; **qp,** quadrate process of quadratojugal; **ru,** rugosities; **sof,** suborbital flange; **sos,** suborbital space; **sqp,** squamosal process of quadratojugal; **sqr,** squamosal ramus of postorbital. Scale bars equal 5 cm.

the jugal articulates medially with the ectopterygoid, although CT scans revealed that this junction is displaced. Overall, the jugal is planar, except for the quadratojugal rami, which are laterally curved. However, the left quadratojugal rami exhibit less lateral convexity due to taphonomic deformation. These rami form the anterior half of the lateral "cheek" under the infratemporal fenestra.

The main body of the jugal is proportionally wider than that in *Majungasaurus* and *Llukalkan*, being more similar to the condition in *Carnotaurus* and some indeterminate abelisaurids from India (Novas *et al.*, 2004). The lateral surface of the bone is completely ornamented with rugosities and anastomosed grooves. There are some rounded and prominent tubercles scattered over the surface.

As in other abelisaurids, the jugal forms the posterior half of the ventral margin of the antorbital fenestra. In more early-diverging ceratosaurs, such as *Ceratosaurus*, the jugal is excluded from this fenestra. As it occurs in abelisaurids, the jugal margin of the antorbital fenestra lacks any external antorbital fossa in *Skorpiovenator*.

The jugal body bears a small anterior triangular process that forms the posteroventral margin of the antorbital fenestra. This process is similar to that present in *Majungasaurus*, but longer than that observed in *Carnotaurus*. The length of the maxillary contact represents approximately 54% of the anteroposterior length of the maxilla. A similar condition is observed in *Carnotaurus*, whereas in other abelisaurids, this proportion is less than 50%.

The lacrimal process is short, with a slightly irregular contact surface. The postorbital process of the jugal is subtriangular in lateral view, with its main axis posterodorsally inclined, and concave posterior and anterior margins. This process narrows dorsally and articulates with the postorbital through a reduced contact surface, as shown by the CT scans. The portion between the postorbital and lacrimal processes, which also forms the ventral margin of the suborbital space, has a surface that is gently curved medially. Additionally, although the right palatine is partially preserved, the contact between the jugal and the palatine is offset. The posterior third of the ventral margin, ventral to the quadratojugal rami and the base of the postorbital process, is straight and anteroposteriorly oriented. Ventral to the orbital fenestra, this margin is projected dorsoanteriorly, forming the articulation with the maxilla.

The quadratojugal processes are robust and show a subtriangular contour in lateral view. The dorsal ramus is slightly longer than the ventral one, while *Carnotaurus* and *Majungasaurus* have the opposite condition.

Quadratojugal. The quadratojugal articulates anteriorly with the jugal, posteromedially with the quadrate and dorsally with the squamosal. Its general morphology is “L-shaped” in lateral view, with an anteriorly directed jugal process, a dorsally directed squamosal process and a small posteroventrally projected quadrate process (Fig. 8E–8F). The jugal process is robust, transversally thick, exhibiting a subcircular cross section. Furthermore, it shows a strong lateral curvature, forming a pronounced “cheek” with the posterior end of the jugal, below the infratemporal fenestra. The lateral surface of this process is strongly ornamented, as is the jugal surface next to it, covered with vertically oriented crests and furrows. Although similar ornamentation on the lateral surface of the jugal process is present in other abelisaurids, the strongly developed rugosity combined with the thick, rounded, and laterally procumbent process in *Skorpiovenator* is considered here an autapomorphy. The contact surfaces for the quadratojugal rami of the jugal consist of shallow dorsal and ventral grooves, as evidenced by CT data; both grooves are bounded medially by a thin ridge.

The squamosal process is slender, with its anteroposterior length being about two-thirds of the dorsoventral height of the jugal process. In other abelisaurids such as *Majungasaurus* and *Carnotaurus*, both processes show similar dimensions in lateral view. The anterior margin of the squamosal process is convex—similar to the condition in *Majungasaurus*, but unlike the nearly straight margin in *Carnotaurus*—and tapers dorsally into a sharp apex. The dorsal tip of the squamosal process articulates posteriorly with the quadratojugal process of the squamosal, forming an oblique contact in lateral view. This morphology is hidden by the disarticulation and distortion of the squamosal on the right side, but is much better preserved on the left side of the skull. The posterior margin of the squamosal process curves medially, forming a vertical contact with the quadrate in posterior view.

The quadrate process is small, subtriangular, and tapers posteriorly, as it occurs in *Carnotaurus*, in contrast to the

subrectangular quadrate process present in *Majungasaurus*, whereas in *Eoabelisaurus* this process is rounded but relatively shorter anteroposteriorly.

Quadrate. The quadrate articulates with the squamosal dorsally, the articular ventrally, the pterygoid anteromedially through the pterygoid flange, and the quadratojugal laterally. In *Skorpiovenator*, both quadrates are preserved in articulation but are severely distorted by plastic deformation (Fig. 9A–9K). Both are broken at mid-height, resulting in misalignment of their shafts. The suture with the quadratojugal on both sides remains unfused.

The quadrate is dorsally narrow and expands ventrally towards the articular end (Fig. 9F–9G). It is a dorsoventrally tall bone, and regardless of the taphonomic deformation, it is posteriorly concave in lateral view (Fig. 9H–9I). CT scans reveal that, in dorsal view, the quadrate head is ovoidal, narrowing posteriorly into a faint crest, with its main axis aligned with the longitudinal axis of the skull (Fig. 9K).

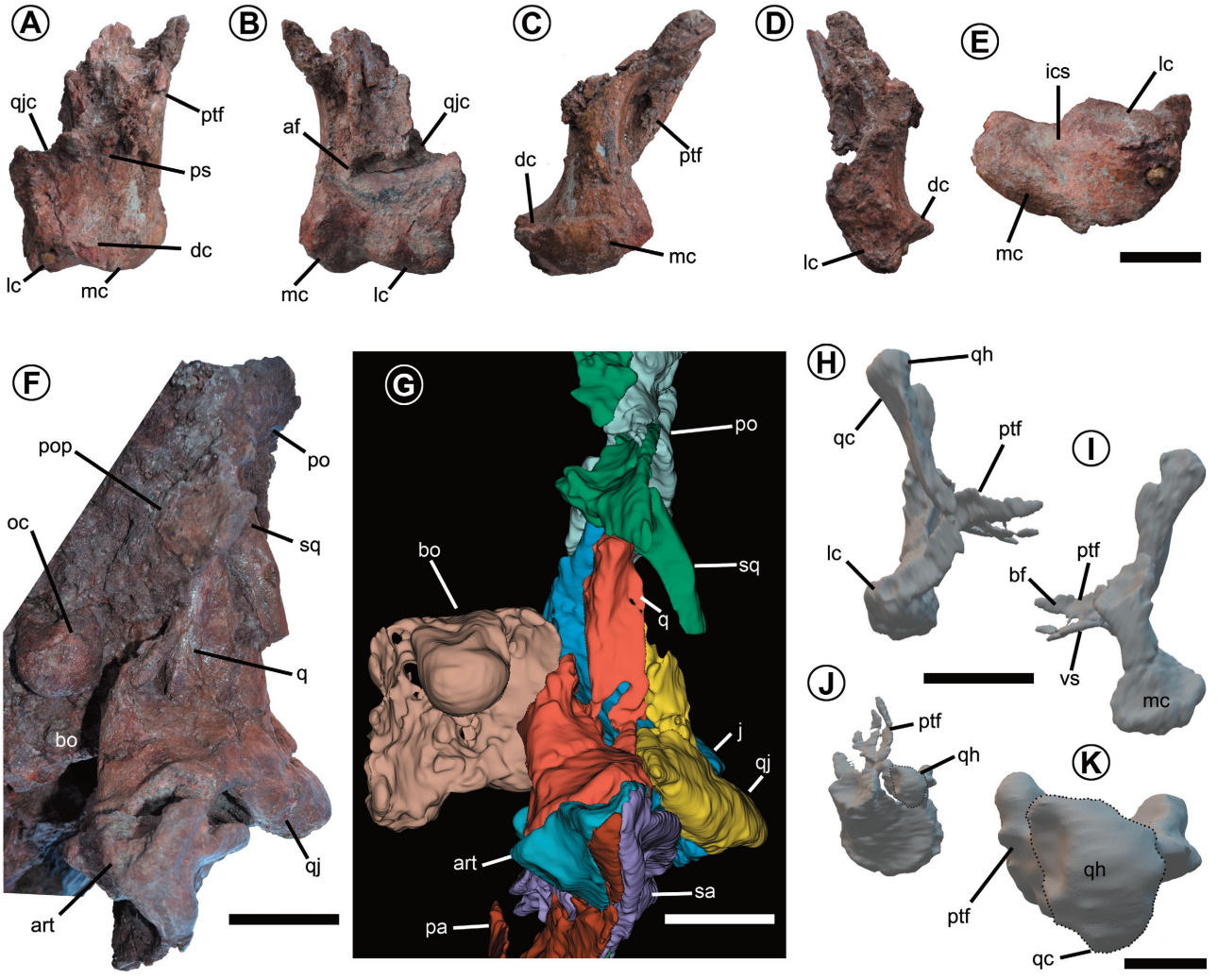


Figure 9. A–K. Quadrate bones of ***Skorpiovenator bustingorryi*** **(MMCh-PV 48)**. Left quadrate in **A,** posterior; **B,** anterior; **C,** medial; **D,** lateral, and **E,** distal views. **F,** right quadrate in posterior view; **G,** rendereded right quadrate (light red) with surrounding bones in posterior view (image derived from CT scans): basioccipital (cream-coloured), articular (blue), prearticular (red), surangular (violet), quadrate (light red), quadratojugal (yellow), jugal (bright blue), squamosal (green), and postorbital (light blue). Isolated and rendered right quadrate in **H,** lateral; **I,** medial; and **J,** dorsal views. **K,** detail of the quadrate head in dorsal view. Abbreviations: **af,** anterior fossa; **art,** articular; **bf,** blind fossa; **bo,** basioccipital; **dc,** dorsal crest; **lc,** lateral condyle; **ics,** intercondylar sulcus; **j,** jugal; **mc,** medial condyle; **oc,** occipital condyle; **pa,** prearticular; **po,** postorbital; **pop,** paroccipital process; **ps,** posterior surface; **ptf,** pterygoid flange;**q,** quadrate; **qc,** quadrate crest; **qh,** quadrate head; **qj,** quadratojugal; **qjc,** quadratojugal contact; **sa,** surangular, **sq,** squamosal; **vs,** ventral shelf. Scale bars equal 5 cm (A–D, F–J), 2 cm (E) and 1 cm (K).

The right quadrate is disarticulated from the squamosal, but keeps its contact with the quadratojugal (Fig. 2A) through a slightly sigmoid suture visible in posterior view. The pterygoid flange is better preserved in the left quadrate (Fig. 2E): it is a wide, laminar process anteromedially projected. Although not completely visible in posterior view, the CT scans revealed that the medial surface of the pterygoid flange is characterized by a large and shallow fossa, which in turn is ventrally bounded by a thick bony shelf that extends posteroventrally to anterodorsally. The same pattern of blind fossa and ventral shelf is present in *Noasaurus*, *Carnotaurus*, *Abelisaurus*, and *Majungasaurus*. In posterior view, the quadrate shows a dorsoventrally elongated small fossa at mid-shaft, with a similar shape and position to that present in *Majungasaurus*. The articular surface for the quadratojugal is rugose and has an ovoidal contour with its main axis anterodorsally oriented (Fig. 9D). This surface lacks the small process present in *Ilokelesia*.

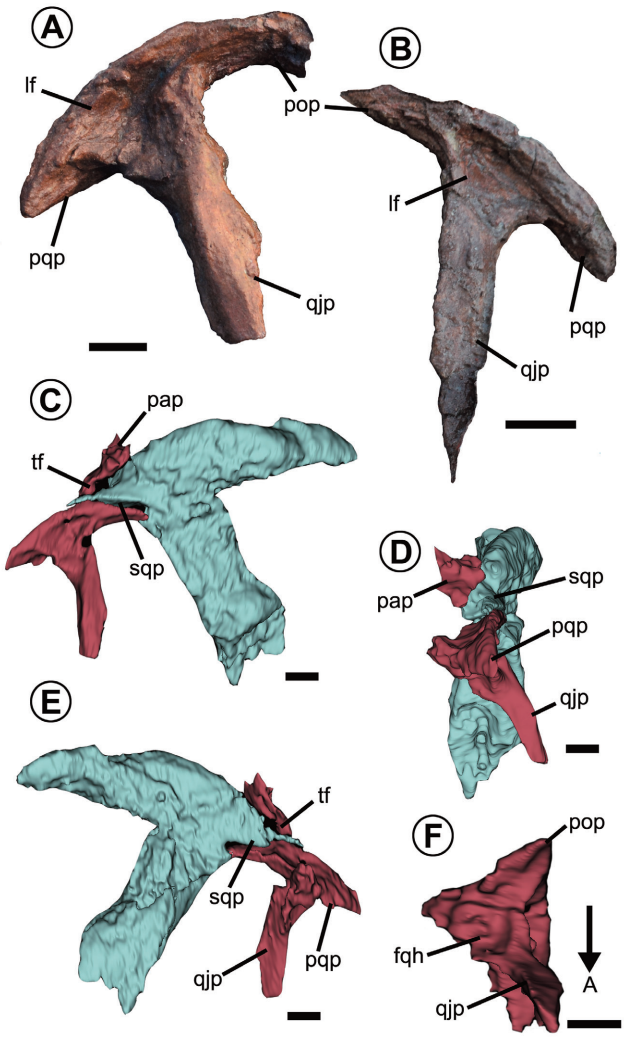


Figure 10. A–F. Squamosals of ***Skorpiovenator bustingorryi*** (**MMCh-PV 48**). **A,** right and **B,** left squamosal in lateral view. Rendered 3D images showing the articular contact between the right squamosal and right postorbital in **C,** lateral; **D,** posterior; and **E,** medial views. **F,** detail of the rendered right squamosal in ventral view showing the articulation area for the quadrate. Abbreviations: **A,** anterior direction; **fqh,** squamosal facet for quadrate head; **lf,** lateral fossa; **pap,** parietal process of squamosal; **pop,** postorbital process of squamosal; **pqp,** postquadratic process; **qjp,** quadratojugal process; **sqp,** squamosal process of postorbital; **tf,** triangular facet of squamosal. Scale bars equal 2 cm.

In ventral view, the articulation with the lower jaw is composed of two anteromedially-posterolaterally oriented condyles separated by a shallow intercondylar sulcus (Fig. 9E), similar to that present in *Abelisaurus* and *Ilokelesia*, but unlike the deeper sulcus in *Carnotaurus*. The medial condyle is twice as large as the lateral one, resembling the condition in *Ilokelesia*. The articular surface of the medial condyle is anteroposteriorly extensive, exhibiting a semi-circular contour in medial view. The articular surface of the lateral condyle is much more restricted and almost planar in lateral view. In posterior view, both condyles are bounded dorsally by a rugose and dorsally concave crest which ends on the articular surface for the quadratojugal. Immediately dorsal to the articular surface of the lateral condyle, on the anterior surface of the shaft, lies a shallow oblique fossa.

Squamosal. The squamosals were recovered in their respective anatomical positions, but with some displacement relative to the surrounding bones on the right side (Fig. 10A–10F). This displacement results in an unnaturally posteroventrally vaulted position, as well as a ventral disarticulation from the quadratojugal and quadrate. The squamosal is a triradiate bone that articulates with the postorbital anteriorly, the quadratojugal ventrally, the parietal dorsomedially, and the paroccipital process of the exoccipital posteromedially. The postorbital process contacts the squamosal process of the postorbital through a triangular articular surface, as in *Majungasaurus*, *Llukalkan*, and *Carnotaurus*. In dorsal view, the contact with the parietal is difficult to establish due to the poorly preserved surface.

The postquadratic process is relatively short and posteroventrally projected, distally tapering into a pointy tip, as in other abelisaurids (Fig. 10A–10B). The posterior surface of this process is flat where it articulates with the paroccipital process. The quadratojugal process is

nearly vertical and, despite its displacement from the quadratojugal due to deformation, it is clear that these elements were originally in contact. This process shows a central widening that is more noticeable in posterior view, a condition similar to that in *Majungasaurus*, whereas such widening appears to be absent in *Koleken*. In lateral view, the quadratojugal process is kinked as in other abelisaurids such as *Koleken*, *Majungasaurus* and *Llukalkan* (Pol *et al.*, 2024). The quadratojugal process is slightly longer than the postquadratic process (Fig. 10B) as in *Carnotaurus*, *Majungasaurus* and *Abelisaurus*; while in *Spectrovenator*, *Koleken* and *Llukalkan* the quadratojugal process is twice as long as the postquadratic process.

The lateral surface of the squamosal, in the confluence of the three processes, is occupied by a shallow and well-defined fossa (Fig. 10A–10B), also present in all South American abelisaurids (*e.g.*, *Abelisaurus*, *Llukalkan*, *Koleken*, *Carnotaurus*, *Viavenator*) but seemingly absent or extremely poorly developed in *Majungasaurus* and *Arcovenator*. The squamosal lateral fossa of *Skorpiovenator* seems to be deeper than in the remaining South American taxa.

Palate

Palatal bones in *Skorpiovenator* are preserved mostly on the right side, which still preserves in contact the pterygoid, ectopterygoid, palatine and vomer (Fig. 11A–11P). The left side is poorly represented, consisting only of fragments of pterygoid and vomer, and a partial palatine; furthermore, the left ectopterygoid is missing. Additionally, it cannot be determined whether epipterygoid bones are preserved. The mediolateral compression of the skull caused the right side of the palate to be elevated relative to its left counterpart, displacing it from its articulations with the upper jaw bones.

Palatine. Each palatine is mostly represented by the vomeropterygoid process and part of the palatine body (Fig. 11A–11J). Remains of the pterygoid ramus are preserved only in the left palatine, whereas maxillary and jugal articular contacts are missing. The vomeropterygoid process is almost three times as long as it is wide, with slightly curved anterior and posterior margins (Fig. 11I–1.J). The lateral surface bears a smooth and shallow fossa, giving it a laterally concave aspect. This fossa is bounded by anterior and posterior ridges, the latter of which is thicker. The morphology of the vomeropterygoid resembles the condition in *Majungasaurus* and *Carnotaurus*; however, in the latter taxon the palatine is severely distorted. Additionally, it is unknown if the vomeropterygoid process of *Skorpiovenator* is distally expanded as in *Majungasaurus* and *Spectrovenator*. The left palatine preserves part of the palatine body and the pterygoid process, which seems to radiate medially from the palatine body.

Pterygoid and vomer. Although both pterygoids are preserved, the right element is better preserved, remaining articulated with most adjacent bones, whereas the left pterygoid is represented only by its anterior portion (Fig. 11A–11G). Alongside the maxilla, the pterygoid is one of the longest cranial elements (see SOI 1, Table S1). It is a triradiate bone consisting of a main body that projects into several processes that articulate with the quadrate posterolaterally, the basisphenoid posteriorly, the ectopterygoid medially, the palatine laterally (although this contact is displaced), the vomer anteriorly, and the contralateral pterygoid medially (Fig. 11E–11F).

The ectopterygoid process contacts the ectopterygoid laterally, and is equal in length to the medial process of the latter. Although distorted, the ectopterygoid process is projected posteroventrally and is slightly curved in lateral view (Fig. 11K), in contrast to the more strongly curved processes of *Carnotaurus*, *Llukalkan*, and *Majungasaurus*. However, this condition may be accentuated by deformation, as the angle of inclination in *Skorpiovenator* is approximately 60°, which is greater than the 45° observed in *Carnotaurus* and *Majungasaurus*. The ectopterygoid contact appears to be through a shallow groove, since CT scans are not clear enough. The posterior portion of the pterygoid is formed by two processes projecting from the pterygoid body: a lateral quadrate process, which articulates with the quadrate (= quadrate process), and a smaller projection that participates in the basipterygoid articulation (also called pterygoid medial process; see Eddy & Clarke, 2011) (Fig. 11K–11N). Both quadrate and pterygoid medial processes form a U-shaped slot that receives the basipterygoid process of the braincase, a condition observable in dorsal view. The pterygoid quadrate process is poorly preserved, but it seems to extend posterolaterally as a transversally thin and laterally convex lamina; however, given the state of preservation, the precise suture with the

quadrate is not discernible. Additionally, there is no evidence of preserved epipterygoid bone over the quadrate process.

The anterior portion of the pterygoid is formed by the vomeropalatine process that articulates with the palatine laterally and the vomer anteriorly. This process consists of an elongate lamina, subtriangular in outline and transversally thick. Due to skull deformation, the vomeropalatine process probably has been laterally rotated, exhibiting the appearance of a tall bone; a similar condition to that in *Carnotaurus* (Cerroni *et al.*, 2020a). Both dorsal and ventral margins of the vomeropalatine process are straight, whereas the lateral surface is concave and dorsally bounded by a crest, similar to that in *Carnotaurus* and *Eoabelisaurus*, although it is not clear whether it has a small dorsal fossa (see Cerroni *et al.*, 2020a: Fig. 20). Abelisaurids that, alongside *Skorpiovenator*, possess a well-developed triangular vomeropalatine process include *Llukalkan*, *Carnotaurus*, and apparently *Eoabelisaurus*. In *Carnotaurus*, however, this process is much more developed, whereas in *Majungasaurus* it appears to be triangular, although it is incompletely preserved. The anterodorsal corner of the vomeropalatine process extends into a straight projection that articulates with the vomer; however, CT scans reveal no discernible sutures between these elements. The few vomerine remains, observed through CT data, indicate that the vomer is a long and straight bone that narrows anteriorly (Fig. 11K–11L).

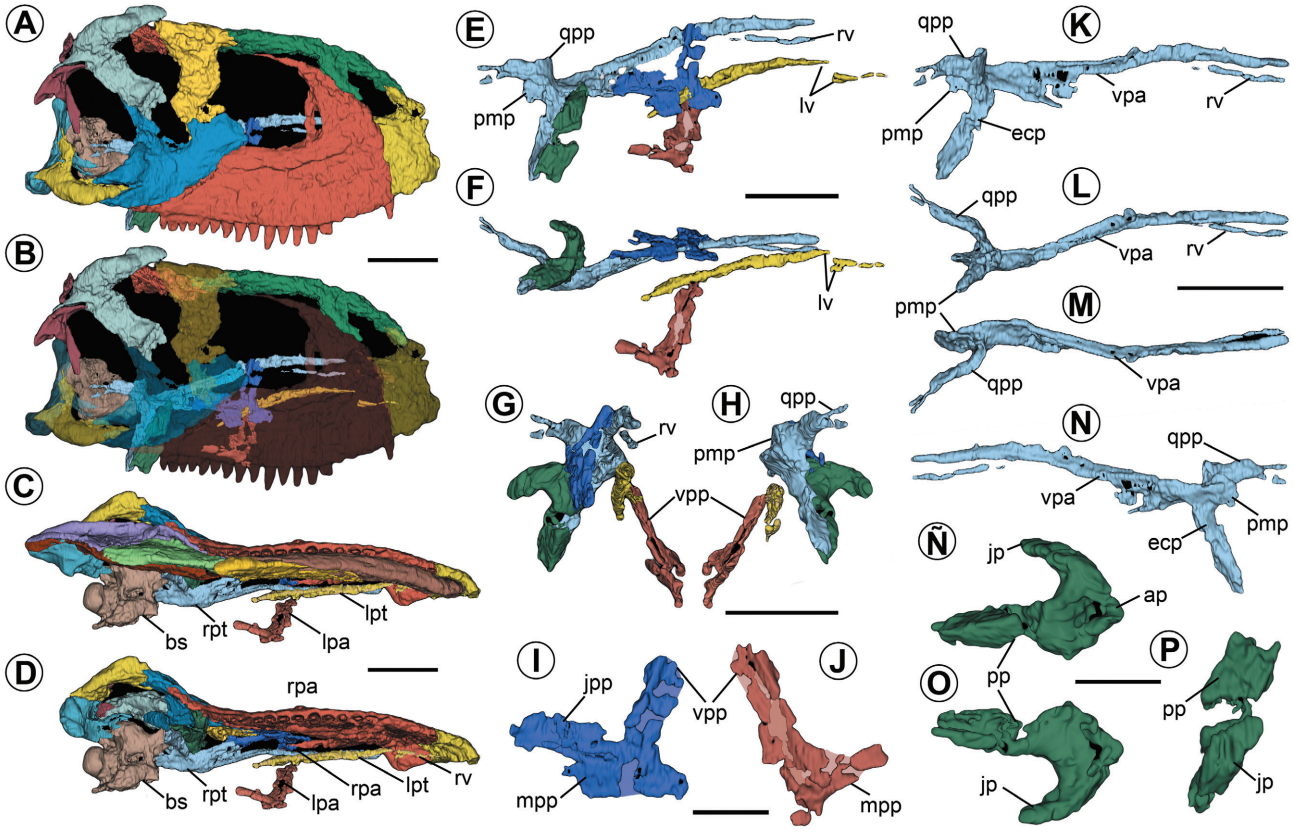


Figure 11. A–P. Rendered palatal bones of ***Skorpiovenator bustingorryi* (MMCh-PV 48)**. **A,** right lateral view of the skull. **B,** right lateral view of semitransparent skull, showing palatal bones with right pterygoid and vomer (light blue), right ectopterygoid (green), right palatine (light purple), left palatine (light red) and left pterygoid and vomer (yellow). **C,** ventral view of the skull with lower jaw in articulation. **D,** ventral view of skull with removed lower jaw bones showing palatal bones. Rendered palatal bones in **E,** right lateral; **F,** ventral; **G,** anterior; and **H,** posterior views. **I,** right and **J,** left palatine in lateral views. Right pterygoid in **K,** lateral; **L,** ventral; **M,** dorsal; and **N,** medial views. Right ectopterygoid in **Ñ,** dorsal; **O,** ventral; and **P,** lateral views. Abbreviations: **ap,** anterior process of ectopterygoid; **bs,** basisphenoid; **ecp,** ectopterygoid process of pterygoid; **jp,** jugal process of ectopterygoid; **jpp,** jugal process of palatine; **lpa,** left palatine; **lpt,** left pterygoid; **lv,** left vomer; **mpp,** maxillary process of palatine; **pmp,** posteromedial process of pterygoid; **pp,** pterygoid process of ectopterygoid; **qpp,** quadrate process of pterygoid; **rpa,** right palatine; **rpt,** right pterygoid; **rv,** right vomer; **vpa,** vomeropalatine process of pterygoid; **vpp,** vomeropterygoid process of palatine. Scale bars equal 10 cm (A–H, K–N) and 5 cm (I–J, Ñ–P).

Apparently, the vomers are separated from each other and located at different levels due to deformation, similar to the position of the pterygoid bones; whereas the remains of the left vomer are close to the premaxillary articulation but slightly offset.

Ectopterygoid. Only the complete right ectopterygoid is preserved (Fig. 11D–11G). Due to deformation on the right side of the skull, the surangular is displaced dorsally and occupies the U-shaped space of the ectopterygoid. As in other abelisaurids, the ectopterygoid is more robust than the other palatal bones (Sampson & Witmer, 2007). Both processes diverge posteroventrally from the ectopterygoid body and their main axes are almost aligned with each other (Fig. 11Ñ–11P). The pterygoid process contacts the pterygoid medially through a shallow facet. This process is twice as long as and transversely thicker than the jugal process. The latter contacts the jugal posterolaterally and tapers distally into a sharp end.

The ectopterygoid body is formed by the confluence of the pterygoid and jugal processes anteriorly. From this point, a small, subtriangular projection extends and tapers anteriorly. The medial margin of this anterior projection is thickened, a condition shared with *Llukalkan* but absent in *Majungasaurus*. On the ventral surface of the anterior projection lies a noticeable, relatively excavated fossa. Although CT scans suggest that this fossa is perforated, this is likely a taphonomic artifact.

Braincase

The braincase (including the skull roof formed by the parietal and frontals) was virtually extracted from the CT data (see SOI 5, SOI 6). The braincase is almost complete but—like the rest of the skull—is heavily fractured, which made the segmentation process highly difficult. It also exhibits some degree of lateroventral compression, resulting in the asymmetrical positioning of paired structures (Fig. 12A–12F). The bones are fused, and no sutures are observed in the CT scans. The fractures obscured most of the sutures and neurovascular foramina.

The general morphology of the main structures was recovered, but the poor preservation obscured most sutural contacts and neurovascular foramina. Additionally, only fragments of the interorbital septum and the cultriform process were preserved.

Frontal. The frontals are the main elements of the cranial roof, as in other theropods (Figs. 2D, 3B, 6A, 12D, SOI 1 Fig. S2). Each frontal articulates with the nasal rostrally, the lacrimal and postorbital laterally, the parietal caudally, and the laterosphenoid, orbitosphenoid, and sphenethmoid ventrally. Alongside the nasal, the frontal shows one of the most distinctive characteristics of *Skorpiovenator*: a double row of large foramina running anteroposteriorly along the dorsal surface of the skull, likely associated with a special neurovascular system (Cerroni *et al*., 2020b).

The contour of the frontal in dorsal view is trapezoidal, with its narrowest point at its anterior end and widening posteriorly to the articulation with the parietal. The paired frontals are fused, with the interfrontal suture completely obliterated and indiscernible (Fig. 6A). The contour of the articulation with the nasals is difficult to discern due to the poor preservation of this sector of the skull roof. However, the articulation appears to be W-shaped, with the frontal exhibiting two small, triangular anterior projections, similar to the condition present in *Rugops* and *Llukalkan*. The contact with the lacrimal and postorbital is not discernible, but in the case of the lacrimal it was interpreted based on the CT scans (Fig. 7G–7H). The contact with the parietal is irregular and elevated in a low transversal crest, positioned in the line of the internal border of the supratemporal fenestrae (Fig. 6A).

The dorsal surface of the bone is irregular, faintly ornamented as in *Ekrixinatosaurus*, but not as developed as the strong granulations and grooves present in *Llukalkan*, *Abelisaurus* or *Niebla*. The frontals are mostly flat medially and convex laterally, and exhibit low double lateral prominences (Fig. 6A, SOI 1 Fig. S2). This contrasts with the condition in *Abelisaurus*, *Aucasaurus*, or *Niebla*, in which these prominences are single on each side. The posterior, larger prominence, positioned near the anterior margin of the supratemporal fenestra, is probably equivalent to those present in other abelisaurids. Additionally, an anterior, smaller prominence, separated by a concave cleft from the posterior prominence on each side, is positioned in the transversal line of the lacrimal-postorbital suture. These paired double prominences are covered by rounded rugosities more developed than in the rest of the frontal surface, and represent a unique trait of *Skorpiovenator.* However, it is worth noting that in *Ekrixinatosaurus* the posterior promi-

nences are present as in other abelisaurids, but the frontals lack their anterior margin, so it is not possible to determine if the anterior prominences were also present. The orbital vault is wide and convex.

Parietal. The paired parietals are fused into a single element, as in other theropods (Fig. 2D, 3B, 6A, 12D). The parietal articulates with the frontals anteriorly, the postorbital anterolaterally, the squamosals posterolaterally, the supraoccipital caudally, and the prootic and opisthotic ventrally.

The parietal eminence is probably formed by both the parietal and supraoccipital. It projects dorsally slightly over the level of the sagittal bar/crest. The sagittal bar (delimited laterally by the median margins of the supratemporal fossae) is anteroposteriorly short and wide, as in *Aucasaurus*. Only a fragment of the laminar nuchal crest is preserved on the right side (Fig. 2E), lateral to the parietal eminence. When complete, the nuchal crest was prominent—approximately three times the height of the foramen magnum—as in most other abelisaurids (*e.g.*, Paulina-Carabajal, 2011b; Filippi *et al.*, 2018).

Supraoccipital. The supraoccipital contacts the parietal rostrally and with the exoccipital-opisthotic complex ventrally, although the precise articular suture is almost indistinguishable superficially. There are no visible sutures with the parietal and the exoccipital-opisthotic complex, and it is not possible to determine if the supraoccipital participates in the dorsal margin of the foramen magnum. This bone is vertically oriented as in *Carnotaurus*, *Llukalkan*, and *Abelisaurus*, but differs from the anterodorsally inclined supraoccipital present in *Majungasaurus* and *Viavenator*.

The supraoccipital forms a large posterior projection, the supraoccipital tuberosity (Fig. 2E, 12C). Ventral to this tuberosity, the supraoccipital crest is present as a promi-

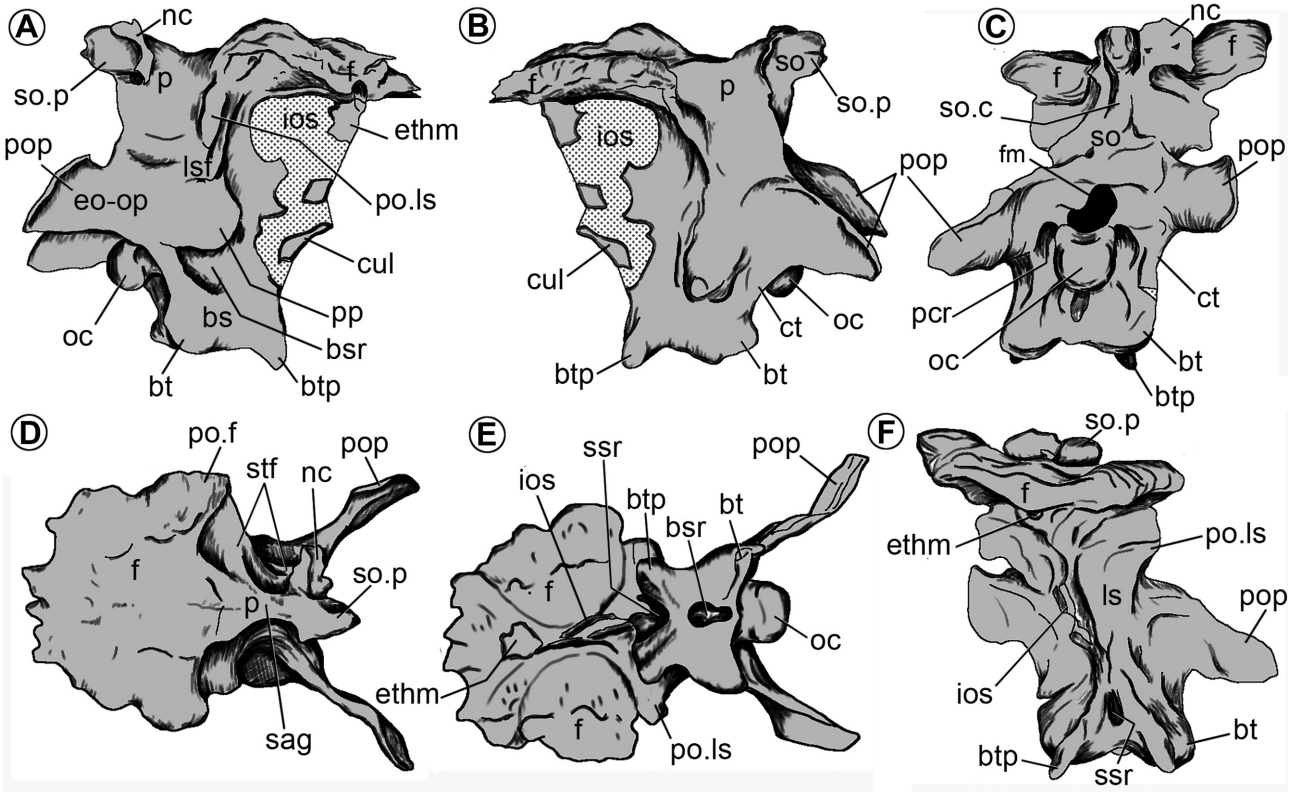


Figure 12. A–F. Line drawings of the braincase of ***Skorpiovenator bustingorryi*** (**MMCh-PV 48**) based from CT scan data. **A,** right lateral; **B,** left lateral; **C,** posterior; **D,** dorsal; **E,** ventral; and **F,** anterior views. Abbreviations: **bs,** basisphenoid; **bsr,** basisphenoid recess; **bt,** basal tubera; **btp,** basipterygoid process; **ct,** crista tuberalis; **cul,** cultriform process; **ethm,** ethmoidal elements (fragments attached to the ventral surface of the frontals); **f,** frontal; **fm,** foramen magnum; **ios,** interorbital septum; **lsf,** laterosphenoid; **ltr,** lateral tympanic recess; **nc,** nuchal crest; **oc,** occipital condyle; **p,** parietal; **pcr,** paracondylar recess; **po.f,** postorbital process of the frontal; **po.ls,** postorbital process of the laterosphenoid; **pop,** paroccipital process; **pp,** preotic pendant; **preo-op,** exoccipital-opisthotic complex; **sag,** sagittal bar/crest; **so,** supraoccipital; **so.c,** supraoccipital crest; **so.p,** supraoccipital posterior projection; **ssr,** subsellar recess; **stf,** supratemporal fossa.

nent median ridge running ventrally, without reaching the foramen magnum. The foramina for the caudal middle cerebral veins are probably located dorsally on both sides of the supraoccipital crest. This position was determined via CT scans, as the external surface of the bone is heavily eroded.

Exoccipital-Opisthotic complex. During the early ontogeny of archosaurs, the exoccipital and the opisthotic become fused into a single element (Currie, 1997), the Exoccipital-Opisthotic complex or otoccipital (Sampson & Witmer, 2007). This complex forms the laterodorsal margin of the foramen magnum (Fig. 2E, 12C).

The exoccipital contacts the supraoccipital dorsomedially, the basioccipital ventrally, and the prootic anteriorly; however, the sutures are obscured by fusion and/or poor preservation. The exoccipitals form the lateral margins of the foramen magnum, and probably the dorsal margin as well. The exoccipitals may have been excluded from the occipital condyle, as the CT scans showed no sutures with the basioccipital. Lateral to the occipital condyle, there are oval paracondylar recesses (Fig. 12C), into which the posterior cranial nerves open. The CT scans showed two passages—one large and another markedly smaller anteriorly—for branches of the CN XII.

The paraoccipital process is better preserved on the right side (Fig. 12A–12F). This process is a blade-like structure, more or less twice the height of the foramen magnum, and slightly posterolaterally inclined distally. The distal end is slightly expanded. The ventral margin of the paraoccipital process is at the level of the dorsal margin of the occipital condyle in posterior view. The ventral ramus of the opisthotic, forming the crista tuberalis, is deep but does not obscure the occipital condyle in lateral view. Ventrally, the crista tuberalis extends to the lateral margins of the basal tubera.

Basicranium. As mentioned, the sutures between basioccipital-basisphenoid, and basisphenoid-parasphenoid are indistinguishable. Some fragments of the cultriform process are preserved.

The basioccipital forms the main body of the occipital condyle and the short condylar neck (Fig. 12C, 12E). The occipital condyle is subcircular in posterior view. The dorsal surface of the condyle is widely concave. The ventral surface of the neck is flat and smooth, lacking a mid-crest, as in *Ilokelesia* and *Aucasaurus* but different from the condition observed in *Abelisaurus*, *Carnotaurus*, and *Majungasaurus*, where there is a median longitudinal crest. The basal tubera are fused forming a vertical quadrangular plate below the occipital condyle (Fig. 12C). Due to the poor surface preservation, there is no evidence of a vertical keel ventral to the condyle. A small, rounded medial fossa lies ventral to the occipital condyle, similar to the condition in *Majungasaurus*. The basituberal web exhibits a concave distal end. The maximum width of this plate is almost three times that of the occipital condyle, and it shows a caudal concavity, as in other abelisaurids.

The basisphenoid forms most of the basicranium, contributing to the anterior portion of the basal tubera, the basipterygoid processes, and most of the floor of the endocranial cavity (Fig. 12E). In ventral view, the anterolateral margins of the basisphenoid body are gently convex as in *Llukalkan* and *Viavenator*. This contrasts with the straight margins present in *Ceratosaurus* and the sigmoid morphology observed in *Majungasaurus*. The basipterygoid process is finger-shaped and relatively short (Fig. 12A–12C), as in *Carnotaurus* and *Niebla*. It is ventrolaterally projected, slightly below the level of the basal tuber. CT scans revealed that the right basipterygoid process remains in contact with the pterygoid, and this articulation occurs through a slot in the pterygoid body (see pterygoid description), as also occurs in *Majungasaurus* and *Carnotaurus*.

The lateral side of the basisphenoid bears a wing-like preotic pendant (probably formed by both prootic and basisphenoid) that overhangs a well-developed lateral tympanic recess. Within the anterior wall of the recess, a large foramen opens for the entrance of the cerebral branch of the internal carotid artery. A large basisphenoidal recess excavates the ventral side of the basisphenoid (Fig. 12E). The recess is drop-shaped, delimited by the basituberal web posteriorly and the basipterygoid web anteriorly. This is different from the almost sub-circular basisphenoidal recess present in *Viavenator* and the triangular recess present in *Llukalkan*, *Niebla* and *Majungasaurus*. The CT scans reveal paired pneumatic recesses associated with the basisphenoid recess, which dorsally excavate the neck of the occipital condyle. The basipterygoid web delimits a well-developed subsellar recess posteriorly, as in other studied abelisaurids. The lateral walls delimiting the subsellar recess project dorsomedially and converge to form the

cultriform process, a blade-like structure strongly projected anterodorsally.

Prootic. The prootic forms the lateral wall of the braincase, contacting the opisthotic posteriorly, the laterosphenoid anteriorly, and the basisphenoid ventrally (Fig. 12A). The only discernible foramen allows the passage of the maxillomandibular nerve (CN $V_{2,3}$). It is large and oval, located posterodorsal to the preotic pendant, and indicates the prootic-laterosphenoid contact. The otic recess, better observed on the left side, indicates the contact of the prootic with the opisthotic. The proximal portion of the preotic pendant seems to be formed by the prootic based on the dorsal position of the structure.

Laterosphenoid-orbitosphenoid. The laterosphenoid and orbitosphenoid form the anterior portion of the lateral wall of the braincase (Fig. 12A–12F). Posteriorly, the laterosphenoid contacts the prootic, likely at the foramen for CN $V_{2,3}$. The postorbital process of the laterosphenoid is blade-shaped, and it projects laterally from the wall of the braincase, delimiting the supratemporal fossa posteriorly. There are no sutures between the laterosphenoid and orbitosphenoid. The cranial foramina III and IV—which may indicate the limit between the two bones—are not discernible. The orbitosphenoids may contact each other and the interorbital septum anteromedially. Fragments of the interorbital septum remain attached to this region.

Ethmoidal-Complex (Sphenethmoid-Mesethmoid). Fragments of the mesethmoid and sphenethmoid are preserved in articulation with the ventral surface of the frontals (Figs.12.A, 12.E, 12.F). They form a tubular structure that lateroventrally encloses the olfactory tracts and bulbs, a condition shared with other abelisaurids.

Lower jaw

Both lower jaws were preserved fully articulated with the skull (Fig. 2A–2C). Given the plastic deformation of the skull, the left mandible is observable in the right lateral view (Fig. 2A). The mandibles are elongate and ventrally curved (Fig. 13A–13G), as in *Carnotaurus*. This contrasts with the straight mandibles registered in *Majungasaurus* or *Spectrovenator*. The external mandibular fenestra is delimited by the dentary anteriorly, the angular posteroventrally, and the surangular posterodorsally (Fig. 13A). This fenestra is large, as is common in deeply-nested abelisaurids, such as *Carnotaurus* and *Majungasaurus*. In ventral view, although slightly masked by the deformation, lower jaws show a "U-shaped" outline (Fig. 2C), as is typical in abelisaurids (Sampson & Witmer, 2007), in contrast to the "V-shaped" condition observed in other theropods (*e.g.*, *Australovenator*, White *et al.*, 2015; *Dilong*, Xu *et al.*, 2004; *Velociraptor*, Barsbold & Osmólska, 1999).

Dentary. Both dentaries are closely appressed to the skull, as they were preserved articulated. Consequently, several features of their dorsal/dentigerous margins, including the morphology of the dentary teeth and alveoli, cannot be determined through direct observation. However, CT data provide some additional anatomical details (Figs. 13.A–13.D, 14.A–14.D). This bone represents about 56% of the total length of the lower jaw.

The dentary contacts the contralateral dentary anteromedially, the angular posterolateroventrally, the angular posterolaterodorsally, the splenial medially, and the supradentary dorsomedially. In lateral view, the dentary exhibits a concave dorsal margin and a convex ventral margin, resulting in an upturned symphysis (Fig. 13A–13B, 14A–14B). This condition is shared with *Carnotaurus*, *Ekrixinatosaurus* and an indeterminate ceratosaur from the Cañadón Asfalto Formation (Pradelli *et al.*, 2024), but contrasts sharply with the predominantly straight lateral profile present in other ceratosaurs, such as *Genyodectes* (Rauhut, 2004) and adult specimens of *Majungasaurus* (Ratsimbaholison *et al.*, 2016). There is some variation of this character within *Ceratosaurus*, with the dentary of the holotype specimen of *Ceratosaurus nasicornis* (UNSM 4735) being completely straight, and the holotype of *C. dentisulcatus* (UMNH-VP 5278) dorsally curved.

The dentary is a transversely thick bone, mostly in its anterior end and mid-length; whereas towards its posterior end it becomes gradually thinner, near the angular contact (Fig. 13D). CT data exhibit the presence of at least 21 teeth, most of them preserved and erupted (Fig. 13A, 14A); however, the morphology of the alveoli cannot be determined.

The anterior/symphyseal margin of the dentary is gently curved, only differentiated from the ventral margin by an obtuse angle of approximately 120° (Fig. 13A). In anterior view, the symphysis thickens dorsally towards the dentigerous margin (Fig. 13E).

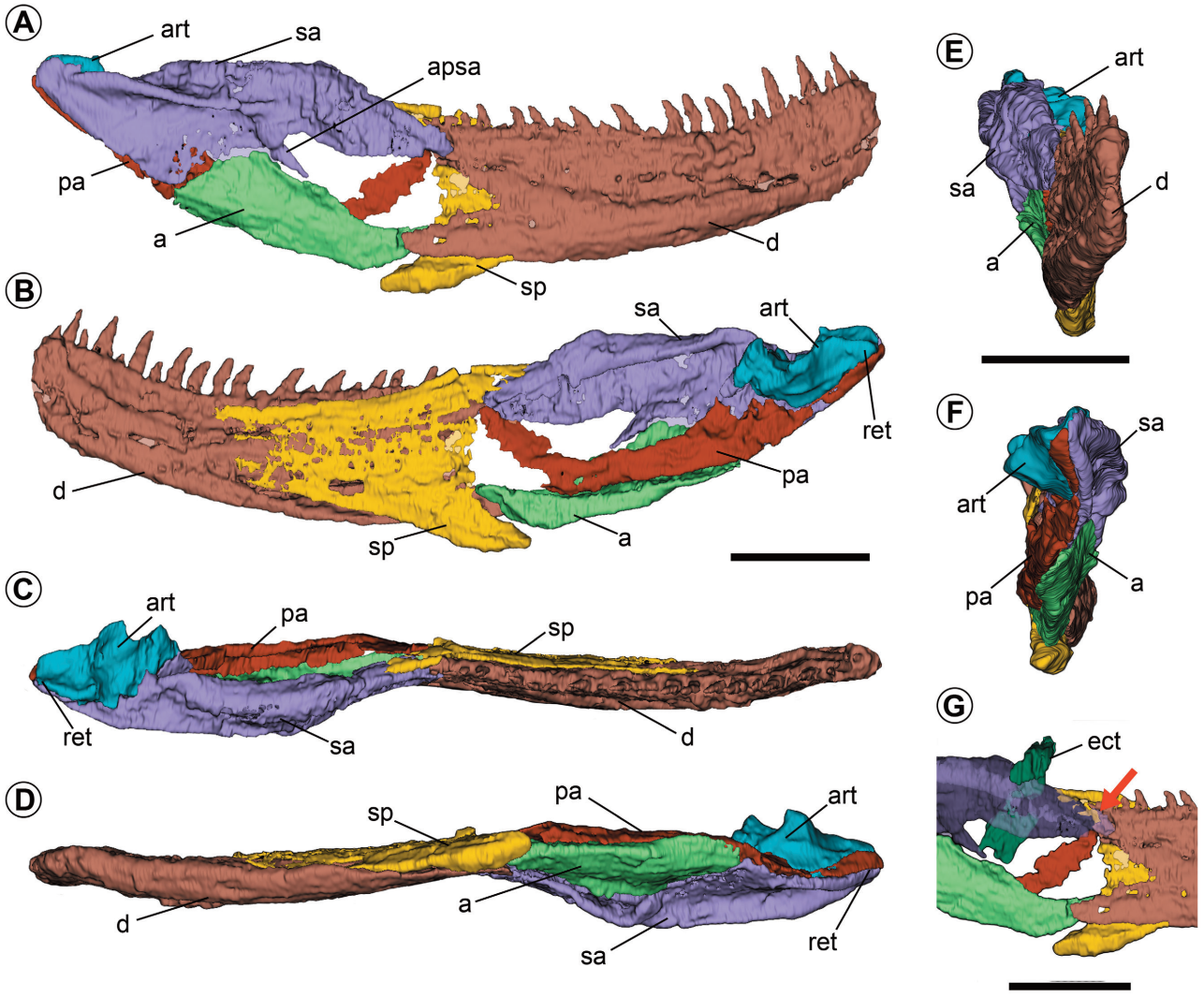


Figure 13. **A–G.** Rendered right lower jaw of ***Skorpiovenator bustingorryi*** **(MMCh-PV 48)**. **A,** lateral view; **B,** medial view; **C,** dorsal view; **D,** ventral view; **E,** anterior view; **F,** posterior view. **G,** detail of the lower jaw showing the right ectopterygoid mounted due to a taphonomic artifact, over the dorsal aspect of the surangular. Red arrow highlights the intramandibular joint. Abbreviations: **a,** angular; **apsa,** angular process of surangular; **art,** articular; **d,** dentary; **ect,** ectopterygoid; **pa,** prearticular; **ret,** retroarticular process; **sa,** surangular; **sp,** splenial. Scale bars equal 10 cm.

The lateral surface of the dentary is longitudinally divided by a conspicuous groove that runs anteroposteriorly, being positioned approximately at mid-height (Fig. 14B). Ventral to this groove, the lateral and ventral surfaces of the dentary are sculptured by rugosities and elongate furrows that extend mostly anteroposteriorly. The ventral half of the lateral surface of the dentary is swollen, exhibiting a distinct lateral convexity in cross-section. In contrast, the dorsal half of the lateral surface is almost flat, bearing a series of dorsoventrally oriented shallow depressions, resembling the condition in *Carnotaurus*, *Majungasaurus*, and *Spectrovenator*.

At its posterior end, the dentary bifurcates anterior to the external mandibular fenestra, forming a posterodorsal process that articulates with the surangular (hidden on the right side by the posterior maxillary teeth) and a posteroventral process that articulates with the angular (Fig. 13A, 14A–14B). CT scans reveal that the surangular process forms a socket that receives the anterior portion of the surangular, which is formed by small additional posterior projections, similar to the condition in the surangular processes of *Carnotaurus* and *Majungasaurus* (Cerroni *et al.*, 2020a). The angular process is slightly more posteriorly projected than the surangular process, as in the condition

in *Carnotaurus* and in contrast to the condition observed in *Majungasaurus*, where both processes show the same length. The angular process is lateromedially compressed and articulates with the anterior ramus of the angular.

In medial view, the splenial and supradentary cover approximately two-thirds of the total surface of the dentary. The splenial contacts the Meckelian groove ventrally and extends from the 10th dentary alveolus to the posterior end of the dentary. CT scans reveal an additional thin ridge on the medial surface of the dentary, sub-parallel to the splenial contact, obscured laterally by the articulated splenial (Fig. 14A). The extent of the adductor fossa reaches up to the 13th alveolus. Anterior to the splenial, the medial surface of the dentary shows the Meckelian groove (which constitutes the rostral extension of the adductor or Meckelian fossa) in the form of a conspicuous and anteroposteriorly oriented sulcus. This sulcus separates the sculptured ventral margin of the bone with the bowed medial surface of the dentary. This surface, in turn, is bounded dorsally by the fused paradental plates, which become dorsoventrally lower posteriorly until they disappear at the level of the splenial foramen. This condition is similar to that observed in *Carnotaurus*, whereas in *Majungasaurus*, the paradental plates extend posteriorly to the level of the posterior margin of the splenial. The symphyseal contact between dentaries is about 43 mm long anteroposteriorly.

Angular. The angular articulates with the surangular dorsally, the dentary anterolaterally, the splenial anteromedially and the prearticular medially (Fig. 13A–13G). It is an elongate, anteriorly acuminated bone that becomes dorsoventrally deeper posteriorly (Fig. 14I–14L). The lateral surface of the angular shows the same ornamentation pattern observed in the dentary, with faint rugosities and grooves. In lateral view, the anterior end of the bone is acutely pointed and rests over a shelf formed laterally by the dentary and ventrally by the splenial. The anterior end is almost at the same level as the anterior end of the surangular, resembling the condition in *Carnotaurus*. In contrast, the angular is shorter in *Majungasaurus*. There is a small and shallow notch on the anterolateral corner of the anterior end that receives the posteroventral process of the dentary. The angular contributes approximately one-quarter of the ventral margin of the mandibular fenestra, between the angular process of the surangular and that of the dentary. In medial view, the angular shows an anteroposteriorly extensive, gently curved suture with the prearticular, ending anteriorly in a triangular process interposed between the prearticular and the splenial (Fig. 15D). This morphology was originally proposed as an autapomorphy of *Skorpiovenator* (Canale *et al.*, 2009), given that the medial exposure of the angular is more restricted in *Majungasaurus* and *Carnotaurus*.

Surangular. The surangular is positioned on the dorsolateral surface of the postdentary region of the mandible and articulates with the dentary anteriorly, the angular ventrally, the prearticular medially, and the articular posteriorly. The surangular is an anteroposteriorly elongate and robust bone, nearly as long as the prearticular. It possesses a strongly convex dorsal margin that extends from the dentary process to the anterior margin of the glenoid fossa (Figs. 13.A–13.D, 14.M–14.N, 15.B). The surangular is notably convex at the level of the mandibular fenestra, bearing a distinct, dorsally projected knob-like structure similar to that of *Carnotaurus*. This contrasts with *Majungasaurus*, where the convexity is weakly developed. On the central portion of the lateral surface of the bone, there is a laterally projected thin crest ("lateral shelf" in *Carnotaurus*, *sensu* Cerroni *et al.*, 2020a), which runs anteroposteriorly and represents the insertion of the *M. adductor externus superficialis* (Fig. 14M). In *Carnotaurus* and *Majungasaurus*, this crest becomes thicker and rounded on its anterior half, while in *Skorpiovenator* it is dorsoventrally thin all along its length. As in other theropods, this lateral shelf roofs a fossa, which covers most of the posterolateral surface of the surangular. Within this fossa, two low, rounded ridges oriented posteroventrally are present ventral to the lateral shelf.

In lateral view, the maximum dorsoventral height of the bone is reached at the level of the posterior end of the angular. The suture line with the latter bone is sigmoidal. Anteriorly, the surangular forms a notch surrounding the posterior end of the external mandibular fenestra. As in *Carnotaurus* and *Majungasaurus*, the angular process of the surangular descends at an acute angle and terminates in a blunt end, forming the posteroventral margin of the external mandibular fenestra (Fig. 14M–14N). This process is situated near the anterior end of the bone as observed in *Carnotaurus*, while in *Majungasaurus* and *Spectrovenator*, this process is located at the mid-length of the surangular. The posterior end of the surangular is laterally bisected by the

lateral crest and is rounded, as seen in *Carnotaurus*, while in *Majungasaurus* it is posteriorly pointed. The surangular-prearticular suture is clearly observable from the glenoid along the entirety of the thin posteroventral mandibular margin, where it forms a prominent ventral keel. The lateral surface of the surangular is smooth on its posterior half, and exhibits faint rugosities on the anterior portion, anterior to the lateral crest.

On both sides of the skull, the dentary process of the surangular is obscured by the maxillary teeth; however, CT scans reveal that this process narrows anteriorly into a pointy end that articulates in a pocket of the dentary. Resembling the condition of *Majungasaurus*, the medial surface of the surangular shows a large concavity that forms the adductor fossa (see Sampson & Witmer, 2007). The dorsal margin of the surangular medially projects a thick lamina that forms the dorsomedial aspect of the adductor fossa; this lamina is continuous along the dorsal aspect of the surangular (Fig. 14N). In medial view, adjacent to the glenoid region, the surangular possesses an anteroventral triangular projection that articulates with the prearticular and the articular, forming part of the anterior margin of the glenoid. Between this projection and the main body of the surangular lies a deep and wide fossa that forms the posterior aspect of the adductor fossa.

Splenial and supradentary. The splenial articulates laterally with the dentary, posteriorly with the prearticular, posteroventrally with the angular, and dorsally with the supradentary. It is a flat and transversally thin bone, with a trapezoidal/triangular outline, which covers most of the medial surface of the dentary (Fig. 13A–13G, 14E–14H, 15A). In lateral view, it is a tall bone; at its posterior end

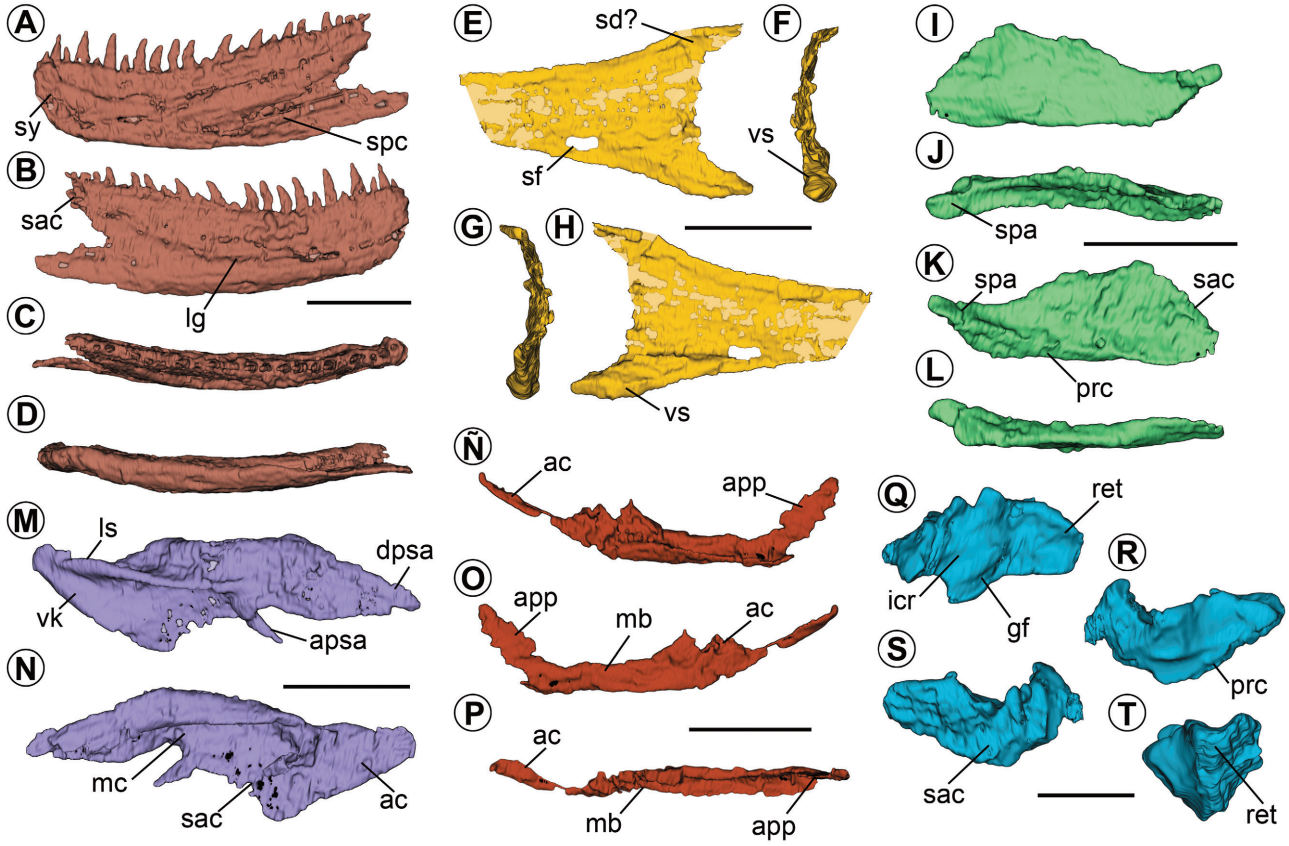


Figure 14. A–T. Rendered right lower jaw bones of ***Skorpiovenator bustingorryi*** **(MMCh-PV 48)**. Dentary in **A,** medial; **B,** lateral; **C,** dorsal; and **D,** ventral views. Splenial in **E,** medial; **F,** posterior; **G,** anterior; and **H,** lateral views. Angular in **I,** lateral; **J,** dorsal; **K,** medial; and **L,** ventral views. Surangular in **M,** lateral and **N,** medial views. Prearticular in **Ñ,** lateral; **O,** medial; and **P,** dorsal views. Articular in **Q,** dorsal; **R,** medial; **S,** lateral; and **T,** posterior views. Abbreviations: **ac,** articular contact; **app,** anterior process of prearticular; **apsa,** angular process of surangular; **dpsa,** dentary process of surangular; **gf,** glenoid fossa; **icr,** intercondylar ridge; **lg,** lateral groove; **ls,** lateral shelf; **mb,** median body; **mc,** medial crest; **prc,** prearticular contact; **ret,** retroarticular process; **sac,** surangular contact; **sd?,** supradentary?; **sf,** splenial foramen; **spa,** splenial process of angular; **spc,** splenial contact; **sy,** symphysis; **vs,** ventral shelf; **vk,** ventral keel. Scale bars equal 10 cm (A–L) and 5 cm (Q–T).

exhibits a curved outline, which becomes dorsoventrally shorter anteriorly. At its rostral end, the splenial splits into two prongs, separated by a shallow notch (Fig. 15A). Both prongs have approximately the same length as in *Ceratosaurus* and *Carnotaurus*, contrasting with the condition in *Majungasaurus*, where the upper prong is more anteriorly projected than the ventral one. The splenial foramen (mylohyoid foramen, Meckelian foramen) is an anteroposteriorly elongated aperture (Fig. 15A), ventrally positioned at the mid-length of the splenial as seen in *Carnotaurus*, which differs from the more anteriorly positioned foramen present in *Majungasaurus* and *Spectrovenator*. The ventral margin of the posterior end is lateromedially thickened and projected posteriorly, forming a broad shelf, as can be observed in *Carnotaurus*, *Majungasaurus* and *Spectrovenator*. This posterior projection articulates with the angular process of the dentary, altogether forming the articular contact that receives the anterior portion of the angular. The splenial is laterally exposed in the lower jaw, ventral to the contact between the dentary and angular (Fig. 13A, 15B), as in *Majungasaurus* and *Spectrovenator*, and to a lesser extent in *Carnotaurus* and *Ceratosaurus*. This exposed portion of the bone bears ornamentation on its lateral and ventral surfaces, similar to that found on other facial bones, particularly the dentary.

The dorsal margin of the splenial contacts the supradentary; however, no sutures are visible. The supradentary exceeds posteriorly the posterior margin of the splenial, partially covering the paradental plates of the dentary and curving outwards.

Prearticular. Although both paired prearticular bones are present and complete, the left one exhibits a better-preserved surface and, due to the plastic deformation of the skull, is more readily observable in medial view (Fig. 15C–15D). The prearticular articulates anterodorsally with the splenial, ventrally with the angular, lateroposteriorly with the surangular, and posterodorsally with the articular. It is unclear if a coronoid bone was present articulating with the prearticular. The prearticular is a thin and anteroposteriorly elongated element, dorsoventrally low in its central region, with both ends expanded (Fig. 14Ñ–14P). Its dorsal margin is gently curved and forms the rim of the medial mandibular fenestra.

Although poorly preserved, the anterior end of the prearticular can be interpreted as a laminar sheet of bone with a trapezoidal outline and directed dorsally. The overall morphology of the prearticular closely resembles the condition in *Spectrovenator* and *Carnotaurus*. The contact with the splenial is limited to the upper half of the anterior margin. The angular is broadly exposed medially and contacts the prearticular ventrally along approximately two-thirds of its length. The CT scans reveal that the angular contact of the prearticular is formed by a short, thin, and laterally directed shelf that rests on the thick ventral ridge of the angular, both structures forming the ventral aspect of the adductor fossa. The posterior end of the bone articulates dorsally with the articular through a curved, dorsally concave suture. Dorsolaterally, the prearticular contacts the triangular projection of the surangular, as can be observed through CT data. From this point, the prearticular extends posteriorly to the distal end of the retroarticular process via a dorsoventrally tall, finger-like lamina (Fig. 15C–15D), distinct from the tapered posterior process observed in *Majungasaurus* and *Carnotaurus*. The contact between the prearticular and surangular forms a conspicuous ventral keel.

Articular. Both articular bones are present (Fig. 15B–15E), and due to the disarticulation of the left distal half of the quadrate, the glenoid surface of the left articular bone is observable. The articular is a short, deep, and robust element that articulates with the prearticular ventrally and the surangular laterally. The articular constitutes the medial two-thirds of the glenoid fossa, whereas the surangular forms the remaining lateral one-third. The glenoid is divided by an anteromedially-posterolaterally oriented ridge into two asymmetrical fossae which articulate with the quadrate condyles (Fig. 15E). The glenoid is anteromedially bordered by a pronounced sharp ridge. Anterior to this ridge, the articular contacts the triangular projection of the surangular. In dorsal view, the lateral contact with the surangular is through a zig-zag suture that extends from the lateral shelf to the posterior fossa of the surangular. Posterior to the glenoid, the dorsal surface of the retroarticular process is covered by the shallow retroarticular fossa (Fig. 15E–15F). This fossa is longer anteroposteriorly than wide, different from the almost equidimensional fossa present in *Majungasaurus* and the anteroposteriorly short fossa present in *Ceratosaurus* and *Carnotaurus*. The retroarticular fossa

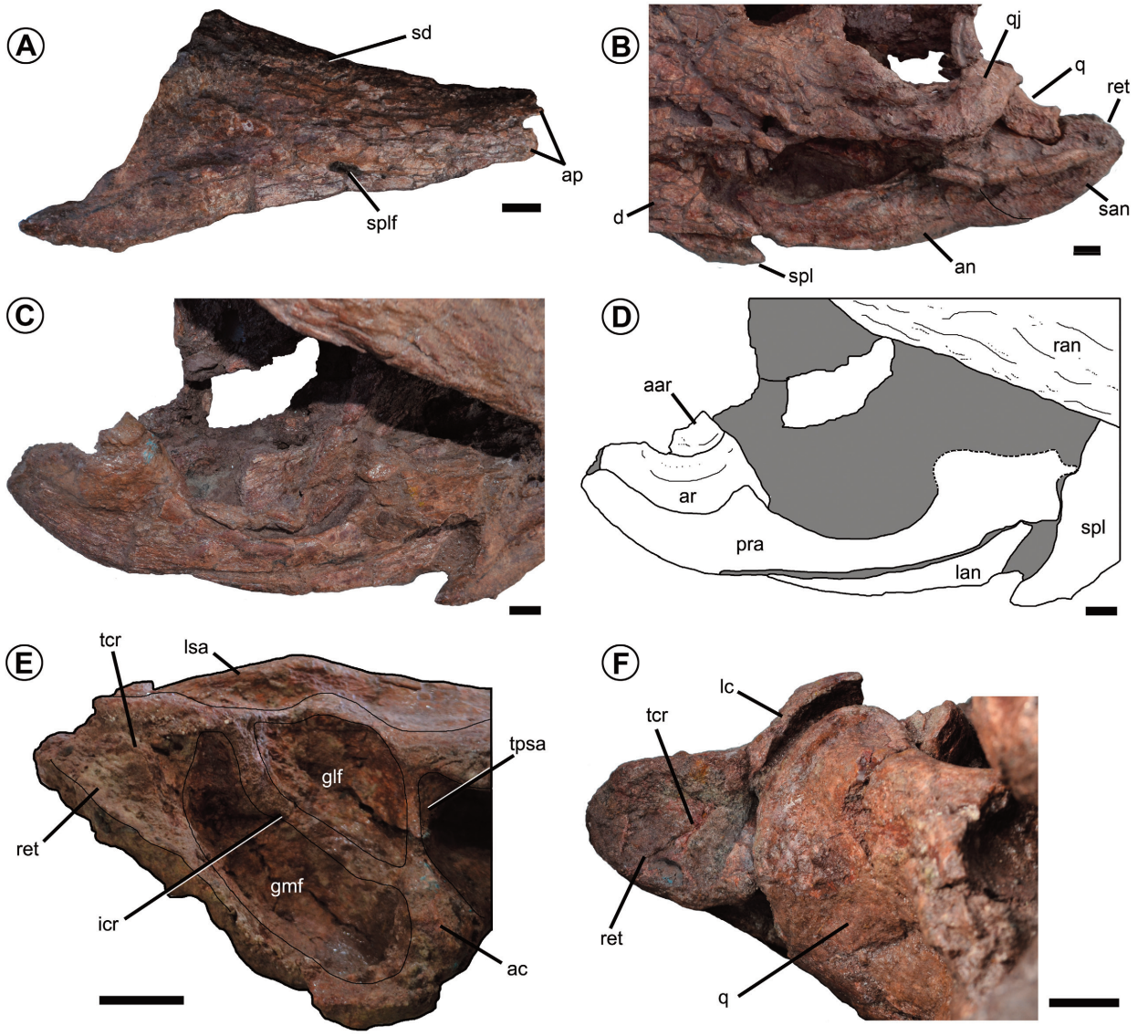


Figure 15. A–F. Postdentary bones of ***Skorpiovenator bustingorryi*** **(MMCh-PV 48)**. **A,** left splenial in medial view; **B,** left postdentary bones in lateral view; **C,** left articular and prearticular in medial view, and **D,** interpretative drawing. **E,** left and **F,** right articular in dorsal view. Abbreviations: **aar,** antarticular; **ac,** anterior crest; **an,** angular; **ap,** anterior prongs; **ar,** articular; **d,** dentary; **icr,** intercondylar ridge; **glf,** glenoid lateral fossa; **gmf,** glenoid medial fossa; **lan,** left angular; **lc,** lateral crest of articular; **lsa,** lateral shelf of surangular; **pra,** prearticular; **q,** quadrate; **qj,** quadratojugal; **ran,** right angular; **ret,** retroarticular process; **san,** surangular; **sd,** supradentary; **spl,** splenial; **splf,** splenial foramen; **tcr,** transverse crest; **tpsa,** triangular projection of surangular. Scale bars equal 2 cm.

is divided by a strongly oblique, posterolaterally oriented, low and thin crest. This crest is also present in *Carnotaurus*, although it is markedly less oblique, being oriented almost transversely to the main axis of the lower jaw. The lateral wall of the retroarticular process is more dorsally projected than the medial one.

A peculiar trait revealed by CT scanning, is the presence of an elongated and small cavity on the lateral aspect of the articular (SOI 1, Fig. S3). Such cavity is also neighboring the suture with the surangular, and partially leading into the last one. Apparently, this cavity is connected to the dorsal surface of the articular through a narrow canal. This canal exits via a foramen located at the surangular-articular suture, although it remains unclear whether this represents the chorda tympani foramen. The internal articular cavity is unlikely to be of pneumatic origin due to the absence of prominent exit foramina; consequently, it is probably related to mandibular innervation.

Antarticular. A small bone is present on the dorsal margin of the anteromedial border of the left articular (Figs. 15C–15D, 16A–16D). It exhibits a widely open suture with the articular. Dorsal to the glenoid cavity, this element bears an articular surface that surrounds the medial condyle of the quadrate anteriorly and medially, resulting in a curved outline in dorsal view. Its anterior portion is more robust than the medial one. A small tip is present on its dorsal margin.

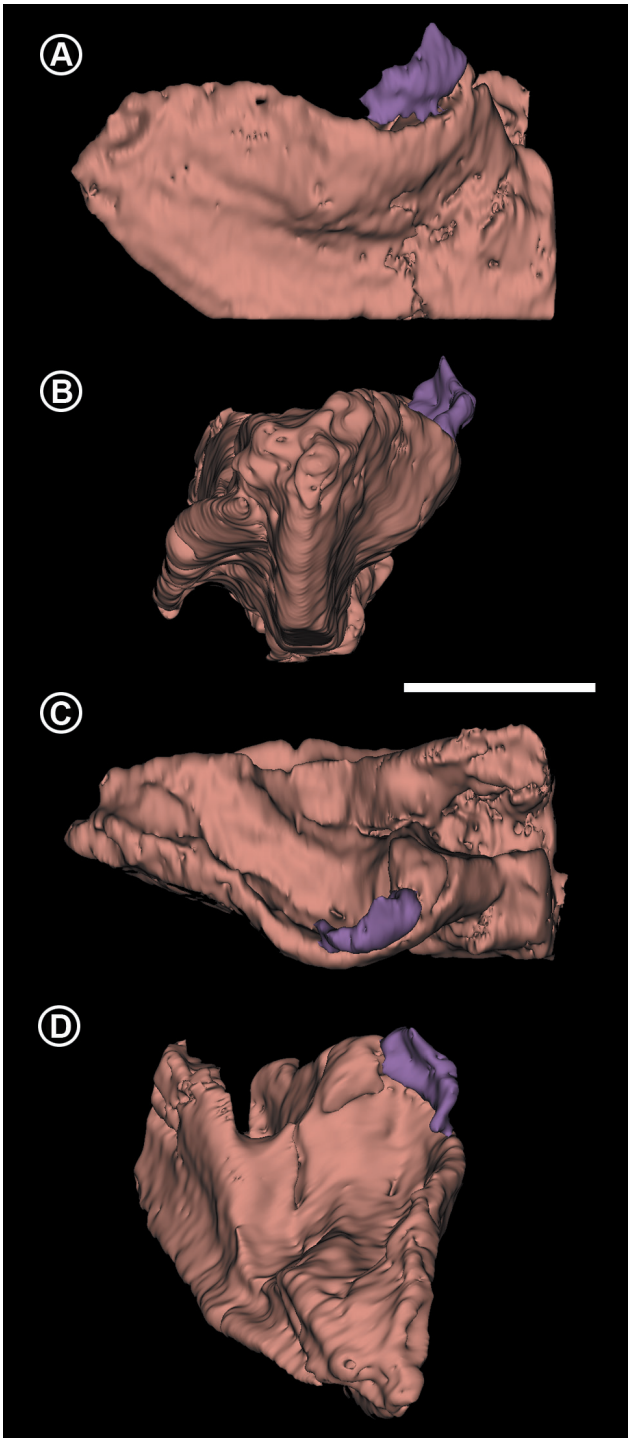


Figure 16. A–D. Left articular bone (light red) and the sesamoid antarticular (violet) positioned above it of ***Skorpiovenator bustingorryi*** (**MMCh-PV 48**). **A,** medial; **B,** posterior; **C,** dorsal; and **D,** posterodorsal views. Scale bar equals 5 cm.

The dorsal margin of the right articular is incompletely preserved; therefore, it is not possible to determine if this element was present bilaterally. This small bone has not been recorded in other abelisaurids with well-preserved articular regions (*e.g.*, *Carnotaurus*, *Majungasaurus*, or *Spectrovenator*); however, it was identified in two species of the allosauroid tetanuran *Allosaurus*: *A. fragilis* and *A. jimmadseni* (Madsen, 1976; Chure and Loewen, 2020). The nature of this element is analyzed in further detail in the Discussion section below.

Teeth

General dentition. Each premaxilla of *Skorpiovenator* exhibits four alveoli, although those on the right side are more clearly discernible. The mesiodistal axes of these alveoli follow the curvature of the premaxilla, preventing any overlap between adjacent teeth. Both of these features, although not previously mentioned for this taxon, are observed in other abelisaurids and are diagnostic characters of Abelisauridae (Hendrickx *et al.*, 2020). Although it is not possible to compare the apicobasal length of the teeth in this region since no teeth are preserved *in situ*, it can be discerned that the first alveolus is slightly smaller than the others. Additionally, three isolated teeth (*i.e.*, MMCh-PV 48/1-2, and 48/6) are preserved within the assemblage, exhibiting characteristics typical of teeth from this region.

The maxillary dentition of *Skorpiovenator* is notable for comprising 19 teeth, making it the only currently known abelisaurid to exhibit such a high maxillary tooth count. The maxillary teeth preserved *in situ* comprise 14 on the right maxilla (rmx1 and rmx6–15 well preserved, rmx16–19 extremely damaged) and 13 on the left maxilla (lmx7?–19?) (Fig. 2A–2B). Additionally, five isolated teeth (MMCh-PV 48/3–5, /8, and /13) are interpreted as likely originating from the maxillary region. Between alveoli 4 and 5, the orientation of the mesiodistal axes shifts diagonally, giving the tooth row an "*en echelon*" disposition. Although many teeth are missing and cannot be compared in detail, it is discernible that the anterior elements are larger than those in the posterior region (SOI 2).

A total of 21 tooth positions can be counted in the right dentary (Fig. 14A–14B), which, along with *Ekrixinatosaurus* (19 teeth; Calvo *et al.*, 2004), represents the highest number of dentary teeth reported among abelisaurids. Although the segmentation quality of the right dentary is not optimal, an "*en echelon*" disposition condition is discernible at least in the 7th and 8th teeth, where the mesiodistal orientation of the erupting tooth is oblique relative to that of the more anterior teeth. Although it remains unclear how far posteriorly this condition extends along the tooth row, at least these two teeth exhibit a position closely similar to that observed in *Majungasaurus* (Smith, 2007). The dentary dentition is characterized by anterior crowns that are apicobasally taller than those in the middle and posterior regions of the tooth row. Furthermore, tomographic segmentation reveals that the anterior teeth display a straight to slightly convex distal profile in lateral view, with the apex positioned at mid-crown level or aligned with the distal carina. In contrast, the mid- and posterior teeth exhibit a concave distal profile in lateral view, with the apex positioned further distally relative to the basal portion of the distal margin.

Mesial Dentition. Three isolated teeth, tentatively assigned to the left premaxilla (MMCh-PV 48/1–2 and /6), together with the first tooth of the right maxilla, represent the mesial dentition of *Skorpiovenator* (Fig. 17A–17E). Unfortunately, segmentation from CT data of the dentary teeth has low resolution, which hinders a clear distinction between the mesial and lateral teeth in this bone. Nevertheless, it is possible to discern that only the teeth from the anteriormost portion of the dentary exhibit a mesial morphology (*i.e.*, likely the first four to six teeth). The mesial teeth exhibit relatively strong labiolingual compression, with a CBR ranging from 0.44 to 0.63, values comparable to those observed in other abelisaurids, such as *Rugops* and "*Abelisaurus*" (see Meso *et al.*, 2021a), whose range lies between 0.5 and 0.65 (Hendrickx *et al.*, 2020). This condition contrasts with the Majungasaurinae clade, whose mesial teeth are notably thicker labiolingually, with CBR index ranging from 0.7 to 1 (Hendrickx *et al.*, 2020). Although it is not possible to confidently calculate the CBR of the first tooth of the right maxilla in *Skorpiovenator*, the measured proportions suggest that it was as robust as those of the premaxilla (SOI 2). In general, the mesial teeth are also characterized by being slightly elongate, with CHR values ranging from 1.24 (rmx 1) to 2.08 (lpm indet.), a range very similar to that observed in other abelisaurids. In addition, in lateral view, the mesial dentition of *Skorpiovenator* exhibits weak mesiodistal curvature, with the distal profile of the crown being straight to slightly convex (Fig. 16A, 16C).

Two of the premaxillary teeth (MMCh-PV 48/1 and /6) are slightly recurved linguodistally, whereas the crown of the first right maxillary tooth appears to curve only distally. Both the mesial and distal carinae are present on the mesial dentition, with well-developed denticles visible along the entire length of the crown. The mesial carina extends to the level of the cervical margin, while the distal carina continues slightly further basally. However, the basal extent of the distal carina is not discernible on the crown of the first right maxillary tooth. In the most mesial teeth, both carinae exhibit a slightly sigmoidal curvature and are lingually displaced. MMCh-PV 48/1 and /6 exhibit a salinon-shaped to slightly J-shaped cross-sectional outline at the base of the crown, with a strongly convex prominent labial margin, and a slightly biconcave or sigmoidal lingual margin. This

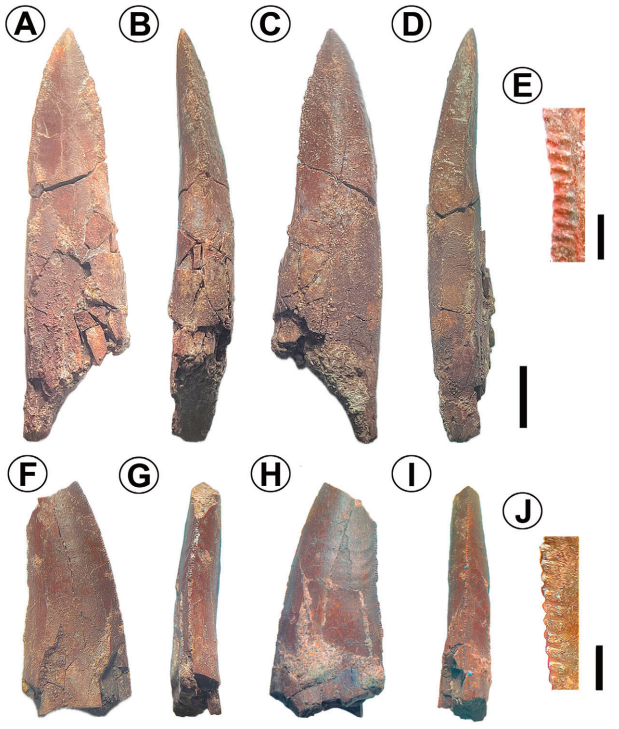


Figure 17. A–J. Loose teeth of ***Skorpiovenator bustingorryi*** **(MMCh-PV 48)**. Mesial tooth in **A,** lingual; **B,** distal; **C,** labial; **D,** mesial views. **E,** mesial tooth, detail of denticles of distal carina. Lateral tooth in **F,** lingual, **G,** distal**, H,** lateral, **I,** mesial views. **J,** lateral tooth, detail of denticles of distal carina. Scale bar equals 1 cm (A–D, F–I) and 1 mm (E–J).

outline results from the presence of apicobasally elongated concave surfaces adjacent to the distal and mesial carinae on the lingual face of the crown. One of these is visible on the labial surface, adjacent to the mesial carina, while the second concave surface is perceptible on the lingual face, adjacent to the distal carina.

Although the roots of the isolated premaxillary teeth are incompletely preserved, the remaining portions are well-preserved and already exceed the crown in length. This suggests that the original root length may have reached approximately 1.5 times the height of the crown. The root tapers apically and exhibits straight to slightly convex mesial and distal profiles in lateral view. The points of maximum convexity are positioned at approximately one-third of the apicobasal height of the root. In mesial or distal view, the long axis of the root in MMCh-PV 48/6 is approximately vertical along the basal two-thirds of its height, gently curving distally in the basal third. In contrast, the roots of MMCh-PV 48/1 and 48/2 are straight along their entire longitudinal extent. At the level of the cervix, a subtle constriction is present between the root and the crown, imparting a concave profile to the mesial and distal margins in lateral view in this portion. This feature is particularly well marked in the most mesial tooth (MMCh-PV 48/6), and slightly less pronounced in MMCh-PV 48/1 and 48/2. The root is hollow and elliptical in cross-section at the basal third of its height in all mesial teeth. A well-defined resorption pit, ranging from shallow to moderately deep, is visible on the lingual surface of each mesial tooth.

Lateral dentition. The description of the lateral dentition of *Skorpiovenator* is based on five isolated teeth (MMCh-PV 48/3–5, /8, and /13), which are tentatively assigned to the maxilla based on their overall morphology (Fig. 17F–17J), and *in situ* teeth of the right and left maxillae (Fig. 2A–2B). The crowns of the lateral dentition differ markedly from those of the mesial dentition in their labiolingual compression (CBR), the position of the carinae along the crown, and the cross-sectional shape at the base of the crown. The isolated teeth are poorly preserved, and the *in situ* teeth of the maxillae (*n.b.*, positioned above the dentary) are difficult to measure due to their preserved position. Additionally, as previously mentioned, the tomographic segmentation of the dentary teeth lacks sufficient resolution. As a result, several measurements—such as the crown base width (CBW)—could not be obtained. Consequently, the labiolingual compression of this dentition could only be tentatively estimated from two teeth, yielding a range of ~0.43 to 0.5. This range is broadly consistent with the lateral dentition of other abelisaurids (Hendrickx *et al.*, 2020). This is further supported by the mid-crown ratio (MCR; SOI 2), which is consistent with the variation observed in other abelisaurids (pers. obs. J.G.M.). Regarding the crown height ratio (CHR), this index exhibits a wide range of variation, from 1.18 (rmx13) to 2.07 (lmx12?), but never exceeds 2.2, as noted by Hendrickx *et al.* (2020). This type of dentition, characterized by apicobasally low crowns, is similar in size to that of some other Gondwanan abelisaurids, such as *Majungasaurus* and *Llukalkan*.

Both the maxillary and dentary teeth exhibit a distal margin that ranges from slightly convex or straight to weakly concave, while the mesial margin is slightly convex (Fig. 17F, 17H). As in the mesial dentition, the lateral crowns exhibit mesial and distal carinae that are denticulate along their entire length. Both carinae extend to the base of the crown or terminate slightly apical to the cervix. The only lateral tooth that preserves a portion of the root (*i.e.*, MMCh-PV 48/3) is poorly preserved, making it difficult to determine whether either the mesial or distal carina extends just below the level of the cervix. Both carinae are centrally positioned on the crown and exhibit a straight apicobasal trajectory. The exception is observed in the two most mesial lateral teeth (MMCh-PV 48/4–5), in which the mesial carina is weakly curved. Although the lingual side of the *in situ* maxillary teeth cannot be observed, their labial halves suggest that their cross-sectional shape is lanceolate to lenticular. This interpretation is consistent with the isolated elements and the majority of the centroposterior dentary series, where the morphology is more readily discernible. Additionally, unlike the mesial teeth, the elements corresponding to the lateral dentition do not exhibit visible longitudinal concavities on the crowns.

Only the specimen MMCh-PV 48/3 preserves a substantial, albeit incomplete, portion of the root, revealing a slight constriction between the crown and the root. Although it is incompletely preserved, it is possible to discern that both the mesial and distal margins are slightly convex in lateral view, a condition also observed in the mesial dentition. Additionally, in mesial or distal view, the basal

portion curves distally, resembling the condition described for the mesial teeth. As for the resorption pit, it appears to be broader; however, due to taphonomic labiolingual compression, its depth cannot be accurately determined.

On the labial margin of the left maxilla, at the level of tooth positions 9 and 10, the tip of a supernumerary tooth is emerging (SOI 1, Fig. S4).

Denticles. The denticle densities in the dentition of *Skorpiovenator* are higher at the bases of both the mesial and distal carinae, particularly in the most mesial lateral teeth, where values reach up to 25 denticles per 5 mm on the mesial base (MB) and 20 on the distal base (DB) (see SOI 2). These densities gradually decrease towards the apex, with apical values ranging from 10 to 13 denticles per 5 mm. The best-preserved premaxillary teeth show consistent values between carinae, ranging from 14 to 16 at the base and decreasing apically (SOI 2). This pattern is also observed in several lateral teeth, where the mesial and distal carinae maintain similar denticle densities along their length. Although data for many maxillary teeth are missing due to preservation, available values suggest a relatively stable denticle size ratio between mesial and distal carinae, with no abrupt or irregular variation. It is noteworthy that the premaxillary tooth MMCh-PV 48/6 exhibits a DSDI of 1, while two isolated teeth identified as the most mesial lateral elements (MMCh-PV 48/4–5) show values ranging from 0.85 to 1. Similarly, elements MMCh-PV 48/8 and 48/13 both yield a DSDI of 1, as does the right maxillary tooth mx7. The tomographic segmentation of the dentary teeth lacks sufficient resolution, preventing detailed observation of any denticle-related features.

Both the mesial and lateral dentition of *Skorpiovenator* are characterized by denticles that share the same overall morphology (Fig. 17E, 17J). Denticles along the mesial carina are perpendicular to slightly mesially inclined. They present a subquadrangular profile in lateral view (Fig. 17E, 17J) and are mesiodistally longer than they are apicobasally tall (DHR equal to 1.5). The external margin of denticles exhibits a parabolic outline, symmetrically to asymmetrically convex in lateral view. While the denticles of the distal carina share a similar overall shape, they differ in being even more elongated mesiodistally relative to their apicobasal height (*n.b.*, with DHR index between 1.8 and 2). Furthermore, the denticles are more strongly inclined relative to the external margin of the crown, and their external profiles appear distinctly asymmetrical in lateral view. Nevertheless, the interdenticular space is narrow between mesial denticles and broad between distal denticles.

Crown ornamentation and enamel surface texture. The enamel surface texture of both mesial and lateral crowns is irregular and lacks any clear orientation. In the mesial dentition (*e.g.*, MMCh-PV 48/6), marginal undulations are present on the lingual surface; these structures are mesiodistally narrow, obliquely oriented, and positioned adjacent to the mesial carina. In contrast, the lateral dentition exhibits marginal undulations adjacent to both mesial and distal carinae on the lingual surface, as well as along the distal margin of the labial surface (Fig. 17H). The marginal undulations near the distal carina are mesiodistally longer than those associated with the mesial carina, with their distalmost ends angled apically. Additionally, the lateral crowns display faint, well-organized transverse undulations, typically occurring in groups of three, with noticeable spacing between adjacent groups.

DISCUSSION

Character analysis: *Skorpiovenator* cranial autapomorphies

The following list details the original characters proposed as autapomorphic of *Skorpiovenator* in its initial description (Canale *et al.*, 2009). Given the significant expansion of our knowledge regarding abelisaurid anatomy since then, we re-evaluate these originally proposed traits and propose new autapomorphies in this present work.

(1) Ascending process of maxilla homogeneously wide rostro-caudally. The maxilla of *Skorpiovenator* exhibits an ascending process that originates vertically from the main body of the bone, consistent with other abelisaurids. However, it is notably broad rostrocaudally. In other abelisaurids, this process typically presents a triangular outline, tapering distinctly dorsally. This morphology is observed in *Carnotaurus*, *Majungasaurus*, *Kryptops*, *Ekrixinatosaurus*, and *Spectrovenator*. While this region of the maxilla is partially incomplete in *Rugops* and *Tralkasaurus*, the preserved portions suggest a triangular morphology similar to that of other abelisaurids. In *Skorpiovenator*, the ventral portion of the ascending process is remarkably wide, extending to the level where it turns caudally along

the nasal. This morphology appears to be unique and thus represents an autapomorphy for *Skorpiovenator*.

(2) Maxillary horizontal ramus dorsoventrally deep with subparallel dorsal and ventral margins. Although abelisaurids possess deep skulls and consequently deep maxillae, they usually exhibit maxillary bodies that acuminate posteriorly towards their contact with the jugal. In *Skorpiovenator*, the dentigerous margin of the maxilla and the dorsal border are subparallel, resulting in a maxillary body that remains homogeneously deep through its anteroposterior length. Conversely, the maxillae of *Majungasaurus*, *Rugops*, *Kryptops*, *Llukalkan*, *Tralkasaurus*, *Aucasaurus*, and *Ekrixinatosaurus* feature a maxillary body that tapers posteriorly towards the contact with the jugal. In *Carnotaurus*, the dorsal margin is extremely short and slightly curved, as it continues ventrally toward the curvature of the anterior margin of the antorbital fenestra. Therefore, we retain this character as autapomorphic of *Skorpiovenator*.

(3) Maxilla/jugal contact subvertical. The strong inclination of the maxilla/jugal contact of more than 45° with respect to the anteroposterior axis of the skull is a character widely distributed in Abelisauridae (Canale *et al.*, 2009; Pol *et al.*, 2024). Although the contact between the maxilla and jugal is extremely inclined in *Skorpiovenator*, it does not differ greatly from the condition observed in *Carnotaurus*, where the central sector of the suture is almost subvertical (Cerroni *et al.*, 2020a, fig. 5). For this reason, we consider this character more widely distributed in Abelisauridae, and it no longer forms part of the diagnosis of *Skorpiovenator*.

(4) 19 maxillary teeth. The number of maxillary teeth is variable among the different species of ceratosaurs, being 12 in *Carnotaurus*, 15 in *Ceratosaurus*, 16 in *Ekrixinatosaurus*, 17 in *Majungasaurus* and 18 in *Spectrovenator*. Although *Rugops* has been suggested to possess more than 20 maxillary teeth (Hendrickx *et al.*, 2020), the holotype preserves 17 teeth, with space potentially available for one additional small tooth. With 19 teeth, *Skorpiovenator* stands out as the abelisaurid with the highest number of maxillary teeth. Although intraspecific ontogenetic variations regarding the number of teeth have been reported in different groups of theropods (Rauhut & Fechner, 2005; Kundrat *et al.*, 2008; Bever & Norell, 2009), including the extreme case of the abelisauroid elaphrosaurine *Limusaurus* where juveniles with complete dentition become completely toothless adults (Wang *et al.*, 2017), the number of teeth in adults appears not to vary. This is observed in *Majungasaurus*, where two maxillae belonging to adult specimens share the same number of alveoli (Sampson & Witmer, 2007). For this reason, this character is maintained in the diagnosis of *Skorpiovenator*.

(5) Lacrimal rostrally projected and with a well-developed suborbital process. This could be separated into two different characters. Regarding the rostral projection of the lacrimal, by the time *Skorpiovenator* was published, this trait represented a novelty. Although *Ceratosaurus* shows a well-developed rostral projection, the overall morphology of the lacrimal is primitive. This bone bears a well-developed fossa and lacks the dermal lamina that covers its lateral surface. However, restricting the comparison to abelisaurids, the Early Cretaceous *Spectrovenator* shows an anterior process of the lacrimal, closely resembling that of *Skorpiovenator*. Furthermore, even *Llukalkan* possesses a small anterior process (besides the long anteromedial projection also observed in *Majungasaurus*). Regarding the suborbital process—a rounded posteriorly directed projection over the posterior margin of the lacrimal which forms the anteroventral margin of the orbit—this feature is not exclusive to *Skorpiovenator*. It is also present in *Spectrovenator*, *Abelisaurus*, *Majungasaurus*, and *Rugops*. Consequently, this character has a wider distribution within Abelisauridae and cannot be considered autapomorphic.

(6) Quadratojugal with pronounced caudal notch. This character refers to the concavity formed between the posterior margin of the dorsal process and the dorsal margin of the posterior process of the quadratojugal in lateral view. Those borders form an angle of approximately 120 degrees between them. When comparing this morphology with that of *Majungasaurus*, *Carnotaurus*, or even non-ceratosaurian theropods such as *Allosaurus*, there is no significant difference among them. Thus, we consider this a non-informative character.

(7) Dentary with caudoventral process bifurcated to receive rostral end of angular. The abelisaurids are characterized, almost since their recognition as a distinct clade, by the enlargement of the mandibular fenestra and a loose contact between dentary and postdentary bones, among other characters (Bonaparte, 1991).

In the original description of *Skorpiovenator*, one of the

synapomorphies was related to an apparently more extensive contact between angular and dentary, through a bifurcation of the latter bone, which receives the most rostral end of the angular. Subsequent preparation of the material, which exposed the left dentary, revealed that the splenial is exposed laterally on both dentaries. Due to preservational artifacts, this exposed portion was previously interpreted as the ventral "process" of the supposed bifurcation on the right dentary. The ventrolateral exposure of part of the splenial was also reported for *Spectrovenator* (Zaher *et al*., 2020) and *Majungasaurus* (Sampson & Witmer, 2007). Due to this anatomical misinterpretation, this character is removed from the diagnosis of *Skorpiovenator*.

(8) Angular with rostral end dorsoventrally deep to fit between splenial and prearticular: In abelisaurids, the splenial and prearticular bones show an extensive contact on the medial side of the mandible, as it can be seen in *Spectrovenator*, *Carnotaurus* and *Majungasaurus*. In *Skorpiovenator*, the angular shows an anterodorsally oriented spike that interposes in the ventral part of the contact between the splenial and prearticular. This morphology remains unique to *Skorpiovenator* among known ceratosaurians; it is therefore retained as a valid autapomorphy for this species.

Autapomorphic characters recognized in this work

(1) Antorbital fossa restricted to the maxilla. Nasal and lacrimal without development of antorbital fossa (Fig. 5A–5C). Within Ceratosauria, considerable variation exists in the development and morphology of the antorbital fossa across the maxillary, nasal, and lacrimal bones. Specifically in abelisaurids, this fossa primarily develops on the maxilla, and partially on the lacrimal, where it is partly covered laterally by dermal overgrowths, although it remains faintly visible. In *Majungasaurus*, this fossa also extends onto the central portion of the nasal bone, which is highly apomorphic and strongly pneumatized. In *Skorpiovenator*, the fossa is greatly reduced and is present only in the rostral portion of the ascending process of the maxilla, being absent in the nasal and lacrimal. This character is challenging to ascertain in several abelisaurid species, as the ascending process of the maxilla is often apically incomplete, which hinders the estimation of the dorsal extent of the fossa. However, in some cases, such as *Rugops*, despite the incomplete maxilla, the lacrimal is also preserved with a developed antorbital fossa, leading to the inference that it was present throughout its dorsal extent beneath the nasal.

(2) Double dorsal protuberances over each frontal bone (Figs. 2.D, 6.A). Frontal ornamentations are common within the clade Abelisauridae, including midline domes as seen in *Majungasaurus* and *Rajasaurus*. South American forms may exhibit low lateral protuberances, such as in *Abelisaurus*, *Aucasaurus*, or *Niebla*, or developed horns, as in *Carnotaurus*. In *Skorpiovenator*, however, the frontals bear paired lateral protuberances on each side. There is a larger, more posterior protuberance, located near the anterior margin of the supratemporal fenestra, which appears to be homologous to those found in other aforementioned abelisaurids. Uniquely, a smaller protuberance is positioned at the level of the lacrimal-postorbital contact, a feature not observed in other related species.

(3) Quadratojugal with a thick jugal process that is rounded in cross-section, laterally procumbent, and covered by strong external rugosities (Figs. 2.E, 8.E-8.F, 15.B). The jugal process of the quadratojugal in abelisaurids exhibits diverse morphologies, although its development generally parallels that of the squamosal process in lateral view. It is typically relatively flat or possesses a gentle lateral curvature, as observed in *Carnotaurus* and *Abelisaurus*. In *Skorpiovenator*, however, the lateral margin of the lower bony temporal bar, predominantly formed by the jugal process of the quadratojugal, is strongly projected laterally with a pronounced curvature. The cross-section of this process is semicircular, being wider mediolaterally than it is tall dorsoventrally. Furthermore, its dorsolateral surface is covered by strong, elongated, and vertical prominences and rugosities, indicating a robustly developed muscle attachment area.

(4) 21 dentary teeth (Fig. 13A–13B, 14A–14B). One of the characteristics of *Skorpiovenator* that could only be observed through CT scans is related to the number of dentary teeth. As with the maxillary dentition, the number of teeth in the dentary varies significantly among different abelisaurid species, with 15 counted in *Carnotaurus*, 16 in *Spectrovenator*, and 17 in *Majungasaurus*. With 21 dentary teeth, *Skorpiovenator* possesses the highest alveolar count in the dentary among abelisaurids, which is here proposed as a new autapomorphic character for this taxon.

(5) Retroarticular fossa of the articular anteroposteriorly longer than lateromedially wide, divided by a strongly oblique crest (Fig. 15E–15F). The retroarticular fossa is a depression located on the dorsal surface of the articular bone, posterior to the glenoid cavity in the lower jaw. In most ceratosaurians, this depression is wider lateromedially than it is long anteroposteriorly, or it presents subequal dimensions, as observed in *Ceratosaurus*, *Spectrovenator*, *Majungasaurus*, and *Carnotaurus*. This fossa is often divided by a sharp crest, which in *Carnotaurus*, for example, lies almost transversally to the main axis of the jaw (Cerroni *et al.*, 2020a, fig. 27). In *Skorpiovenator*, however, the fossa is considerably longer than wide and is divided by a strongly oblique crest.

Phylogenetic analysis

Based on the data matrix published by Pol *et al.* (2024), we rescored 47 cranial characters for *Skorpiovenator* (most of which were previously coded as missing data; see SOI 1, Text S3), and changed several states for skull characters in various abelisaurid taxa based on our own observations (see SOI 1, Text S2). We added nine cranial characters and modified two existing ones, all detailed in the SOI 1, Text S1. The heuristic search was performed under equal and implied weighted parsimonies, in order to find optimal results. Although implied weighting yielded trees with improved resolution, all the analyses show broadly similar topologies, especially regarding the phylogenetic position of *Skorpiovenator* (SOI I, Fig. S5).

For the equal weights, we ran the phylogenetic analysis using the exact same parameters used by Pol *et al.* (2024), which resulted in more than 10000 MPTs (overflow), with a length of 590 steps, a best score hit of 59 out of 1000, a CI of 0.483, and an RI of 0.730. After a second round of TBR found more than 99999 MPTs. The subsequent consensus tree shows a huge polytomy that includes all ceratosaurs plus Ceratosauridae (*Genyodectes* + *Ceratosaurus*). We applied the iterPCR method in order to find the unstable taxa, which resulted in the identification of the following nine OTUs: *Thanos*, *Kurupi*, *Elemgasem*, *Quilmesaurus*, *Afromimus*, *Kryptops*, *Huinculsaurus*, *Dahalokely*, and the Abelisauridae indet. MPCN-PV 69. When these taxa are pruned, the reduced consensus shows a well-resolved topology, with polytomies at the base of Noasauridae, the node that reunites *Genusaurus*, *Rugops*, and the clade formed by Majungasaurinae + Brachyrostra, and within Furileusauria. This uncertainty of internal relationships is mirrored in the low nodal support values, recovering a Bremer index higher than 1 only for the clades Neotheropoda (v. 3), Averostra (v. 2), Ceratosauria (v. 2), Elaphrosaurinae (v. 2), the clade that includes *Elaphrosaurus* + CGCCG_20011 (v. 2), and Abelisauridae (v. 2). Resampling methodology also shows low support (see Bootstrap and Jackknife GC values in Supplementary Material), with a single Bootstrap absolute value higher than 50% retrieved for the clade Theropoda (v. 98; see Supplementary Material) and Jackknife values above 50% reported for Theropoda (v. 98), Ceratosauria (v. 50), and the clade that includes *Elaphrosaurus* + CGCCG_20011 (v. 56) (see SOI 1, Fig. S5).

For the implied weighted parsimony, we used a range of concavity constant values (k) of 3, 6, 9, and 12; the results obtained with $k = 3$ outperformed the rest (see SOI 1, Fig. S5). With Piwe = 3, the best score hit was achieved in 217 of 1000 replicates, resulting in 2130 trees with a length of 61.175. A second round of TBR found more than 99999 (overflow). We applied the iterPCR method in order to identify the unstable taxa, and after that we used the command "Unique" that eliminates the duplicated MPTs, leaving 141 trees. The reduced consensus of this analysis shows a well-resolved topology (Fig. 18), similar to that obtained with equal weight, but with the following main differences.

The internal relationships within Noasauridae are better resolved, with a recovered subclade uniting *Masiakasaurus*, *Noasaurus*, and *Afromimus*. An unexpected result is that the fragmentary taxon *Quilmesaurus*, previously considered an abelisaurid (Juárez Valieri *et al.*, 2007; Tortosa *et al.*, 2014; Aranciaga Rolando *et al.*, 2020) is recovered within Noasauridae. This taxon was excluded as unstable under the iterPCR method in the equal weights analysis. Another notable difference is the Cenomanian taxon from Patagonia, *Xenotarsosaurus*, which occupies a position at the base of Abelisauridae alongside *Eoabelisaurus*, whereas in the equal weights analysis it is recovered as a derived taxon within Furileusauria. Finally, the relationships within Furileusauria are better resolved, with *Abelisaurus* as the basal taxon and two subclades, one formed by *Aucasaurus*, *Llukalkan*, and *Viavenator*, and the other comprising *Carnotaurus*, *Pycnonemosaurus*, *Niebla*, and *Koleken*.

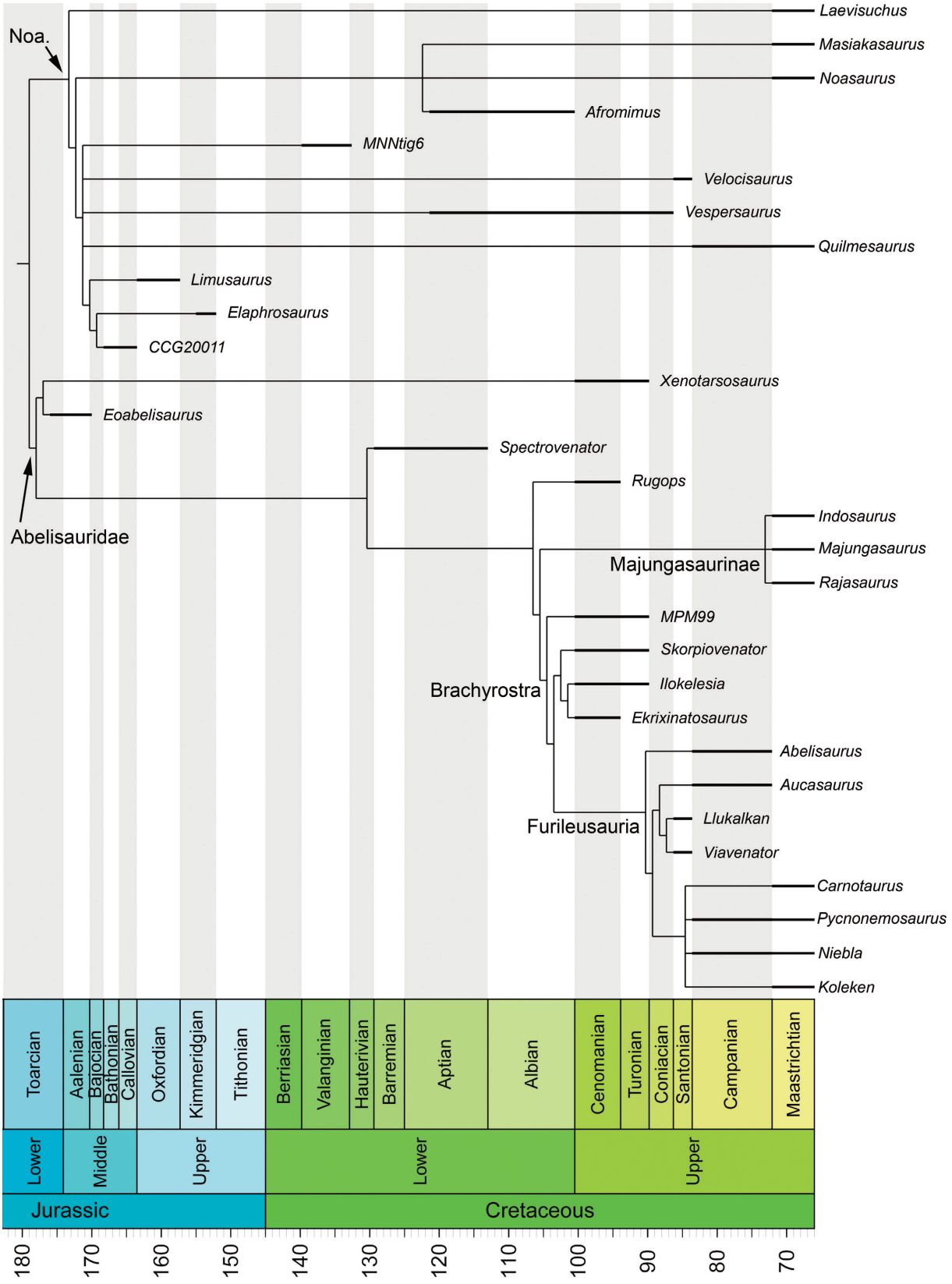


Figure 18: Time calibrated reduced strict consensus tree of Ceratosaurian theropods, showing the phylogenetic relationships of ***Skorpiovenator bustingorryi***, after the exclusion of the taxa *Thanos*, *Kurupi*, *Elemgasem*, MPCN-PV 69, *Rahiolisaurus*, *Kryptops*, *Genusaurus*, *Dahalokely* and *Arcovenator*. Obtained under implied weighting parsimony of the matrix (k = 3). Abbreviation: Noa. = Noasauridae.

One of the most remarkable general differences compared to the results of the original dataset published by Pol *et al.* (2024) is the position of *Abelisaurus*. Here, it is not recovered as a Majungasaurinae, but deeply nested within Brachyrostra as a Furileusaurian. Some of the characters present in this taxon that support this new placement are the knob located over the dorsalmost postorbital–squamosal contact (char. 42; state 1) and the depression present over the lateral surface of the squamosal (char. 248; state 1). Pol and collaborators (op cit.) already noted the weak support of the previously reported affinities between *Abelisaurus* and Majungasaurines. Given this new topology, the synonymy between Majungasaurinae and Abelisaurinae proposed in that work is no longer valid.

Skorpiovenator, previously recorded as a basal brachyrostran by Pol *et al.* (2024), is nested in a distinct clade of Cenomanian—Turonian abelisaurids, with *Ilokelesia* and *Ekrixinatosaurus*. This node is supported by the following synapomorphies: 6 (0): Anterior ramus of the maxilla absent, 27 (1): bulge on the anteromedial rim of supratemporal fossa, 39 (1): Postorbital, strongly inflated and bulked dorsal margin, 43 (1): Angle between dorsal margin of upper temporal arc, formed by the posterior process of postorbital and anterior process of squamosal of more than 45°, 120 (1): postzygodiapophyseal lamina in mid-cervical vertebrae reduced, indicated by a low ridge in parts, 253 (1): Angular process of surangular located close to the anterior end.

This mid- to large-sized abelisaurid clade, known until now only from the Neuquén Province in North Patagonia, is positioned as the sister taxon to the later-diversified Furileusauria. It was likely impacted by the Turonian extinction event, which eradicated carcharodontosaurid and spinosaurid theropods, as well as rebbachisaurid sauropods, in the Southern Hemisphere.

Skull traits discussion

Skull ornaments and ornamentation. As observed in abelisaurid skulls in general (Sampson & Witmer, 2007; Novas, 2009), *Skorpiovenator* possesses facial bones covered by a wide variety of ornamentation, as previously described for each particular bone, including grooves, crests, foramina, and protuberances that give it a rugose appearance. As a general pattern, most of the cranial bones exhibit a primary ornamentation consisting of rounded rugosities surrounded by anastomosing grooves. This texture is present on the premaxilla, lateral crests of the nasal, lacrimal, postorbital, jugal, quadratojugal, and angular bones, as well as on the lateral surface of the splenial. In contrast, the maxilla and, to some extent, the dentary are ornamented by elongated horizontal and vertical crests and grooves. These ornamentations would represent mineralized dermis, marking the locations where the integument and the underlying bone would have been essentially fused (Hieronymous & Witmer, 2004; Sampson & Witmer, 2007).

Ceratosaurian theropods are well-known for their tendency to develop varied and enlarged cranial ornaments of several shapes and sizes, such as the median nasal crest of *Ceratosaurus*, the frontal prominences of *Abelisaurus* and *Aucasaurus*, the large frontal horns of *Carnotaurus*, or the midline boss of *Majungasaurus* and *Rajasaurus*. The aforementioned taxa generally represent medium- to large-sized forms. In this context, a positive correlation between cranial ornamentation and large body size has been proposed for theropod dinosaurs (Gates *et al.*, 2016). Furthermore, a pulse of high evolutionary rates towards the end of the Early Cretaceous has been suggested, marked by the emergence of features typical of Cretaceous abelisaurids, such as a tall and short skull with heavily ornamented dermal bones (Pol *et al.*, 2024). Regarding the distinct types of cranial ornamentation, Carrano and Sampson (2008) posited that within Ceratosauria, these structures lack systematic value, being instead species-specific and exhibiting low taxonomic relevance. It is important to note that the diversity of the group was considerably lower at that time. Specifically concerning *Skorpiovenator*, Delcourt (2018) stated that its frontals, like those of *Ekrixinatosaurus*, are flat, suggesting a basal position relative to Furileusauria. However, as demonstrated in this study, *Skorpiovenator* possesses frontal prominences similar to those found in *Abelisaurus*, *Aucasaurus*, or *Niebla*. Moreover, the lateral prominences of *Skorpiovenator* are double, a unique trait of this taxon, as discussed previously. Firsthand observations of the *Ekrixinatosaurus* holotype reveal the presence of such lateral protuberances as well. Based on the phylogenetic analysis conducted here, the presence of paired protuberances on the frontals is inferred to be a synapomorphy for all Brachyrostra more derived than *Arcovenator* (Char. 24: 2). This trait, therefore, represents a common feature among

South American forms, and it is apomorphically developed to an extreme degree in *Carnotaurus*.

Another notable character of *Skorpiovenator* is the presence of anteroposteriorly elongated protuberances with papillary ornamentation on the anterior end of the nasals. Although preservation of this region is relatively poor, certain preserved sections indicate they constituted two low and elongated crests. In the Cenomanian abelisaurid *Rugops* from Niger, two areas with similar ornamentation are observed, though they are not as developed as in *Skorpiovenator*. This difference could be attributed to the apparently juvenile state of the specimen, suggesting these structures might have achieved greater development later in ontogeny, perhaps similar to that seen in *Skorpiovenator*. These paired, low, and deeply ornamented crests, perhaps covered by an "armor-like dermis" (Hieronymus *et al.*, 2009; Delcourt, 2018), contribute to the diverse types of cranial structures present in ceratosaurians. It is important to highlight that both *Skorpiovenator* and *Rugops* exhibit a transversely concave nasal bone configuration with a series of developed foramina, in addition to sharing the fenestra between the frontal, postorbital, and lacrimal. It is possible that the basal phylogenetic position of *Rugops* is an artifact of the juvenile condition of this taxon, and it might be more closely related to other Cenomanian forms such as *Skorpiovenator*, *Ekrixinatosaurus*, or *Ilokelesia*.

Mandibular fenestra. Another distinctive characteristic of *Skorpiovenator*, which was misinterpreted in the original publication (Canale *et al.*, 2009), concerns the development of the mandibular fenestra. It was described as small and with extensive articulation between dentary and surangular. At that time, only the right side of the specimen was studied, where this region is somewhat deformed and poorly visible. As explained above, the lateral exposure of the splenial was erroneously interpreted as an extra reinforcement for the dentary. On the left side of the specimen, however, this region is better preserved, revealing a large mandibular fenestra with a reduced articulation between the dentary and the post-dentary bones. These features are present in other Late Cretaceous abelisaurids, such as *Carnotaurus* or *Majungasaurus* (and possibly the noasaurid *Masiakasaurus*), and have been interpreted as related to some form of intramandibular movement, a limited and passive kinesis (Bonaparte, 1991; Sampson & Witmer, 2007). Based on these observations from *Skorpiovenator*, it can be established that these mandibular characteristics were already present in abelisaurids by at least the early Late Cretaceous.

Antarticular bone. A noteworthy feature is the presence of this small additional ossification on the articular bone of the mandible. The antarticular was first recognized and named for a theropod by Madsen (1976) on his osteology of *Allosaurus fragilis*, and was later identified in *Allosaurus jimmadseni* (Chure & Loewen, 2020). Its presence was also postulated for the tyrannosaurid *Bagaraatan* (Osmólska, 1996), although this was subsequently reinterpreted as an artifact resulting from a breakage of the medial edge of the surangular (Słowiak *et al.*, 2024).

Regarding the nature of the antarticular, Madsen (1976) noted its resemblance to mammalian sesamoids without inferring homology. We agree that the most plausible hypothesis is that it represents a sesamoid bone. Sesamoids have been defined as "*periarticular skeletal elements, which initially form in juxtaposition to or independently of bones and joints. They are commonly related to tendons and ligaments, have a genetic basis and, once they are formed, epigenetic stimuli drive their growth and development to the acquisition of their definitive tissue composition, which can be diverse, for example, cartilage, fibrocartilage, or bone*" (Abdala *et al.*, 2019). These elements are positioned to envelop bony prominences (Sarin *et al.*, 1999); as incompressible tissues, they prevent the flattening of ligaments and tendons (Tsai & Holliday, 2011). Their occurrence is typically associated with postcranial articulations and more rarely with the skull. Regarding the latter, the most common records are in Osteichthyes fish, and within Tetrapoda, in amphibians, squamates, crocodylians, and birds (Abdala *et al.*, 2019). Specifically, associated with the craniomandibular articulation, this type of structure has been described in salamanders (Ponssa & Abdala, 2020) and in various bird species and groups (Vanden Berge & Storer, 1995), such as the passerine *Callaeas cinerea* (Burton, 1973), the coraciiform *Momotus momota* (Korzun *et al.*, 2004), and charadriiforms of the family Thinocoridae (Korzun *et al.*, 2009).

In the case of the elements recognized in *Skorpiovenator* and *Allosaurus*, their location—coupled with the fact that they are ossifications clearly separate from the articular rather than overgrowths, and considering records of similar

structures in other tetrapod groups, particularly birds—strongly suggests they correspond to sesamoid bones. This element likely ossified within the internal jugomandibular ligament, as occurs in the aforementioned avian examples. This ligament would have undergone considerable compression against the medial condyle of the quadrate during jaw closure and feeding. As is characteristic of sesamoids, while they have a genetic basis, their ultimate formation is related to mechanical stress.

The occurrence in *Skorpiovenator* represents the first record of such an element associated with the craniomandibular articulation in a theropod outside Tetanurae. This highlights that a feature so widely distributed in various extant bird groups is present in a theropod clade phylogenetically distant from the avian lineage, such as Abelisauridae.

Dentition. The dentition of *Skorpiovenator* exhibits clear adaptations for a carnivorous diet, consistent with a lifestyle involving a selective or specialized feeding strategy. The combination of apicobasally low crowns, elongated roots, and a constriction between the crown and root suggests that these teeth were capable of withstanding high mechanical stresses in multiple directions (Hendrickx *et al.*, 2019). The mesial carina is serrated and extends to the cervix, while the denticles on both mesial and lateral teeth are slightly apically inclined. This morphology allows the crown to penetrate deeply into flesh along its entire height, resulting in significant wounds (Hendrickx *et al.*, 2019). The constriction between the crown and root, combined with a basal cross-section of the crown shaped like a salinon or a J-profile, further enhances resistance to multi-directional stresses. Additional structural reinforcements may be provided by marginal undulations and transverse enamel ridges (Hendrickx *et al.*, 2019).

Together, this dental morphology, in conjunction with the cranial, cervical, and postcranial anatomy of *Skorpiovenator*, as well as that of *Majungasaurus* and *Carnotaurus*, likely indicates that these abelisaurids were hypercarnivorous ambush predators that engaged in "bite-and-hold" or "head-hunting" strategies (Therrien *et al.*, 2005; Sampson & Witmer, 2007; Snively & Russell, 2007; Delcourt, 2018; Meso *et al.*, 2021a, b). Nevertheless, certain features suggest that *Skorpiovenator* may have exhibited a more specialized or selective feeding behavior. For instance, the crown base ratio (CBR) values in both mesial and lateral teeth are lower than in any other known abelisaurid. Furthermore, *Skorpiovenator* possesses the highest number of teeth in both the maxilla and dentary among members of its clade.

CONCLUSIONS

This work presents a detailed anatomical description of the only known skull of the abelisaurid species *Skorpiovenator bustingorryi* from the early Late Cretaceous of Patagonia, Argentina. This work expands upon previous descriptions and also provides novel information regarding anatomical sections whose technical preparation was recently completed, including data obtained through CT scans. *Skorpiovenator* represents a unique abelisaurid theropod, largely characterized by a set of derived cranial traits. Among those recognized in the present work are the high number of teeth in both the maxilla and dentary (higher than in any other known abelisaurid), the reduced antorbital fossa on the maxilla, and the thick and pronounced lateral "cheek" formed by the jugal and quadratojugal.

The phylogenetic analysis conducted here places *Skorpiovenator* as a brachyrostran abelisaurid, forming a small clade with other Cenomanian Patagonian taxa such as *Ekrixinatosaurus* and *Ilokelesia*. Some synapomorphies supporting this clade include the complete absence of the anterior maxillary process and the strongly oblique dorsal sector of the postorbital-squamosal complex. This small clade of abelisaurids, which represents the sister group to the more diversified, later-occurring Furileusauria, appears to have been affected by the Turonian extinction event.

Among the specific cranial features of *Skorpiovenator* are its paired frontal prominences, a character recovered here as synapomorphic for brachyrostrans more derived than *Arcovenator*. Moreover, the prominences of *Skorpiovenator* are double on each side, which represents another autapomorphic trait of this species recognized in this study. Furthermore, the anterior portion of the nasals exhibits low, anteroposteriorly elongated protuberances characterized by a dense papillary ornamentation. This characteristic is shared with the Cenomanian abelisaurid *Rugops* from Niger. A key reinterpretation of the original work on *Skorpiovenator* concerns the size of the mandibular fenestra, which is here

reconstructed as wide, with loose contacts between the dentary and postdentary bones, similar to that observed in Late Cretaceous abelisaurids such as *Carnotaurus* and *Majungasaurus*.

Notably, the presence of a small extra bone positioned dorsal to the articular has been identified as a sesamoid antarticular. Similar sesamoids occur in various extant vertebrate groups, particularly in birds, where they occupy an identical position. This constitutes the first record of a sesamoid bone associated with the craniomandibular articulation in a non-tetanuran theropod dinosaur.

ACKNOWLEDGMENTS

We are deeply thankful to the technicians Rogelio Zapata, Andrés Moretti, Christian Albornoz, María Castro, Javier Ochoa, Francisco Castro, Marta Soto, Mara Ripoll, Natalia Gonzalez for their help during the excavation and technical preparation of the specimen, especially Javier "Sapo" Ochoa for the disarticulation of the skull from the neck and in-depth preparation of the skull. We also thank Dr. Agustín Scanferla, the discoverer of the holotype specimen of *Skorpiovenator*. Thanks to the late Manuel Bustingorry, and his family for allowing us to enter his property. Thanks to Dr. Ignacio "Nacho" Cerda, for his insights and bibliography contribution regarding the identification of the sesamoid antarticular bone. Thanks to Diego Pol and Martín Ezcurra for the invitation to participate in this special volume of Ameghiniana. We are also grateful to Jorge A. Gonzalez for his skillful drawings of the retrodeformed version of the skull. We are deeply grateful to the Clínica Moguillansky (Neuquén city), especially to Dra. Graciela Bianchi, Dr. Gustavo Cuevas, technical coordinator Eliana Guareschi, and the technician Angeles Antiao, who made possible the CT scanning of *Skorpiovenator*. We also thank Luciano Pradelli and an anonymous reviewer for providing important suggestions on the manuscript. This research was financially supported by the Municipalidad of Villa El Chocón (to JIC)

REFERENCES

Abdala, V., Vera, M. C., Amador, L. I., Fontanarrosa, G., Fratani, J., & Ponssa, M. L. (2019). Sesamoids in tetrapods: the origin of new skeletal morphologies. *Biological Reviews*, *94* (6), 2011–2032.

Aranciaga-Rolando, A. M., Cerroni, M. A., Marsà, J. A. G., Motta, M. J., Rozadilla, S., Brisson Egli, F. B., & Novas, F. E. (2021). A new medium-sized abelisaurid (Theropoda, Dinosauria) from the Late Cretaceous (Maastrichtian) Allen Formation of Northern Patagonia, Argentina. *Journal of South American Earth Sciences*, *105*, 102915.

Baiano, M. A., Coria, R. A., & Cau, A. (2020). A new abelisauroid (Dinosauria: Theropoda) from the Huincul Formation (lower Upper Cretaceous, Neuquén Basin) of Patagonia, Argentina. *Cretaceous Research*, *110*, 104408. https://doi.org/10.1016/j.cretres.2020.104408

Baiano, M. A., Coria, R. A., Canale, J. I., & Gianechini, F. A. (2021). New abelisaurid material from the Anacleto Formation (Campanian, Upper Cretaceous) of Patagonia, Argentina, shed light on the diagnosis of the Abelisauridae (Theropoda, Ceratosauria). *Journal of South American Earth Sciences*, *110*, 103402.

Baiano, M. A., Coria, R., Chiappe, L. M., Zurriaguz, V., & Coria, L. (2023). Osteology of the axial skeleton of *Aucasaurus garridoi*: phylogenetic and paleobiological inferences. *PeerJ*, *11*, e16236.

Baiano, M. A., Pol, D., Bellardini, F., Windholz, G. J., Cerda, I. A., Garrido, A. C., & Coria, R. A. (2022). *Elemgasem nubilus*: a new brachyrostran abelisaurid (Theropoda, Ceratosauria) from the Portezuelo Formation (Upper Cretaceous) of Patagonia, Argentina. *Papers in Paleontology*, *8*(5), e1462.

Bapst, D. W., (2012). Paleotree: an R package for paleontological and phylogenetic analyses of evolution. *Methods in Ecology and Evolution 3*, 803–807.

Barsbold, R., & Osmólska, H. (1999). The skull of *Velociraptor* (Theropoda) from the Late Cretaceous of Mongolia. *Acta Palaeontologica Polonica*, *44*(2), 189–219.

Berge, J. C. V., & Storer, R. W. (1995). Intratendinous ossification in birds: a review. *Journal of Morphology*, *226*(1), 47–77.

Bever, G. S., & Norell, M. A. (2009). The perinate skull of *Byronosaurus* (Troodontidae) with observations on the cranial ontogeny of paravian theropods. *American Museum Novitates*, *3657*, 1–51.

Bonaparte, J. F. (1985). A horned Cretaceous carnosaur from Patagonia. *National Geographic Research*, *1*, 149–151.

Bonaparte, J. F., & Novas, F. E. (1985). *Abelisaurus comahuensis*, n.g., n.sp., Carnosauria from the Late Cretaceous of Patagonia. *Ameghiniana*, *21*, 259–265.

Bonaparte, J. F. (1991). The Gondwanian theropod families Abelisauridae and Noasauridae. *Historical Biology*, *5*, 1–25.

Burton, P. (1973). Structure of the depressor mandibulae muscle in the Kokako *Callaeas cinerea*. *Ibis*, *115*, 138–140.

Calvo, J. O., Rubilar-Rogers, D., Moreno, K. (2004). A new abelisauridae (Dinosauria: Theropoda) from northwest Patagonia. *Ameghiniana*, *41*(4), 555–563.

Canale, J. I., Scanferla, C. A., Agnolín, F. L., & Novas, F. E. (2009). New carnivorous dinosaur from the Late Cretaceous of NW Patagonia and the evolution of abelisaurid theropods. *Naturwissenschaften*, *96*, 409–414.

Carrano, M. T., Sampson, S. D., & Forster, C. A. (2002). The osteology of *Masiakasaurus knopfleri*, a small abelisauroid (Dinosauria: Theropoda) from the Late Cretaceous of Madagascar. *Journal of Vertebrate Paleontology*, *22*, 510–534.

Carrano, M. T., & Sampson, S. D. (2008). The phylogeny of Ceratosauria (Dinosauria: Theropoda). *Journal of Systematic Palaeontology*, *6*, 183–236.

Carrano, M. T., Loewen, M. A., & Sertich, J. J. (2011). New materials of *Masiakasaurus knopfleri* Sampson, Carrano, and Forster, 2001, and implications for the morphology of the Noasauridae (Theropoda: Ceratosauria). *Smithsonian Contributions to Paleobiology*, *95*, 1–53.

Cerroni, M. A., Canale, J. I., & Novas, F. E. (2020a). The skull of *Carnotaurus sastrei* Bonaparte 1985 revisited: insights from craniofacial bones, palate and lower jaw. *Historical Biology*, *33*(10), 2444-2485.

Cerroni, M. A., Canale, J. I., Novas, F. E., & Paulina-Carabajal, A. (2020b). An exceptional neurovascular system in abelisaurid theropod skull: New evidence from *Skorpiovenator bustingorryi*. *Journal of Anatomy*, *240*(4), 612–626.

Cerroni, M. A., Motta, M. J., Agnolín, F. L., Rolando, A. A., Egli, F. B., & Novas, F. E. (2020c). A new abelisaurid from the Huincul Formation (Cenomanian–Turonian; upper Cretaceous) of Río Negro Province, Argentina. *Journal of South American Earth Sciences*, *98*, 102445.

Cerroni, M. A., Baiano, M. A., Canale, J. I., Agnolín, F. L., Otero, A. & Novas, F. E. (2022). Appendicular osteology of *Skorpiovenator bustingorryi* (Theropoda, Abelisauridae) with comments on

phylogenetic features of abelisaurids. *Journal of Systematic Palaeontology*, *20*, 1–32.

Chure, D. J., & Loewen, M. A. (2020). Cranial anatomy of *Allosaurus jimmadseni*, a new species from the lower part of the Morrison Formation (Upper Jurassic) of Western North America. *PeerJ* 8:e7803. https://doi.org/10.7717/peerj.7803.

Coria, R. A., & Salgado, L. (1995). A new giant carnivorous dinosaur from the Cretaceous of Patagonia. *Nature*, *377*, 224–226.

Coria, R. A., & Salgado, L. (1998). A Basal Abelisauria Novas, 1992 (Theropoda Ceratosauria) from the Cretaceous of Patagonia, Argentina. *Gaia*, *15*, 89–102.

Coria, R. A., Chiappe, L. M., & Dingus, L. (2002). A new close relative of *Carnotaurus sastrei* Bonaparte 1985 (Theropoda: Abelisauridae) from the Late Cretaceous of Patagonia. *Journal of Vertebrate Paleontology*, *22*, 460–465.

Currie, P. J. (1997). Braincase anatomy. In P.J. Currie, and K. Padian (Eds.), *Encyclopedia of Dinosaurs* (pp. 81–83). Academic Press.

Delcourt, R. (2018). Ceratosaur palaeobiology: New insights on evolution and ecology of the southern rulers. *Scientific Reports*, *8*(1). https://doi.org/10.1038/s41598-018-28154-x

de Souza, G. A., Soares, M. B., Weinschütz, L. C., Wilner, E., Lopes, R. T., de Araújo, O. M., & Kellner, A. W. (2021). The first edentulous ceratosaur from South America. *Scientific Reports*, *11*(1), 22281.

Eddy, D. R., & Clarke, J. A. (2011). New information on the cranial anatomy of *Acrocanthosaurus atokensis* and its implications for the phylogeny of Allosauroidea (Dinosauria: Theropoda). *PloS One*, *6*(3), e17932. https://doi.org/10.1371/journal.pone.0017932

Ezcurra, M. D. (2024). Exploring the effects of weighting against homoplasy in genealogies of palaeontological phylogenetic matrices. *Cladistics*, *40*(3), 242–281.

Fedorov, A., Beichel, R., Kalpathy-Cramer, J., Finet, J., Fillion-Robin, J. C., Pujol, S., & Buatti, J. (2012). 3D Slicer as an image computing platform for the Quantitative Imaging Network. *Magnetic Resonance Imaging*, *30*, 1323–1341.

Filippi, L. S., Mendez, A. H., Gianechini, F. A., Valieri, R. D. J., & Garrido, A. C. (2018). Osteology of *Viavenator exxoni* (Abelisauridae; Furileusauria) from the Bajo de la Carpa Formation, NW Patagonia, Argentina. *Cretaceous Research*, *83*, 95–119.

Garrido, A. C. (2010). Estratigrafía del Grupo Neuquén, Cretácico Superior de la Cuenca Neuquina (Argentina): nueva propuesta de ordenamiento litoestratigráfico. *Revista del Museo Argentino de Ciencias Naturales*, *12*, 121–177.

Gates, T., Organ, C., & Zanno, L. (2016). Bony cranial ornamentation linked to rapid evolution of gigantic theropod dinosaurs. *Nature communications*, *7*, 12931.

Gianechini, F. A., Mendez, A. H., Filippi, L. S., Paulina-Carabajal, A., Juárez-Valieri, R. D., & Garrido, A. C. (2021). A new furileusaurian abelisaurid from La Invernada (Upper Cretaceous, Santonian, Bajo de la Carpa Formation), northern Patagonia, Argentina. *Journal of Vertebrate Paleontology*, *40*(6), e1877151.

Goloboff, P. A. (1997). Self-Weighted Optimization: Tree Searches and Character State Reconstructions under Implied Transformation Costs. *Cladistics*, *13*(3), 225–245.

Goloboff, P. A., Farris, J. S., & Nixon, K. C. (2008). TNT, a free program for phylogenetic analysis. *Cladistics*, *24*, 774–786.

Goloboff, P. A., & Szumik, C. A. (2015). Identifying unstable taxa: efficient implementation of triplet-based measures of stability, and comparison with Phyutility and RogueNaRok. *Molecular Phylogenetics and Evolution*, *88*, 93–104.

Goloboff, P. A., Torres, A., & Arias, J. S. (2018). Weighted parsimony outperforms other methods of phylogenetic inference under models appropriate for morphology. *Cladistics*, *34*(4), 407–437.

Goloboff, P. A., & Morales, M. E. (2023). TNT version 1.6, with a graphical interface for MacOS and Linux, including new routines in parallel. *Cladistics*, *39*, 144–153.

Hendrickx, C., Mateus, O., & Araújo, R. (2015). A proposed terminology of theropod teeth (Dinosauria, Saurischia). *Journal of Vertebrate Paleontology*, *35*: e982797. https://doi.org/10.1080/02724634.2015.982797

Hendrickx, C., Mateus, O., da Lourinhã, M., Araújo, R., da Lourinhã, M., & Choiniere, J. (2019). The distribution of dental features in non-avian theropod dinosaurs: Taxonomic potential, degree of homoplasy, and major evolutionary trends. *Palaeontologia Electronica* 22.3.74 1–110. https://doi.org/10.26879/820

Hendrickx, C., Tschopp, E., & Ezcurra, M. (2020). Taxonomic identification of isolated theropod teeth: the case of the shed tooth crown associated with *Aerosteon* (Theropoda: Megaraptora) and the dentition of Abelisauridae. *Cretaceous Research*, *108*, 104312. https://doi.org/10.1016/j.cretres.2019.104312

Hendrickx, C., Cerroni, M. A., Agnolín, F. L, Catalano, S., Ribeiro, C. F, Delcourt, R. (2024). Osteology, relationship, and feeding ecology of the theropod dinosaur *Noasaurus leali*, from the Late Cretaceous of North-Western Argentina. *Zoological Journal of the Linnean Society*, *202*(4), zlae150.

Hieronymus, T. L., & Witmer, L. M. (2003). Dermal enthesis: anatomy and histology of rhinoceros horn attachment. *Integrative and Comparative Biology 43*, 6, 874–874.

Hieronymus, T. L., & Witmer, L. M. (2004). Cranial rugosity and dinosaur 'horns:' rhino and giraffe as model systems for skin reconstruction in fossil taxa. *Journal of Vertebrate Paleontology*, *24*(3, Supplement):70A.

Hieronymus, T. L., Witmer, L. M., Tanke, D. H., & Currie, P. J. (2009). The facial integument of centrosaurine ceratopsids: morphological and histological correlates of novel skin structures. *The Anatomical Record: Advances in Integrative Anatomy and Evolutionary Biology: Advances in Integrative Anatomy and Evolutionary Biology*, *292* (9), 1370–1396.

Ibiricu, L. M., Baiano, M. A., Martinez, R. D., Alvarez, B. N., Lamanna, M. C., & Casal, G. A. (2021). A detailed osteological description of *Xenotarsosaurus bonapartei* (Theropoda: Abelisauridae): implications for abelisauroid phylogeny. *Cretaceous Research*, *124*, 104829.

Juárez Valieri, R. D., Fiorelli, L. E., & Cruz, L. E. (2007). *Quilmesaurus curriei* Coria, 2001 (Dinosauria, Theropoda): Su validez taxonómica y relaciones filogenéticas. *Rev. Mus. Argentino Cienc. Nat., n.s. 9*(1), 59–66.

Korzun, L. P., Erard, C., & Gasc, J. P. (2004). Morphofunctional study of the bill and hyoid apparatus of *Momotus momota* (Aves, Coraciiformes, Momotidae): implications for omnivorous feeding adaptation in motmots. *Comptes Rendus Biologies*, *327*, 319–333.

Korzun, L. P., Érard, C., Gasc, J. P., & Dzerzhinsky, F. J. (2009). Adaptation of seedsnipes (Aves, Charadriiformes, Thinocoridae) to browsing: a study of their feeding apparatus. *Zoosystema*, *31*(2), 347–368.

Langer, M. C., de Oliveira Martins, N., Manzig, P. C., de Souza, Ferreira, G., de Almeida Marsola, J. C., Fortes, E., Lima, R., Santana, L. C. F., da Silva Vidal, L., da Silva Lorencato, R. H., & Ezcurra, M. D. (2019). A new desert-dwelling dinosaur (Theropoda, Noasaurinae) from the Cretaceous of south Brazil. *Scientific Reports*, *9*, 9379. https://doi.org/10.1038/s41598-019-45306-9

Lamanna, M. C., Martinez, R. D., & Smith, J. B. (2002). A definitive

abelisaurid theropod dinosaur from the early Late Cretaceous of Patagonia. *Journal of Vertebrate Paleontology*, *22*(1), 58–69.

Lamanna, M. C., Casal, G. A., & Martinez, R. D. (2011). A new abelisaurid specimen, including a partial skull, from the "middle" Cretaceous of central Patagonia. *Ameghiniana*, *48*(4), R177.

Madsen, J. H. (1976). *Allosaurus fragilis*: a revised osteology. *Utah Geological and Mineral Survey Bulletin* 109,163.

Madsen, J. H., & Welles, S. P. (2000). *Ceratosaurus* (Dinosauria, Theropoda): a revised osteology. *Utah Geological Survey Miscellaneous Publications MP-00–2*, 1–80.

Marsh, O. C. (1881). Classification of the Dinosauria. American. *Journal of Science (Series 3) 23*, 81–86.

Marsh, O. C. (1884). Principal characters of American Jurassic dinosaurs; Part VIII, the order Theropoda. *American Journal of Science*, *3*(160), 329–340.

Meso, J. G., Hendrickx, C., Baiano, M. A., Canale, J. I., Salgado, L., & Díaz Martínez, I. (2021a). Isolated theropod teeth associated with a sauropod skeleton from the Late Cretaceous Allen Formation of Río Negro, Patagonia, Argentina. *Acta Palaeontologica Polonica*, *66*(2), 409–423.

Meso, J. G., Valieri, R. J., Porfiri, J. D., Correa, S. A. S., Martinelli, A. G., Casal, G. A., Canudo, J. I., Poblete, F., & Dos Santos, D. (2021b). Testing the persistence of Carcharodontosauridae (Theropoda) in the Upper Cretaceous of Patagonia based on dental evidence. *Cretaceous Research*, *125*, 104875. https://doi.org/10.1016/j.cretres.2021.104875

Novas, F. E., Agnolín, F. L, & Bandyopadhyay, S. (2004). Cretaceous theropods from India: a review of specimens described by Huene and Matley (1933). *Revista del Museo Argentino de Ciencias Naturales*, *6*, 67–103.

Novas, F. E. (2009). *The age of dinosaurs in South America*. Indiana University Press, Bloomington. Pp. 452.

Novas, F. E., Agnolín, F. L., Ezcurra, M. D., Porfiri, J., & Canale, J. I. (2013). Evolution of the carnivorous dinosaurs during the Cretaceous: the evidence from Patagonia. *Cretaceous Research*, *45*, 174–215. https://doi.org/10.1016/j.cretres.2013.04.001

Owen, R. (1842). Report on British Fossil Reptiles, Part II. In J. Murray (Ed.), *Report of the Eleventh Meeting of the British Association for the Advancement of Science* (pp. 60–204). John Murray.

Paulina-Carabajal, A. (2011a). The braincase anatomy of *Carnotaurus sastrei* (Theropoda: Abelisauridae) from the Upper Cretaceous of Patagonia. *Journal of Vertebrate Paleontology*, *31*, 378–386.

Paulina-Carabajal, A. (2011b). Braincases of abelisaurid theropods from the upper Cretaceous of north Patagonia. *Palaeontology*, *54*(4), 793–806.

Paulina-Carabajal, A., & Filippi, L. (2018). Neuroanatomy of the abelisaurid theropod *Viavenator*: The most complete reconstruction of a cranial endocast and inner ear for a South American representative of the clade. *Cretaceous Research*, 83, 84–94.

Pradelli, L. A., Pol, D., & Ezcurra, M. D. (2024). New dinosaur remains increase theropod diversity in the Cañadón Asfalto Formation (Lower Jurassic), Chubut Province, Argentina. *Journal of Systematic Palaeontology*, *22*(1). https://doi.org/10.1080/14772019.2024.2318262

Ponssa, M. L., & Abdala, V. (2020). Sesamoids in Caudata and Gymnophiona (Lissamphibia): absences and evidence. PeerJ 8:e10595. https://doi.org/10.7717/peerj.10595

Pol, D., & Escapa, I. H. (2009). Unstable taxa in cladistic analysis: identification and the assessment of relevant characters. *Cladistics*, 25(5), 515–527.

Pol, D., & Rauhut, O. W. (2012). A Middle Jurassic abelisaurid from Patagonia and the early diversification of theropod dinosaurs. *Proceedings of the Royal Society B: Biological Sciences*, *279*, 3170–3175.

Pol, D., Baiano, M. A., Černý, D., Novas, F., Cerda, I. A., & Pittman, M. (2024). A new abelisaurid dinosaur from the end Cretaceous of Patagonia and evolutionary rates among the Ceratosauria. *Cladistics*, *40*(3), 307–356.

Porter, W. R. (2015) *Physiological implications of dinosaur cephalic vascular systems* (PhD dissertation, University of Ohio, Athens, OH, USA).

Rauhut, O. W. M. (2004). Provenance and anatomy of *Genyodectes serus*, a large-toothed ceratosaur (Dinosauria: Theropoda) from Patagonia. *Journal of Vertebrate Paleontology*, *24*(4), 894–902.

Rauhut, O. W. M., & Fechner, R. (2005). Early development of the facial region in a non-avian theropod dinosaur. *Proceedings of the Royal Society B: Biological Sciences*, *272*(1568), 1179–1183.

Ratsimbaholison, N. O., Felice, R. N., & O'Connor, P. M. (2016). Ontogenetic changes in the craniomandibular skeleton of the abelisaurid dinosaur *Majungasaurus crenatissimus* from the Late Cretaceous of Madagascar. *Acta Palaeontologica Polonica*, *61*(2), 281–292.

Rauhut, O. W., & Carrano, M. T. (2016). The theropod dinosaur *Elaphrosaurus bambergi*, from the Late Jurassic of Tendaguru, Tanzania. *Zoological Journal of Linnean Society*, *178*, 546–610.

Sampson, S. D., & Witmer, L. M. (2007). Craniofacial anatomy of *Majungasaurus crenatissimus* (Theropoda: Abelisauridae) from the Late Cretaceous of Madagascar. *Journal of Vertebrate Paleontology*, *27*, 32–104.

Sampson, S. D., Witmer, L. M., Forster, C. A., Krause, D. W., O'Connor, P. M., Dodson, P., & Ravoavy, F. (1998). Predatory dinosaur remains from Madagascar: implications for the Cretaceous biogeography of Gondwana. *Science*, *280*, 1048–1051.

Sarin, V. K., Erickson, G. M., Giori, N. J., Bergman, A. G., & Carter, D. R. (1999). Coincident development of sesamoid bones and clues to their evolution. *Anatomical Record*, *257*, 174–180.

Seeley, H. G. (1887). I. On the classification of the fossil animals commonly named Dinosauria. *Proceedings of the Royal Society of London*, *43* (258–265), 165–171.

Sereno, P. C., Dutheil, D. B., Iarochene, M., Larsson, H. C. E., Lyon, G. H., Magwene, P. M., Sidor, C. A., Varricchio, D. J., & Wilson, J. A. (1996). Predatory dinosaurs from the Sahara and Late Cretaceous faunal differentiation. *Science*, *272*, 986–991.

Sereno, P. C, Wilson, J. A., & Conrad, J. L. (2004). New dinosaurs link southern landmasses in the Mid–Cretaceous. *Proceedings of the Royal Society B: Biological Sciences*, *271*(1546), 1325–1330.

Sereno, P. C., & Brusatte, S. L. (2008). Basal abelisaurid and carcharodontosaurid theropods from the Lower Cretaceous Elrhaz Formation of Niger. *Acta Palaeontologica Polonica*, *53*(1), 15–46.

Simón, M. E., Salgado, L., & Calvo, J. O. (2017), A new titanosaur sauropod from the Upper Cretaceous of Patagonia, Neuquén Province, Argentina. *Ameghiniana*, 55, 1–29.

Simón, M. E., & Salgado, L. (2023). A new gigantic titanosaurian sauropod from the early Late Cretaceous of Patagonia (Neuquén Province, Argentina). *Acta Palaeontologica Polonica*, *68*(4), 719–735.

Simón, M. E., & Salgado, L. (2025). New rebbachisaurid (Dinosauria, Sauropoda) from the Huincul Formation (upper Cenomanian-Turonian) of Villa El Chocón (Neuquén Province, Argentina). *Cretaceous Research*, *173*, 106137. https://doi.org/10.1016/j.cretres.2025.106137

Słowiak, J., Brusatte, S. L., & Szczygielski, T. (2024). Reassessment of the enigmatic Late Cretaceous theropod dinosaur, *Bagaraatan*

ostromi. *Zoological Journal of the Linnean Society*, 202(3), zlad169.

Smith, J. B. (2007). Dental morphology and variation in *Majungasaurus crenatissimus* (Theropoda: Abelisauridae) from the Late Cretaceous of Madagascar. *Journal of Vertebrate Paleontology*, *Memoir 8*, 27, 103–126.

Smith, J. B., Vann, D. R., & Dodson, P. (2005). Dental morphology and variation in theropod dinosaurs: Implications for the taxonomic identification of isolated teeth. *The Anatomical Record Part A: Discoveries in Molecular*, *Cellular*, *and Evolutionary Biology*, *285*A, 699–736.

Smith, J. B., & Dodson, P. (2003). A proposal for a standard terminology of anatomical notation and orientation in fossil vertebrate dentitions. *Journal of Vertebrate Paleontology*, *23*, 1–12.

Snively, E., & Russell, A. P. (2007). Functional variation of neck muscles and their relation to feeding style in Tyrannosauridae and other large theropod dinosaurs. *The Anatomical Record: Advances in Integrative Anatomy and Evolutionary Biology 290*, 934–957.

Therrien, F., Henderson, D. M., & Ruff, C. B. (2005). Bite me: biomechanical models of theropod mandibles and implications for feeding behavior. In K. Carpenter (Ed.), *The Carnivorous Dinosaurs*, 179–237. Indiana University Press, Bloomington.

Tortosa, T., Buffetaut, E., Vialle, N., Dutour, Y., Turini, E., & Cheylan, G. (2014). A new abelisaurid dinosaur from the Late Cretaceous of southern France: palaeobiogeographical implications. *Annales de Paléontologie*, *100*, 63–86. http://dx.doi.org/10.1016/j.annpal.2013.10.003

Tsai, H. P., & Holliday, C. M. (2011). Ontogeny of the *Alligator* cartilage transiliens and its significance for sauropsid jaw muscle evolution. *PLOS ONE*, *6*(9):e24935. https://doi.org/10.1371/journal.pone.0024935

Tykoski, R. S., & Rowe, T. (2004). Ceratosauria. In D. B. Weishampel, P. Dodson, & H. Osmolska (Eds.), *The Dinosauria* (pp. 47–70). Berkeley, University of California Press.

Kundrát, M., Cruickshank, A. R. I., Manning, T. W., & Nudds, J. (2008). Embryos of therizinosauroid theropods from the Upper Cretaceous of China: diagnosis and analysis of ossification patterns. *Acta Zoologica*, *89*, 231–251.

Wang, S., Stiegler, J., Amiot, R., Xu, W., Du, G., Clark, J. M., & Xu, X. (2017). Extreme Ontogenetic Changes in a Ceratosaurian Theropod. *Current Biology*, *27*(1), 144–148.

White, M. A., Bell, P. R., Cook, A. G., Poropat, S. F., & Elliott, D. A. (2015). The dentary of *Australovenator wintonensis* (Theropoda, Megaraptoridae); implications for megaraptorid dentition. *PeerJ*, *3*, e1512. https://doi.org/10.7717/peerj.1512

Witmer, L. M. (1997). The evolution of the antorbital cavity of archosaurs: a study in soft tissue reconstruction in the fossil record with an analysis of the function of pneumaticity. *Journal of Vertebrate Paleontology*, *Memoir 3*, 1–73.

Xu, X., Norell, M. A., Kuang, X., Wang, X., Zhao, Q., & Jia, C. (2004). Basal tyrannosauroids from China and evidence for protofeathers in tyrannosauroids. *Nature*, *431*, 680–684.

Zaher, H., Pol, D., Navarro, B. A., Delcourt, R., & Carvalho, A. B. (2020). An Early Cretaceous theropod dinosaur from Brazil sheds light on the cranial evolution of the Abelisauridae. *Comptes Rendus Palevol*, *19*(6), 101–115.

doi: 10.5710/AMGH.20.08.2026.3665

Submitted: 27 August 2025
Accepted: 20 August 2026
Published: 21 August 2026